

Structure and properties of transparent conductive ZnO films grown by pulsed laser deposition (PLD)

by

Yu-Hsiu, Lin



**UNIVERSITY OF
BIRMINGHAM**

A dissertation submitted to
the University of Birmingham
for the degree of
Master of Research

School of Metallurgy and Materials

University of Birmingham

September 2009

UNIVERSITY OF
BIRMINGHAM

University of Birmingham Research Archive

e-theses repository

This unpublished thesis/dissertation is copyright of the author and/or third parties. The intellectual property rights of the author or third parties in respect of this work are as defined by The Copyright Designs and Patents Act 1988 or as modified by any successor legislation.

Any use made of information contained in this thesis/dissertation must be in accordance with that legislation and must be properly acknowledged. Further distribution or reproduction in any format is prohibited without the permission of the copyright holder.

Acknowledgements

I would like to acknowledge sincerely to my supervisor Prof. Abell for his kindness, excellent explanations throughout my study.

I would also like to express my sincere gratitude to Dr Stephen N Kukureka for his enlightening ideas and patient guidance.

Special thanks are given to Mr Bradshaw for his technical support during my experiment.

Many thanks are given to all staff in school of Metallurgy and Materials and especially to my colleagues of the superconductivity group for their help and support during my Master studies.

Finally, I would like to thank my family and friends for the invaluable help and endless encouragement.

.

Abstract

Zinc Oxide (ZnO) has attracted interest due to its potential applications including nonlinear optical devices, blue-violet emission device, buffer layer for GaN-based devices, visible-range transparent electrodes for solar cell and flat panel displays, surface acoustic wave devices, piezoelectric and piezo-optic devices, gas sensors for oxygen, and integrated optical devices such as optical waveguides. Furthermore, ZnO is nontoxic and inexpensive and has comparable electrical and optical properties to commercially available Indium Tin Oxide (ITO).

ZnO thin films were grown on glass substrates by the pulsed laser deposition (PLD) technique using a KrF excimer laser with wavelength of 248nm. The influence of ambient oxygen pressure, substrate temperature, laser fluence, the number of pulses and doping with silicon was investigated. The structural, optical and electrical properties of ZnO thin films were investigated using X-ray diffraction (XRD), atomic force microscopy (AFM), scanning electronic microscopy (SEM), spectrophotometers and resistance measurement by the four-point probe.

Regarding the influence of oxygen pressure, XRD measurements indicate that the ZnO thin films deposited at the oxygen pressure of 10 mTorr (1.3 Pa) crystallize well. AFM results show that the surface roughness of ZnO film increases with an increase of oxygen pressure. The electrical resistivity showed a minimum for an oxygen partial pressure of 10 mTorr (1.3 Pa).

The effect of the substrate temperatures in the range of 100°C to 500°C on the properties of ZnO thin films was investigated with the oxygen pressure kept at 10 mTorr. The lowest resistivity was observed for a substrate temperature of 200 C.

The effect of post-growth annealing showed that for temperatures < 300°C, it is observed that the resistivity of the ZnO films decreases slightly. As the annealing temperature increases up to 500°C, the resistivity of the ZnO films increases dramatically. Furthermore, The ZnO films show an increase of transmittance with annealing temperature, which probably indicates that the annealing treatment improved the crystallinity.

ZnO thin films were deposited using a different number of pulses in order to investigate the thickness dependence of the structural, electrical and optical properties of the films. It was found that correlation between thickness and resistivity of ZnO thin films is negative due to the thicker films having fewer point defects such as oxygen vacancies. The transmittance of ZnO thin films is decreased due to the thickness effect.

Laser energy density was varied in the range from 1.16 J/cm² to 2.73 J/cm² and it was observed that the resistivity of ZnO thin films declines with increasing laser fluence up to 1.51 J/cm². However, at higher fluences up to 2.27 J/cm², the resistivity dramatically increases, and the relatively low resistivity of the ZnO thin films of 3.1x10⁻³ Ω/cm is found at a laser fluence of 1.51J/cm². The optical transmittance increases with increase of laser fluence, from 1.16 J/cm² to 2.27 J/cm² in the range of wavelength of 350 nm to 450 nm. However, as the laser fluence increases up to 2.73 J/cm², the optical transmittance significantly declines.

The influence of impurity doping was investigated by using a 2 wt% Si-ZnO target. It was observed that the doped films had lower resistivity than pure ZnO films (from $9 \times 10^{-3} \, \Omega \, \text{cm}$ to $7 \times 10^{-4} \, \Omega \, \text{cm}$). Probably due to the increase in carrier concentration with doping the Si ions entering into the ZnO lattice caused a shift in the absorption edge and the average transmittance increased to 85 % in the visible region after doping with 2 wt% silicon.

Contents

1	Introduction.....	7
1.1	Zinc oxide.....	7
1.2	Challenges in this project	8
1.3	Aims and objectives.....	8
1.4	Organization of the thesis	8
2	Literature Review	10
2.1	Transparent conducting oxides (TCOs).....	10
2.1.1	ZnO structure.....	10
2.1.2	Electrical properties of ZnO	11
2.1.3	Optical properties of ZnO	12
2.1.4	Effect of doping ZnO with impurity	13
2.2	Pulsed laser deposition (PLD)	14
2.2.1	Introduction to PLD	14
2.2.2	The growth of thin films by PLD	14
2.2.3	The advantages of PLD	15
2.2.4	The disadvantages of PLD.....	16
2.3	Other ZnO thin film fabrication methods.....	17
2.3.1	RF magnetron sputtering.....	17
2.3.2	Molecular-beam epitaxy.....	18
2.3.3	Chemical-vapor deposition.....	18
2.4	Application of ZnO thin films.....	19
3	Experimental Procedures	21
3.1	PLD.....	21
3.2	Conductivity measurement	21
3.3	Transparency measurement.....	22

3.4	Structure	23
3.5	Surface Morphology	24
3.5.1	Scanning electron microscope (SEM)	24
3.5.2	Atomic force microscope (AFM)	24
3.6	Thickness measurement	25
4	Results and discussion	26
4.1	Influence of oxygen pressure	26
4.1.1	Electrical properties	26
4.1.2	Optical properties	27
4.1.3	Surface morphology	27
4.1.4	Structural properties	28
4.2	Influence of substrate temperature	28
4.2.1	Electrical properties	29
4.2.2	Optical properties	29
4.2.3	Surface morphology	29
4.2.4	Structural properties	30
4.3	Influence of annealing	30
4.3.1	Electrical properties	31
4.3.2	Optical properties	31
4.3.3	Surface morphology	31
4.3.4	Structural properties	32
4.4	Influence of the number of pulses on ZnO films	32
4.4.1	Structural properties	32
4.4.2	Optical properties	33
4.4.3	Electrical properties	33
4.5	Influence of laser fluence on ZnO films	33
4.5.1	Structural properties	34

4.5.2	Electrical properties.....	34
4.5.3	Optical properties.....	34
4.6	Influence of doping with silicon	35
4.6.1	Electrical and optical properties.....	35
4.6.2	Structural properties	36
5	Conclusions.....	37
5.1	Conclusions.....	37
6	Future work	39
7	References	40
	Appendix.....	45
	Figures and tables from Chapter 2	45
	Figures and tables from Chapter 4	61

Figure 2-1 Stick and ball representation of ZnO crystal structures: (a) cubic rock-salt(B1), (b) cubic zinc blend (B3), and (c) hexagonal wurztie (B4). The shaded gray and black spheres denote Zn and O atoms, respectively.[79]	46
Figure 2-2 Schematic representation of a wurtzitic ZnO structure having lattice constant a in the basal plane and c in the basal direction; u parameter is expressed as the bond length or the nearest-neighbor distant b divided by c (0.375 in ideal crystal), and α and β (109.47° in ideal crystal) are the bond angles.[79].....	46
Figure 2-3 (a) Mechanism of photon absorption for non-metallic materials in which an electron is excited across the band gap, leaving behind a hole in the valence band. The energy of the photon absorbed is ΔE , which is necessarily greater than the band gap energy E_g . (b) Emission of a photon of light by a direct electron transition across the band gap. [21]47	
Figure 2-4 The spectrum of electromagnetic radiation, including wavelength ranges for the various colors in the visible spectrum.[21].....	47
Figure 2-5 The relation between absorption and the energy band: Metal	48
Figure 2-6 The relation between absorption and the energy band: Semiconductors.....	48
Figure 2-7 The Schematic description of a PLD experimental set-up[55]	49
Figure 2-8 Schematic of the PLD process[18].....	49
Figure 2-9 Film growth modes—layer-by-layer: (a) Frank-Van der Merwe, island; (b) Volmer–Weber (c),	50
Figure 2-10 The process of sputter (1) (from http://www.ajaint.com/whatis.htm).....	50
Figure 2-11 The process of sputter (2) (from http://www.ajaint.com/whatis.htm).....	51
Figure 2-12 The magnet sputter (from http://www.ajaint.com/whatis.htm).....	51
Figure 2-13 The Schematic description of MBE.....	52
Figure 2-14 Sequence of gas transportation and reaction process contributing to CVD film growth[9]	53
Figure 2-15 The Schematic of CVD (from Chi Mei Corporation established Chi Mei Optoelectronics LTD.).....	54
Figure 2-16 The structure of transparent thin-film transistor (from Chi Mei Corporation established Chi Mei Optoelectronics LTD.).....	54
Figure 2-17 The picture of the PLD system used in University of Birmingham.....	55
Figure 2-18 Schematic diagram of a Four point -Probe.....	55
Figure 2-19 (a) Demonstration of how two waves that have the same wavelength λ and remain in phase after a scattering event after a scattering (b) Demonstration of how two waves that have the same wavelength λ and become out of the phase after a scattering event after a scattering[21]	56
Figure 2-20 Diffraction of x-rays by plans of atoms.[21]	57
Figure 2-21 The Schematic diagram of transmittance (from http://en.wikipedia.org/wiki/Wiki)	57
Figure 2-22 The picture of Spectrophotometer	58
Figure 2-23 The picture of SEM JEOL 7000.....	58
Figure 2-24 The Schematic diagram of a SEM (from Professor Ian Jones' lecture)	59
Figure 2-25 The picture of Field emission (from Professor Ian Jones' lecture)	59
Figure 2-26 The Schematic diagram of AFM (from http://en.wikipedia.org/wiki/Wiki)	60
Figure 2-27 The picture of cross section of ZnO thin films by SEM	60
Figure 4-28 Resistivity of ZnO films deposited at various ambient oxygen pressures ($D=55\text{mm}$, $T_s=300^\circ\text{C}$, Laser fluence= $2.7\text{J}/\text{cm}^2$).....	62


Figure 4-29 A plot of electron concentration and resistivity vs. oxygen pressure as result of Hall measurements. The results from samples grown with 1mTorr and 200°C and 300°C are also plotted.[80].....	62
Figure 4-30 Transmittance spectra of ZnO films on glass substrate grown at different ambient oxygen pressures. (D=55mm, Ts=300°C, Laser fluence=2.7J/cm ²).....	63
Figure 4-31 AFM 3D images (2×2μm) of ZnO with varying ambient oxygen pressure. (D=55mm, Ts=300°C, Laser fluence=2.7J/cm ²).....	63
Figure 4-32 Roughness of ZnO films deposited by PLD (D=55mm, Ts=300°C, Laser fluence=2.7J/cm ²).....	64
Figure 4-33 XRD pattern of ZnO films deposited by PLD with varying oxygen pressures. (D=55mm, Ts=300°C, Laser fluence=2.7J/cm ²).....	65
Figure 4-34 peak intensity of XRD pattern of ZnO films deposited by PLD with varying oxygen pressures. (D=55mm, Ts=300°C, Laser fluence=2.7J/cm ²).....	66
Figure 4-35 Variation in the FWHM of (002) reflections of The ZnO films as a function of oxygen pressures. (D=55mm, Ts=300°C, Laser fluence=2.7J/cm ²).....	67
Figure 4-36 Resistivity of ZnO films deposited at various Substrate temperatures (D=55mm, Po2=10mTorr, Laser fluence=2.7J/cm ²).....	68
Figure 4-37 The electrical properties of ZnO thin films deposited at various temperatures[14].....	68
Figure 4-38 Optical transmittance spectra of the ZnO thin films grown at various substrate temperature. (D=55mm, Po2=10mTorr, Laser fluence=2.7J/cm ²).....	69
Figure 4-39 AFM image of ZnO thin films deposited at various substrate temperatures.....	70
Figure 4-40 Roughness of ZnO thin films deposited at various temperatures.....	70
Figure 4-41 FWHM of (002) XRD peaks from ZnO thin films deposited at various temperatures.....	71
Figure 4-42 XRD patterns of ZnO thin films deposited at various substrate temperatures.....	71
Figure 4-43 Peak intensity of (002) diffraction peak for the ZnO films deposited at various temperatures.....	72
Figure 4-44 Resistivity of ZnO films deposited at various annealing temperatures (D=55mm, Po2=10mTorr, Ts=200°C, Laser fluence=2.7J/cm ²).....	73
Figure 4-45 the optical transmittance spectrum of ZnO thin films deposited on glass substrate for as-deposited, and post-growth annealed at various annealing temperatures. (D=55mm, Po2=10mTorr, Ts=200°C, Laser fluence=2.7J/cm ²).....	74
Figure 4-46 Peak intensity of (002) diffraction peak for the ZnO films deposited at various annealing temperatures (D=55mm, Po2=10mTorr, Ts=200°C, Laser fluence=2.7J/cm ²).....	75
Figure 4-47 AFM image of ZnO thin films deposited at various annealing temperatures. (D=55mm, Po2=10mTorr, Ts=200°C, Laser fluence=2.7J/cm ²).....	76
Figure 4-48 The SEM image of ZnO thin film: (a) as grow, and (b) annealing at 500°C for 2h in oxygen (D=55mm, Po2=10mTorr, Ts=200°C, Laser fluence=2.7J/cm ²).....	77
Figure 4-49 Roughness of ZnO thin film deposited at various annealing temperatures. (D=55mm, Po2=10mTorr, Ts=200°C, Laser fluence=2.7J/cm ²).....	78
Figure 4-50 The XRD pattern of ZnO thin films deposited at various annealing temperatures. . (D=55mm, Po2=10mTorr, Ts=200°C, Laser fluence=2.7J/cm ²).....	79
Figure 4-51 X-ray diffraction spectra of ZnO thin film deposited at the various number of laser pulses. (D=55mm, Po2=	

10mTorr, $T_s=200^\circ\text{C}$, Laser fluence= $2.7\text{J}/\text{cm}^2$)	80
Figure 4-52 Peak intensity of (002) diffraction peak for the ZnO films deposited at the various number of laser pulses. ($D=55\text{mm}$, $Po_2=10\text{mTorr}$, $T_s=200^\circ\text{C}$, Laser fluence= $2.7\text{J}/\text{cm}^2$)	81
Figure 4-53 the optical transmittance spectrum of ZnO thin films deposited on glass substrate with the various number of laser pulses. ($D=55\text{mm}$, $Po_2=10\text{mTorr}$, $T_s=200^\circ\text{C}$, Laser fluence= $2.7\text{J}/\text{cm}^2$)	82
Figure 4-54 The resistivity of ZnO thin films deposited at the various number of laser pulses.....	83
Figure 4-55 X-ray diffraction spectra of ZnO thin film deposited at various laser fluence. ($D=55\text{mm}$, $Po_2=10\text{mTorr}$, $T_s=200^\circ\text{C}$).....	84
Figure 4-56 Peak intensity of (002) diffraction peak for the ZnO films deposited at various laser fluence ($D=55\text{mm}$, $Po_2=10\text{mTorr}$, $T_s=200^\circ\text{C}$)	85
Figure 4-57 Resistivity of ZnO thin films deposited at various laser fluence	86
Figure 4-58 the optical transmittance spectrum of ZnO thin films deposited on glass substrates with the various laser fluence ($D=55\text{mm}$, $Po_2=10\text{mTorr}$, $T_s=200^\circ\text{C}$, the number of laser pulse=5000)	87
Figure 4-59 Resistivity, and carrier concentration as a function of Si-ZnO thin films ($D=55\text{mm}$, $Po_2=5\text{mTorr}$, $T_s=200^\circ\text{C}$, the number of laser pulse=5000).....	88
Figure 4-60 Absorption spectra of pure ZnO thin film and 2wt% Si-doped ZnO.....	89
Figure 4-61 X-ray diffraction spectra of ZnO thin film and Si-ZnO thin film ($D=55\text{mm}$, $Po_2=5\text{mTorr}$ & 10mTorr , $T_s=200^\circ\text{C}$, Laser fluence= $2.7\text{J}/\text{cm}^2$)	90

1 Introduction

1.1 Zinc oxide

Much of the academic literature on transparent conductive oxides (TCO) films by pulsed laser deposition (PLD) is focussed on Indium Tin Oxide (ITO) thin films. However in recent years, due to the wide application of ITO materials, the cost of ITO materials is rising, which is forcing many scientists to search for new kind of materials to replace ITO. Of these new kinds of materials, ZnO thin films have attracted the most attention, because unlike the more commonly used ITO, ZnO is a non-toxic and inexpensive material due to abundant ZnO resources. We can find obvious evidence in the fact that more than 1500 papers have been published on ZnO thin films growth and properties of ZnO in this decade.

Zinc oxide (ZnO) is an  n-type semiconductor having a band gap of 3.3 eV at room temperature, large exciton binding energy (60 meV) and optical transparency [1, 2]. The properties of ZnO with a direct band gap and high exciton binding energy are much higher than those of other widely used wide-band-gap materials, for example, ZnSe (20 meV) and GaN (21 meV). Moreover, the ZnO thin films can be deposited at a lower temperature than ZnSe and GaN. Therefore, its wide-band-gap properties enable ZnO to become a potential material for short-wavelength optoelectronic devices, such as UV lasers, blue to UV light-emitting diodes and UV detectors [3, 4], which can be applied to high density data storage systems, solid-state lighting, secure communications and bio-detection.

The growth method of ZnO thin films has been considered by major techniques, such as magnetron sputtering [5, 6], chemical vapour deposition (CVD) [7-10], metallo-organic vapour phase epitaxy (MOVPE) [11], sol-gel processing [12], spray pyrolysis [13] and pulsed laser deposition (PLD) [14]. Of these methods, the PLD technique is considered as a very effective method to growth high-quality films with complex composition. Additionally, thin films deposited by PLD can result in better crystal structure at lower temperature than by other techniques, which is caused by the higher energy of the ablated particles in the laser-produced plasma plume [15]. Moreover, there are still other advantages of using the PLD technique making it so effective. For example, deposition processes in controllable oxygen ambient pressure result in high controllability of thin film chemical element composition and grain growth processes. Thus, in this project, ZnO thin films are deposited on glass substrates by PLD, and the influence of film growth conditions, such as substrate temperature, ambient oxygen pressure, laser fluence and the number of laser pulses on the structural, optical and electrical properties of ZnO thin films was studied.

1.2 Challenges in this project

A high quality ZnO thin film can be deposited by PLD under certain process conditions, but, it is well known that different process machines or different ZnO targets would make the conditions a little different, sometimes totally different. Therefore, for understanding a new material (ZnO) and new equipment (PLD), firstly we should systematically arrange a series of experiments to find out the relative optimized PLD conditions.

For investigating the influence of different parameters of PLD on ZnO thin films, in each experiment we can only vary one parameter and keep the other parameters at the same level. If there is any change in the the parameters of PLD, the experiment should be done all over again.

To commercialize ZnO is each researcher's purpose, but the electrical properties of ZnO are always a weakness compared with ITO. Therefore, in this project we dope the pure ZnO with 2%wt silicon in order to grow a low resistivity and high transmission thin film. Therefore, for achieving the optimized properties of thin film by using new targets, we should re-arrange a series of experiments to optimize the PLD parameters.

1.3 Aims and objectives

- I. To optimize the pulsed laser deposition of ZnO thin films with respect to conductivity and optical transparency by varying oxygen pressure, laser energy density and substrate temperature.
- II. To investigate the influence of oxygen pressure, substrate temperature and laser fluence and annealing treatment on ZnO thin films
- III. To optimize the pulsed laser deposition of 2%wt Si-ZnO thin films with respect to conductivity and optical transparency by varying oxygen pressures, substrate temperatures.

1.4 Organization of the thesis

Chapter 2 gives background theory of ZnO and pulsed laser deposition technique. A literature review of ZnO deposition by PLD and other methods is given.

Chapter 3 explains the ZnO deposition and its characterization.

Chapter 4 contains detailed deposition results for the ZnO thin films by PLD. The effect of the oxygen pressure, substrate temperatures, laser fluence, the number of laser pulses, and doping with Si on the conductivity and optical properties of the ZnO thin films is discussed. The surface morphology and roughness of the thin films and their crystal structure are also investigated.

Chapter 5 concludes the thesis. The main findings of the project are summarized.

Chapter 6 Further work which needs to be done is given.

2 Literature Review

2.1 Transparent conducting oxides (TCOs)

Transparent conducting oxide (TCO) films have been used extensively in the optoelectronics industry, such as the LCD industry, due to their high electrical conductivity, high optical transmittance in the visible region, and high reflectance in the infrared (IR) region. After Badeker [16] reported the first research about TCO, TCO films have started to be widely utilized as an essential part of many optoelectronic applications such as, solar collectors, gas sensors and liquid crystal displays.

Over these last few decades, a large number of TCO materials have been investigated such as In_2O_3 , SnO_2 , ZnO and CdO as well as their doped oxides; most effort has been concentrated on creating thin films to improve the electrical conductivity and optical transparency of the films. Additionally, it is well known that most of the TCO materials are n-type semiconductors. So, there has also been some effort on developing p-type TCO films, such as N-doped ZnO [17].

Of all the TCO films, ITO thin films are the most widely used in specific applications, such as flat panel displays, solar cells and LEDs, but due to the cost issue impurity-doped ZnO films also began to attract much attention because they are non toxic and inexpensive and have comparable electrical and optical properties to ITO [18].

2.1.1 ZnO structure

ZnO belongs to the group of II-VI binary compound semiconductors which crystallize in either a cubic zinc-blende or hexagonal wurtzite structure where each anion is surrounded by four cations at the corners of a tetrahedron, and vice versa. The bonding of this tetrahedral coordination is characteristic of sp^3 covalent bonding, but these materials also have substantial ionic character. Therefore, as shown in Figure 2-1, the crystal structures of ZnO are wurtzite (B4), zinc blende (B3), and rock-salt (B1). Under ambient conditions, the thermodynamically stable phase is wurtzite, while the zinc-blende ZnO structure is only revealed by growth on cubic substrates; moreover, the rock-salt (NaCl) structure probably grows at relatively high pressure. Therefore, the structure of ZnO thin films deposited by PLD belongs to the wurtzite structure.

The wurtzite structure has a hexagonal unit cell with two lattice parameters, a and c , in the ratio of $c/a = \sqrt{8/3} = 1.633$. The schematic structure is shown in Figure 2-2, and this

structure has two interpenetrating hexagonal-close-packed (hcp) sub-lattices. Each sub-lattice consists of one type of atom represented with respect to each other along the threefold c-axis by the amount of $u=3/8=0.375$ (in an ideal wurtzite structure) in fractional coordinates.

2.1.2 Electrical properties of ZnO

The electrical resistivity (ρ) of ZnO films is determined by the carrier concentration (N) and carrier mobility (μ), which is also presented as $\rho=1/(Ne\mu)$ where e is the electron charge. It is known that e is a constant, so, for obtaining low resistivity, the carrier concentration (N) and carrier mobility (μ) should be simultaneously maximized, and most research papers have suggested that the method of achieving maximum carrier concentration is by oxygen vacancies and doping.

Oxygen vacancies can be created by controlling the substrate temperature or ambient oxygen pressure. The literature [18] indicates "If an oxygen vacancy is created in a perfect crystal, two electrons are created in the crystal and contributed as ionized donors." But, if there is too much oxygen created in the thin films, suboxides will form, causing the resistivity to rise."

In addition to the oxygen vacancies, doping also can change the electrical conduction of TCOs. As host cations are substituted by elements with a valence higher than that of the host, the extra electrons can become conduction electrons. To avoid the charge neutrality, substitution of a higher valence element creates extra electrons.

It is well known that pure zinc oxide films usually have a characteristic high resistivity due to their low carrier concentration. Therefore, in order to decrease resistivity, we can increase either the carrier concentration or the carrier mobility in zinc oxide thin films. The former is probably obtained by oxygen and/or zinc non-stoichiometry, or doping with an impurity. However, Hu *et al.* [19] pronounced that non-stoichiometric films have excellent electrical and optical properties, but they become very unstable as the ambient temperature becomes higher. On the other hand, for obtaining stable low resistivity ZnO thin films, doped ZnO thin film is probably a good approach.

In conclusion, the majority of research for achieving low resistivity ZnO thin films is focused on increasing the free carrier concentration in thin films through use of dopants and oxygen vacancies. But, Johson *et al.* [20] in 1947 stated that increasing the carrier density via doping or oxygen vacancies is self-limiting because the increase of the number of free carriers decreases the mobility of carriers due to carrier-carrier scattering. Therefore, there is a trade-off relation between the carrier density and the carrier mobility for obtaining low resistivity.

2.1.3 Optical properties of ZnO

When light proceeds from one medium into another, several phenomena occur. Some of the light radiation may be transmitted through the medium, some will be absorbed, and some will be reflected at the interface on the surface. Moreover, the intensity I_0 of the beam incident on the surface of the thin films must equal the sum of the intensities of the transmitted, absorbed, and reflected beams, which can be written as $I_0 = I_T + I_A + I_R$. An alternate form of the above equation is $T + A + R = 1$, where T , A , R , respectively, are the transmissivity (I_T/I_0), absorptivity (I_A/I_0), and reflectivity (I_R/I_0). Thus, materials that are capable of transmitting light with relatively little absorption and reflection are transparent.

The optical phenomena that occur within solid materials, such as ZnO thin films, involve interactions between the electromagnetic radiation and atoms, ions and electrons. Of these interactions, electronic polarization and electron energy transitions are the most important. Nevertheless, absorption by electronic polarization is only explained for the light frequencies in the vicinity of the relaxation frequency of the constituent atoms [21]. Thus, for non-metallic materials like ZnO films at short wavelength ($\lambda < 400\text{nm}$), absorption phenomena can be explained by the fundamental energy gap [18], which depends on the electron energy band structure of the materials; band structures for semiconductors like ZnO thin films are an important property.

As demonstrated in Figure 2-3, absorption of a photon of light probably occurs by the promotion or excitation of an electron from the nearly filled valence band, across the band gap, and into an empty state within the conduction band; a free electron in the conduction band and a hole in the valence band are created. Furthermore, the energy of excitation ΔE is related to the absorbed photon frequency based on the electron transitions equation: $\Delta E = h\nu$. Thus, absorption phenomena can take place only if the photon energy is greater than the band gap E_g , that is represented as: $h\nu > E_g$.

Based on the above theory in which the absorption occurs by $h\nu > E_g$, we extend our discussion to metallic materials. As shown in Figure 2-5, since metallic materials lack a band gap, every photon has enough energy to excite the electron into a higher energy unoccupied state. In contrast, for semiconductors like ZnO thin films, the absorption phenomenon occurs when the energy of the photon in some range of wavelength is greater than E_g while the transparency phenomenon occurs as that of photon under some range of wavelength is smaller than E_g . Hence, that is the reason why the ZnO thin films are only transparent in the visible range; visible light lies within a very narrow region of the spectrum with wavelengths ranging between 400 nm to 700 nm [22] (shown in Figure

2-4).

The transmittance and reflectance data can be used to calculate absorption coefficients of the films at different wavelengths. The absorption coefficient, α , is given by the relation:

$$\alpha = \frac{1}{t} \ln \frac{(1-R)^2}{T} \quad [23]$$

where t is the film thickness, T is the transmittance and R is the reflectance. Additionally, the absorption coefficient data also can be transferred to another equation relative to the band gap (E_g), which can be represented as the following:

$$\alpha h\nu \approx (h\nu - E_g)^{\frac{1}{2}}$$

where $h\nu$ is the photon energy [24].

2.1.4 Effect of doping ZnO with impurity

Recently, doped zinc oxide thin films have been widely studied for their application as conducting electrode materials in flat-panel displays or solar devices. Unlike the more commonly used indium tin oxide (ITO), zinc oxide is a non-toxic and inexpensive material. Furthermore, it is a II-VI n-type semiconductor with band gap of approximately 3.3 eV at room temperature and a hexagonal wurtzite structure [25]. Pure zinc oxide films are highly transparent in the visible range (light wavelength of 400-700 nm) and have high electrical conductivity. However, non-stoichiometric or impurity (Group III elements or Group IV elements) doped zinc oxide films have electrical conductivities as well as high optical transparent. Non-stoichiometric zinc oxide films have unstable electrical properties at high temperature because the sheet resistance of ZnO thin films increases under either oxygen chemisorption and desorption [26] or heat treatment in vacuum or in ambient oxygen pressure at 300 °C~400 °C [27]. Turning to impurity doped ZnO thin films, unlike non-stoichiometric ZnO thin films, impurity doped ZnO thin films possess stable electrical and optical properties. Among the zinc oxide films doped with group II elements such as barium, aluminum, gallium and indium, aluminum-doped zinc oxide (AZO) thin films show the lowest electrical resistivity [28]. Aluminum-doped zinc oxide (AZO) has a low resistivity of $2-4 \times 10^{-4} \Omega \text{ cm}$ [28-30], which is quite similar to that of ITO films, which is about $1-2 \times 10^{-4} \Omega \text{ cm}$ [31-33], and AZO also shows good optical transmission in the visible and near infrared (IR) regions. Thus, AZO films have been used as transparent conducting electrodes in solar cells [19, 34]. In addition to doping with Group III elements, doping ZnO with Group IV elements such as [35, 36] Ge, Sn, Ti, Si is also a good way to obtain low resistivity transparent materials in order to replace ITO because Ge, Ti, Zr could substitute on the Zn atom site. For example, Sn can serve as a doubly ionized donor with the incorporation of SnO_2 as a solute in ZnO and, consequently, provide a high electron carrier concentration. It is, therefore,

expected that the Sn doped ZnO (SZO) will have a higher electrical conductivity and better field emission properties compared with undoped ZnO [36].

2.2 Pulsed laser deposition (PLD)

2.2.1 Introduction to PLD

Pulsed laser deposition (PLD) is a physical vapour deposition process, which involves a deposition process in a vacuum system. Functionally, it shares some process characteristics in common with molecular beam deposition and some with sputter deposition. As shown schematically in Figure 2-7, a pulsed laser is directed on to a target of the material, such as pure ZnO target, to perform a deposition process. Each laser pulse ablates a small amount of the material creating a plasma plume. Then, the ablated material is ejected from the target in a highly forward-directed plume. The ablated species condense on the substrate placed opposite to the target (Figure 2-8).

2.2.2 The growth of thin films by PLD

During vapour-phase epitaxial growth on a flat substrate, nucleation and growth of islands play important roles. Nucleation leads to the formation of surface steps and growth of islands causes the lateral movement of these steps. Since they occur far from thermodynamic equilibrium both of them are determined by kinetics that also further affects the final surface morphology.

For a thermodynamically stable system, the thermodynamic approach to crystal growth can be used to describe crystal growth close to equilibrium. Local fluctuations from equilibrium lead to nucleation, which gives rise to a phase transition from the gas to the solid phase. Markov *et al.* [37] stated that the gas phase is a prerequisite for the formation of these nuclei whereas the formation probability is determined by the activation energy, and nuclei will be formed until a critical density is reached. Then, the nuclei will grow and crystallization proceeds.

Bauer [38] further used the thermodynamic approach to determine growth modes of thin films, and stated that the balance between the free energies of the thin film surface (γ_F), substrate surface (γ_S), and the interface between film and substrate (γ_I) is used to determine the film morphology. So, based on this concept, there are three types of film modes, shown schematically in Figure 2-9. In layer-by-layer growth (Figure 2-9(a) Frank-van Merwe growth mode), the total surface energy ($\gamma_F + \gamma_I$) of the wetted substrate

is lower than the surface energy of the bare substrate γ_s . Strong bonding between film and substrate reduces γ_i such that $\gamma_F + \gamma_i < \gamma_s$. On the contrary, if there is no bonding between film and substrate, three-dimensional (3D) islands are formed. The film does not wet the substrate because this would lead to an increase of the total surface energy, and this growth mode is called the Volmer-Weber growth mode (See Figure 2-9(b)). Turning to the third type of growth mode, heteroepitaxial growth, is called the Stranski-Krastanov growth mode (Figure 2-9(c)). During this type of growth mode, the lattice mismatch between substrate and film gives rise to biaxial strain, causing an elastic energy that grows with increasing layer thickness. Moreover, misfit dislocations at the substrate-film interface will be created if the layer thickness is over a critical thickness, where it is thermodynamically favorable to introduce dislocations due to the increase of the elastic energy, relieved by the dislocations, in the interfacial energy.

2.2.3 The advantages of PLD

Many techniques such as magnetron sputtering[5, 6], chemical vapour deposition (CVD)[8], metallorganic vapour phase epitaxy (MOVPE)[11], sol-gel[12], spray pyrolysis[13], and pulsed laser deposition (PLD) have been used to deposit ZnO films. Among these techniques, the PLD technique has been proved to be a very effective method to deposit high-quality films. That is because of the following reasons:

- Films grown by PLD can be realized at low temperature
The most important characteristics in PLD is the ability to implement stoichiometric transfer of ablated material from targets to substrate for many materials. This comes from the non-equilibrium nature of the ablation process itself due to absorption of high laser density by a small volume of material. However, if the laser fluence is too low, the laser pulse simply heats the target. In this case, the evaporative flux from a target would be determined by the vapour pressures of the constituents. In contrast, as the laser fluence is increased, the ablation threshold is reached where the laser energy ablation is higher than that needed for evaporation. Consequently, absorption by the ablated species occurs, resulting in the formation of plasma at the target surface. Therefore, with appropriate choice of ablation wavelength and absorbing target, high-energy densities are absorbed by a small volume of material, resulting in vapourization that is not dependent on the target temperature.[15]
- High controllability of composition of thin films and growth process with controllable gas partial pressure, such as ambient oxygen pressure.
The purpose of ambient gas introduced into PLD chamber can be explained by two reasons. First, the formation of thin film materials often requires a reactive species, such as molecular oxygen for oxides, as a component of the flux. Interaction of ablated

species with the background gas often produces molecular species in the ablation plume, and these species can cause phase formation. Secondly, the background gas can also be used to reduce the kinetic energies of the ablated species, which can moderate the plume energies to much less than 1 eV [39]. Consequently, interaction with ambient gas slows the ablation plume expansion.

- The complex material films can be deposited by PLD
PLD can provide stoichiometric transfer of material from the target, generation of energetic species, hyperthermal reaction between the ablated cations and the background gas in the ablation plasma. Moreover, its background pressure can decrease up to ultrahigh vacuum. So, films could be deposited by PLD from single, stoichiometric targets of materials or multiple targets for each element.
- Uniform thin films can be produced by PLD
- The thickness distribution of the thin films is determined by the highly forward-directed nature of the ablation plume which is quite non-uniform, and that is because the distribution of material deposited from the ablation plume is symmetric with the target surface normal and can be represented as a $\cos^n(\theta)$ distribution, where n can vary from 4-30. However, using faster scanning of the ablation beam over the target and rotating the substrate, PLD can produce uniform coverage over large areas [18].
- The biggest advantage is that it is versatile. A very wide range of materials, including oxides, metals, semiconductors and even polymers, can be grown by PLD. All that is required is a target of the desired composition. It is unlike Molecular Beam Epitaxy (MBE) and Chemical Vapour Deposition (CVD), where a different source of precursors is required for each element of the compound.[9]
- It has the ability to maintain target composition in the deposited thin films. Because of the very short duration and high energy of the laser pulse, the target material plumes instantly toward the substrate: every component of the phase has a similar deposition rate. This makes optimization of the deposition process much easier [18].
- The energy associated with the high ionic content in laser ablation plumes (typically of the order of 10% and rising with increasing incident laser power density) and high particle velocities (of the order of 10^6 cm s^{-1}) appear to aid crystal growth and lower the substrate temperature required for epitaxy.
- Other advantages are that PLD is clean, low cost relative to CVD, and capable of producing multi-layers simply by switching between several different targets [40].

2.2.4 The disadvantages of PLD

Although PLD has been successfully applied to many research areas, it still has some

disadvantages, that include:[41]

- The ablation plume cross section is generally small (in the order of cm^2) due to a limited laser spot size. This, in turn, limits the sample size that can be prepared by PLD. In addition, this also creates difficulty in controlling thickness uniformity across the sample: this problem can be overcome, to some extent, by scanning the laser beam on a larger size target.
- The plume of ablated material is highly forward directed, which causes poor conformal step coverage. It also makes thickness monitoring difficult.
- Finally, there is an intrinsic “splashing” associated with laser ablation itself, which produces droplets or big particles of the target material on the substrate surface. From an industrial perspective, this is particularly serious as it will result in device failure.

2.3 Other ZnO thin film fabrication methods

2.3.1 RF magnetron sputtering

Sputtering is a technique used to deposit thin films of a material on to a substrate. First, it will create gaseous plasma and then accelerating the ions from this plasma on to the target. The target material is eroded by the arriving ions via energy transfer and molecules. (See Figure 2-10) When these natural particles are ejected they will travel in a straight line unless they come into contact with something, such as other material particles. At this moment, the substrate placed in the path of these ejected particles will be coated by a thin film of the source material (See Figure 2-11).

Although sputtering is proven to be a useful technique in the deposition of thin films, it has two major problems - the deposition rate is slow and the electron bombardment of the substrate is extensive, causing overheating and structural damage. So, the development of magnetron sputtering deals with both of these issues simultaneously. It uses magnets behind the cathode to trap the free electrons in a magnetic field above the target surface (See Figure 2-12). These electrons are not free to bombard the substrate, but in traditional sputtering they do. The trapped electrons form curved circuitous paths in the magnetic field, enhancing their probability of ionizing a neutral gas molecule by several orders of magnitude. This increase in available ions significantly increases the rate at which target material is eroded and subsequently deposited on to the substrate.

In early ZnO research, RF magnetron sputtering was one of the most used growth techniques. Due to its low cost and low operation temperature [10], magnetron sputtering was a preferred method, when compared to sol gel and chemical-vapour

deposition[7]. The growth usually took place in the chamber ambient with $O_2/Ar + O_2$ ratios ranging from 0 to 1 at a pressure of 10^{-3} - 10^{-2} Torr (0.13Pa-1.3Pa), O_2 was used as the reactive gas and Ar acting as the sputtering enhancing gas.

2.3.2 Molecular-beam epitaxy

Molecular beam epitaxy (MBE) was developed in the early 1970s as a means of growing high-purity epitaxial layers of compound semiconductors [42]. MBE can produce high-quality layers with a very abrupt interface and good control of thickness, doping and composition due to the high degree of control possible with MBE. So, MBE is a valuable tool in the development of sophisticated electronic and optoelectronic devices.

Molecular beam epitaxy implements deposition in high vacuum or ultra high vacuum (10^{-8} Pa). The most important characteristic of MBE is the slow deposition rate (probably less than 1000 nm per hour), which allows the films to grow epitaxially.

In MBE, the molecular beams are typically from thermally evaporated elemental sources, and the gaseous elements then condense on the substrates. This means that evaporated atoms do not interact with each other or the vacuum chamber gases until they reach the substrate due to the long mean free paths of the atoms. During deposition, RHEED (Reflection High Energy Electron Diffraction) is used to monitor the growth of the crystal layers (see Figure 2-13). The computer controls shutters in front of each source, allowing precise control of the thickness of each layer, down to a single layer of atoms.

For ZnO thin films deposited by molecular-beam epitaxy (MBE), Zn metal and O_2 are usually used as the source material. High purity Zn metal is evaporated from an effusion cell, where the cell temperature can be varied to examine the effect of Zn flux on the growth rate and material properties. The oxygen radical beam, which can be generated by ECR or a RF plasma source, is directed on the film surface to obtain high oxidation efficiency. When the oxygen plasma is used, the chamber pressure is around 10^{-5} Torr during deposition.

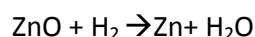
2.3.3 Chemical-vapor deposition

Chemical vapour deposition (CVD) is the process of chemically reacting a volatile compound of a material to be deposited, with other gases, to produce a non-volatile solid that deposits atomistically on a suitably placed substrate. It differs from physical vapour deposition (PVD), which relies on material transfer from condensed-phase evaporant or sputter target sources. Because CVD processes do not require vacuum or unusual levels of power, they were practised commercially prior to PVD [7].

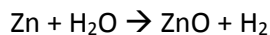
The fundamental sequential steps that occur in every CVD process are sketched in Figure 2-14 and include:

1. Convective and diffusive transport of reactants from the gas inlets to the reaction zone
2. Chemical reactions in the gas phase to produce new reactive species and by-products.
3. Transport of the initial reactants and their products to the substrate surface
4. Adsorption (chemical and physical) and diffusion of these species on the substrate surface.
5. Heterogeneous reactions catalyzed by the surface leading to film formation
6. Desorption of the volatile by-products of surface reactions
7. Convective and diffusive transport

In the CVD method, ZnO deposition occurs as a result of chemical reactions of the vapour-phase precursor on the substrate (shown in Figure 2-15), which are delivered into the growth zone by the carrier gas, which is hydrogen (H₂). The reactions occur in a reactor in which a necessary temperature profile is created in the gas flow direction. The typical pressure is ≤ 133 Pa and the flow rate is about 40 ml/min. Targets made from Zn powder are placed in the evaporation zone where the temperature is about 770 °C. The following chemical reaction between the Zn target and H₂ carrier gas takes place in the evaporation zone:



On the substrate, where the temperature was kept in the range of 590-610 °C, the reverse reaction occurs:



The ZnO films grown by this method show quite high crystal, electrical and luminescence properties [43].

2.4 Application of ZnO thin films

Having the property of wide band-gap causes ZnO to not only be a material transparent in the visible and near UV-visible regions, but also be electrical conductive (n-type). Moreover, the cost of ZnO compared to ITO is relatively lower. ZnO has been used therefore for transparent conducting electrodes instead of expensive ITO for flat-panel display and solar cells [44]. In addition to pure ZnO thin films, doping with various elements (Al, Ga, In) is an efficient way to increase the electrical conductivity [45, 46]. Among these doped ZnO thin films, Al-doped zinc oxide (AZO) thin films have been used as an anode contact for organic light-emitting diodes (OLED).

As shown in Figure 2-16, ITO has been used as an active channel layer in a transparent thin-film transistor (TFT) that can be operated in the presence of visible light in a LCD

display for a while. But due to the improvement of ZnO optical and electrical properties, ZnO thin films also have been used as an active channel layer in a TFT [47].

Another interesting point of ZnO thin film application is to grow (0001)-oriented ZnO thin films by PLD on an amorphous substrate. Such textured film on a GaAs substrate has acted as an alignment layer for the growth of c-axis-oriented GaN films [48]. Although the textured ZnO films do not exhibit outstanding crystalline quality, very strong emission features associated with exciton transitions were observed, which further lead ZnO thin films on GaAs to become a plausible system for short-wavelength visible or UV-light emitting diodes (LEDs).

3 Experimental Procedures

3.1 PLD

ZnO thin films were deposited on glass substrates in a vacuum chamber using a 248nm KrF excimer laser (Lambda Physics LPX 300). The laser emits 25 ns pulses with a repetition rate of 10Hz. High purity O₂ gas was introduced through independent mass flow controllers and the process pressure was kept in the range from 5m Torr to 10m Torr. The PLD system used in this project is shown in Figure 2-17.

The ZnO target was brought from PI-KEM Ltd.[49] It has a diameter of 25 mm. It is composed of 99.999 % high pure ZnO. The Si doped ZnO target was brought from PI-KEM Ltd[49]. It has a diameter of 25mm. It is composed of 98wt% ZnO and 2wt% silicon.

The laser beam with a typical energy of 350 mJ was generated outside the chamber. The optical instruments, such as lenses, mirrors and apertures, whose objective was to steer and focus the laser beam with an incident angle of 45° toward the target with a rotating speed of 10rpm, through a vacuum window, were placed before the port of the deposition chamber. A 10Hz frequency of pulses was supplied for depositing of ZnO films, while the power density of the laser beam at the target surface was about 2.7 J/cm².

The glass substrates used in the depositions are borosilicate Corning 1737 brought from Corning technologies Ltd [50]. The size of the as received substrate is 75 mmx50 mm. It was cut by a diamond knife into 10x10 mm pieces. The substrates were glued on to the heater with silver paint from Agar scientific Ltd [51] to ensure a good thermal contact. The silver paint is composed of very fine silver flakes suspended in methyl iso-butylketone. Before deposition, the substrates were cleaned by using acetone for 10 min and ethanol for 10 min with ultrasonic agitation. Then, they were rinsed with distilled water and dried by compressed air. Finally glass substrates were clamped on to the heater, which can adjust the substrate's temperature to around a temperature of 200°C.

For obtaining the optimized properties of ZnO thin films, several parameters listed in Table 4-1, Table 4-2 and Table 4-3, and the following chapter investigates all parameters.

3.2 Conductivity measurement

The average electrical resistance of the ZnO thin films was calculated by the four-point probe method, by measuring at nine different positions but in symmetrical places on each film, and using an EXCEL program to analyse all values. As shown in Figure 2-18, the 4-point probe system consists of four equally spaced tungsten tips with finite radius. Each

tip is supported by a spring to minimize sample damage when the samples are measured. A high impedance current source is used to supply current through the outer two probes; a voltmeter measures the voltage across the inner two probes (see Figure 2-18) to determine the sample resistance.

In reference [52], for bulk samples where the sample thickness $t \gg s$, the probe spacing, we assume a spherical protrusion of current emanating from the outer probe tips. The differential resistance is:

$$\Delta R = \rho \left(\frac{dx}{A} \right)$$

Then integration between the inner probes tips (where the voltage is measured) gives:

$$R = \int_s^{2s} \rho \frac{dx}{2\pi x^2} = \frac{\rho}{2\pi} \left[-\frac{1}{x} \right]_s^{2s} = \frac{1}{2s} \frac{\rho}{2\pi}$$

where s is probe spacing. Additionally, the superposition of current at the outer two tips can be $R=V/2I$. Therefore, we further modify the expression for bulk resistivity:

$$\rho = 2\pi s \left(\frac{V}{I} \right)$$

If the thin films are very thin (thickness $t \ll s$), we obtain current rings instead of spheres. So, we can put the expression for the area $A=2\pi xt$ into the resistance equation.

$$R = \int_s^{2s} \frac{\rho}{2\pi xt} \frac{dx}{x} = \frac{\rho}{2\pi t} \ln(x) \Big|_s^{2s} = \frac{\rho}{2\pi t} \ln 2$$

Thus, for $R=V/2I$, the sheet resistivity for a thin sheet is:

$$\rho = \frac{\pi t}{\ln 2} \left(\frac{V}{I} \right)$$

Since the equation for resistivity of thin films is obtained, we can use 4-point probe to measure the resistance of thin films, and then using this equation to calculate the resistivity.

3.3 Transparency measurement

In optics theory[21], the transmittance is the fraction of incident light at specific wavelength that passes through a sample, and we will measure the same sample two to three times, then use an EXCEL program to draw a transparency spectrum to analyze the

optical property. As shown in Figure 2-21, the transmittance (T) can be expressed as the following equation:

$$T = \frac{I}{I_0}$$

where I_0 is the intensity of the incident light and I is the intensity of the light coming out of the sample. Therefore, based on the above theory, we can use the model 6130 double beam spectrophotometer (brought from Jenway company [53]) to measure the transmittance of all our samples. The transmittance was measured as a function of wavelength (300 – 1000 nm), and a typical result is shown in Figure 4-30. Furthermore, transmittance is related to absorbance A as:

$$A = -\ln T = -\ln\left(\frac{I}{I_0}\right)$$

3.4 Structure

The crystal structure of the ZnO films was investigated by X-ray- diffraction (XRD) analysis using a Siemens goniometer with a Cu $K\alpha$ radiation source. Cullity [54] stated that diffraction occurs when a wave interacts with a series of regularly spaced obstacles that are capable of scattering the wave and have spacings that are comparable in magnitude to the wavelength. Moreover, the diffraction is a consequence of specific phase relationships that are established between two or more waves that have been scattered by the obstacles.

As shown in Figure 2-19, in the beginning, they all have the same wavelength (λ) and both waves suffer the scattering event. If this path length difference is an integral number of wavelengths, as noted in Figure 2-19 (a), these scattered waves are still in phase. It is called a mutual reinforcement of one another. However, in Figure 2-19(b), where the path length difference after scattering is some integral number of half wavelengths, the scattered waves are out of phase. Therefore, Bragg used this phenomenon to discover the Bragg law ($n\lambda = 2d \sin \theta$) to examine material structure.

In practice, we can measure the angle (θ) by the angle between the arms of the diffractometer when they move. As the arm moves at constant angular velocity, a recorder automatically plots the diffracted beam intensity as function of 2θ ; 2θ is termed the diffraction angle, which is measured experimentally. Figure 4-33 shows a diffraction pattern for ZnO thin films. The high-intensity peaks result when the Bragg diffraction condition is satisfied by some set of crystallographic planes.

3.5 Surface Morphology

The surface morphology of ZnO thin films was investigated by scanning electron microscopy (SEM) (see Figure 2-23) and atomic force microscopy (AFM) in contact mode.

3.5.1 Scanning electron microscope (SEM)

As shown in Figure 2-20, the scanning electron microscope generates a beam of electrons, which come from a filament (see Figure 2-25). The filament is a loop of tungsten which functions as a cathode. A voltage is applied to the loop (in this research, we use 10 kVA), making it to heat up. The anode, which is positive with regard to the filament, forms powerful attractive forces for electrons. This makes the electrons accelerate toward the anode. Some accelerate right by the anode and down the column to the sample.

The beam is collimated by an electromagnetic condenser lenses, focused by an object lens, and scanned across the surface of the sample by electromagnetic deflection coils. The primary imaging method is done by collecting secondary elements that are released by the sample. The secondary electrons are detected by a scintillation material that produces flashes of light from the electrons. The light flashes are then detected and amplified by a photomultiplier tube. By correlating the sample scan position with resulting signal, an image can be formatted, which is similar to what would be seen through an optical microscope.

3.5.2 Atomic force microscope (AFM)

As shown in Figure 2-26, the AFM consist of a micro-scale cantilever with a sharp tip at its end which is used to scan the sample surface. The cantilever is typically silicon or silicon nitride with a tip radius of curvature on the order of nanometers. Although AFM has two types of measurement, that is contact mode and tapping mode, we only used contact mode to measure all samples.

In contact mode measurement, the tip automatically approaches extremely near surface of sample, and forces between the tip and the sample and lead to a deflection of the cantilever are Van der Waals forces. Typically, the deflection is measured using a laser spot reflected from the top of the cantilever into an array of photodiodes.

Then, the single collector will receive all the difference of sample surface. The PC monitor will show the morphology of sample. The AFM software also can calculate the range of the root mean square (RMS) of sample surface roughness, which is a statistical measure of the magnitude of a varying quantity.

3.6 Thickness measurement

Because all the samples were extremely thin, that is around 250~300nm, the only practical way to measure the thickness of the films was to use the SEM to image cross-sections of the films and then use the SEM software to calculate the thickness of thin films automatically. (See Figure 2-27) Normally, each sample was measured two to three times, then the EXCEL program was used to compare all samples.

4 Results and discussion

4.1 Influence of oxygen pressure

The oxygen pressure was always considered to be one of the most important parameters of the PLD growth process. It sensitively affects the epitaxial quality, surface morphology and optoelectronic properties[55]. Moreover, oxygen pressure is also used to control densities of vacancies of oxygen and defects that influence film conductivity; too numerous oxygen vacancies will act as defects without donating electrons and will decrease the conductivity by decreasing the conduction electrons. Consequently, a certain degree of ambient oxygen pressure in the film growth was required with the purpose of conductivity improvement. In this section, for investigating the influence of oxygen pressure on ZnO thin films, we only varied the oxygen pressure and kept other parameters the same. The detailed information is shown in Table 4-1.

4.1.1 Electrical properties

Figure 4-28 indicates the variation of electrical properties as a function of ambient oxygen pressure for ZnO films deposited on glass substrates. The resistivity increases slowly with increasing oxygen pressure to 10 mTorr (1.3 Pa) and then dramatically increases with a further increase in P_{O_2} up to 50mTorr (6.7Pa). It can be clearly observed that the resistivity of the ZnO film is very sensitive to the ambient oxygen pressure, and a low range of resistivity can be obtained in a small range of oxygen pressures between 10mTorr(1.3Pa) and 20mTorr (2.6Pa)..

The ambient oxygen pressure affects accordingly the electrical properties of the ZnO films,[56, 57] which results from stoichiometry effects, and this argument can be seen in Figure 4-29. As the oxygen pressure increases, the electron concentration tends to decrease while the resistivity of the film increases, being associated with a decrease in the density of oxygen vacancies as shallow donors; this also is a sign that the ZnO film approaches an improved stoichiometry with an increased oxygen supply.

Additionally, Zheng and Kwok [58] also declared that the sensitivity to the ambient oxygen pressure can be explained by a characteristic of PLD. They observed that at low oxygen pressures, the density of various species is not uniform on the surface of the substrate due to the different velocity for each species. This also creates defect centers in the film, which increase the film resistivity. Nevertheless, if the oxygen pressure is too high, the velocity of various species in the laser-generated plume will be slowed down because of

the collisions with oxygen molecules, and then the surface activation of the species will be decreased. Therefore, the high oxygen pressure leads to low mobility of species, and this low mobility of species further causes the low crystal quality.

In conclusion, the ambient oxygen pressure is sensitively relative to the electrical resistivity of ZnO films because of mobility of species and stoichiometry effects. Thus, for achieving high conductivity ZnO film, the supply of the ambient oxygen pressure would be at around 10mTorr.

4.1.2 Optical properties

Figure 4-30 shows the transmittance spectra from wavelengths of 300 nm to 1000 nm for ZnO films on glass substrates at different ambient oxygen pressures. The observed transmittances are improved with raising ambient oxygen pressures, and average transmittance taken across the wavelength of 91 % can be achieved at the ambient oxygen pressure of 50 mTorr. This result also indicates that the transmittance is very sensitive to the ambient oxygen pressure, and Jin *et al.*[56] declared that “one important quality of the UV emission may be the stoichiometry of the ZnO which usually has a lot of oxygen vacancies in its lattice.” It is thus expected that the ZnO film grown at higher oxygen pressure of 50 mTorr probably has more improved stoichiometry with fewer oxygen vacancies.

4.1.3 Surface morphology

Figure 4-31 shows five AFM images of the ZnO films grown on glass substrates by PLD at an ambient oxygen pressure of 10 mTorr to 50 mTorr. It is clear that the particle size increases with an increase in the ambient oxygen pressure. Moreover, Figure 4-32 also indicates that the roughness of ZnO films deposited in $D=55\text{mm}$, laser fluence= $2.7\text{J}/\text{cm}^2$ and $T_s=300^\circ\text{C}$ increases with an increase in the ambient oxygen pressure.

This increase in surface roughness with increasing oxygen pressure may be attributed to an enhanced particulate formation in the laser induced plume, which is a typical characteristic of high-pressure laser ablation [59]. On the other hand, if a laser ablation experiment is done in vacuum, there are no collisions between the ejected species before they reach the substrate. At this moment, particulates are predominantly formed from solidified liquid droplets that are expelled from the target by the recoil pressure. As a result, we can observe that the vapour species are grown as a uniform background film. However, if the ambient oxygen pressure increases, the vapour species would face enough collisions so that nucleation and growth of these vapour species to form particulates can occur before they arrive at the substrate. Then, the formation of particulates shifts from

liquid droplets to vapour species. From the time when the growth mechanism changes to diffusion, the resident time of particulate in the vapour control decides the size of the particulate. Consequently, it can be observed that with increasing residence time the particulates are becoming larger.

4.1.4 Structural properties

Figure 4-33 shows the XRD patterns of ZnO films grown on glass substrates at various oxygen pressures. It is clearly observed that ZnO films in the oxygen pressure regime of 5 mTorr to 50 mTorr are completely c-axis oriented in the film's normal direction without any trace of differently aligned planes. Yoo *et al.*[44] indicated that ZnO films usually grow with c-axis preferred orientation under typical growth conditions, which is attributed to the lowest surface energy of the (002) basal plane in ZnO, leading to a preferred growth in the (002) direction.

It can be seen from Figure 4-34 that the peak intensity values of the (002) diffraction orientation are quite similar for the ZnO films grown in an oxygen pressure regime of 5 mTorr to 20 mTorr. However, for the ZnO films grown in the regime of 30 mTorr to 50 mTorr, the intensity of (002) diffraction orientations is extremely low, indicating that the ZnO film grown in higher oxygen pressures has a very low crystalline quality.

As shown in Figure 4-35, the full width at half maximum (FWHM) of the (002) XRD peaks of the ZnO films stays quite low for all the films deposited in the oxygen pressure regime of 5 mTorr to 20 mTorr, but rapidly increases as the oxygen pressure increases up to 30 mTorr. It is well known that the smaller the FWHM, the higher the film crystallinity. Therefore, the result of the FWHM is consistent with that of peak intensity values (002), again supporting the result that the ZnO films deposited above a certain oxygen pressure show a deteriorating crystalline quality.

4.2 Influence of substrate temperature

From section 4.1, it can be concluded that for obtaining higher conductive ZnO film, the relatively optimized oxygen pressure would be 10 mTorr based on Figure 4-28. So, as Table 4-2 shows, using the PLD technique, ZnO films of 10 mTorr oxygen pressure were grown for various substrate temperatures on to glass substrates and their electrical properties, optical properties, morphological and crystal properties were examined.

In the literature [60], the dependence of the film's quality on the growth temperature can be attributed primarily to the mobility of the atoms during the deposition and the growth. At low substrate temperature, vapour species with a low surface energy are arriving on the substrate surface, and these low mobility species in the absence of a thermal diffusion

process further hinder the crystallization of the films. However, at the high substrate temperature, the species have enough mobility to arrange the atoms at suitable positions in the crystalline cell. Additionally, the increase of the growth temperature makes diffused oxygen and zinc atoms increase on the surface, which can lead to a decrease of the oxygen and zinc vacancies. As a result, the density of the defects is reduced and higher crystallinity films are grown.

4.2.1 Electrical properties

As shown in Figure 4-36, the resistivity decreases from 8.63×10^{-2} to 9.01×10^{-3} with a substrate temperature increase from 100°C to 200°C but if the substrate temperature is increased from 200°C to 500°C, the resistivity increases from 9.01×10^{-3} to 4.26×10^{-1} . This result is partially similar to the research from Kang *et al.*[14] (as shown in Figure 4-37) but the result is not similar to Figure 4-37 between 100°C and 200°C. So, it is believed that as the substrate temperature is increased, the number of oxygen atoms absorbed on the thin film will increase, causing a decrease of the defect density. As a result, the carrier concentration declines. Therefore, this result further indicates that when the substrate temperature is increased from 100°C to 500°C, the ZnO films become closer to the stoichiometric composition.

4.2.2 Optical properties

Figure 4-38 shows the transmittance spectra of ZnO films grown at the substrate temperatures of 100°C, 200°C, 300°C, 400°C and 500°C at a fixed oxygen pressure of 10 mTorr. From these transmittance spectra, it can be observed that there is a slight relation between the substrate temperature and the transmittance. At a substrate temperature lower than 100°C, Zn and O₂ molecules could not have enough energy to form stoichiometric ZnO thin films, so we can see the transmittance spectrum of the ZnO film grown at a temperature of 100°C is worse than others. However, the relative higher transmittance of the ZnO film deposited at substrate temperature of 400°C indicates the stoichiometry of the ZnO films has been improved when the substrate temperature increases up to 400°C. But, on increasing the substrate temperature above 400°C, the transmittance of the ZnO film surprisingly decreases. Bae *et al.*[61] indicated that ZnO films grown at 400°C are more stoichiometric than other films deposited above 400°C.

4.2.3 Surface morphology

Figure 4-39 shows the AFM images of the surface morphologies of the ZnO thin films

deposited at various substrate temperatures. In the case of the thin films deposited at 100°C, small grains were observed. However, as the substrate temperature is increased up to 500°C, the surface morphology is observed to consist of larger and more uniform grains. Moreover, the surface roughness is increased from 1 nm to 19 nm with increasing substrate temperature up to 500°C (shown in Figure 4-40). This increase of the surface roughness may be due to the increase of the grain size. This result is also observed in Figure 4-41, which is the FWHM of the (200) XRD peaks from ZnO thin films deposited at various temperatures. It is well known that smaller FWHM value we observe, the larger grain size we obtain.

The growth of grains along the substrate surface is controlled by the substrate temperature which is relative to the surface diffusion ability of atoms[59]; at a substrate temperature of 100°C, the growth of grains along the substrate is limited. As a result, the grain size is small. As the substrate temperature increases up to 200°C, the growth of grain size is enhanced, the films also become relatively compact. However, compared with the grain size of films grown at substrate temperature of 100°C, that of the films grown at substrate temperature of 200°C is relatively larger, which is attributed to grain refinement by recrystallization of the ZnO films at the appropriate temperature (200°C)[62]. When the substrate temperature increases up to 500°C, the high temperature can provide more energy for mobility of particles on the surface. Consequently, the grain size of ZnO thin films is larger at 500°C than at lower temperatures.

4.2.4 Structural properties

Figure 4-42 indicates the XRD pattern for the ZnO films deposited at various substrate temperatures. As shown in Figure 4-42, only the (002) diffraction peaks were observed. This indicated that the ZnO films have a c-axis preferred orientation perpendicular to the substrate surface, and this result can be explained by the fact that, in the case of the ZnO films having a wurtzite hexagonal crystal structure, the (002) plane has the lowest surface energy density [63]. Moreover, Figure 4-43 further indicates, the ZnO thin film deposited at 100°C shows a relatively low (002) diffraction peak. This is attributed to the low atomic mobility, which limits the crystal growth during the crystallization process. However, as the substrate temperature increases up to 500°C, there is enough thermal energy to supply to atoms on the substrate, which increases the surface mobility. As a result, it leads to an increased peak intensity in the (002) plane orientation (shown in Figure 4-43).

4.3 Influence of annealing

From section 4.1 and 4.2, we can obviously see that the relatively optimized deposition

parameters are $D=55\text{mm}$, $P_{O_2}=10\text{mTorr}$, $T_s=200^\circ\text{C}$. In this section, we examine the effect of post-growth annealing (for 2 hours) of ZnO thin films on the structural as well as electrical properties in order to find a new way to improve the various properties of ZnO thin films. The detailed parameters are shown in Table 4-3.

4.3.1 Electrical properties

Figure 4-44 shows the resistivity of the ZnO films as a function of annealing temperature. For annealing temperature $< 300^\circ\text{C}$, it is observed that the resistivity of the ZnO films decreases slightly. As the annealing temperature increases up to 500°C , the resistivity of the ZnO films increases dramatically. This result is similar to the result of Kang *et al.* [64] and Stamataki *et al.* [65], so we probably could attribute this phenomenon to the decline of the carrier concentration as the annealing temperature increases. Additionally, Kang *et al.* [64] and Stamataki *et al.* [65] believe that this is because the number of Zn interstitials decreases probably due to Zn evaporation by increasing annealing temperature, or the oxygen vacancies, which contribute the free carriers, declined by oxygen diffusion into the film with annealing treatment.

4.3.2 Optical properties

Figure 4-45 shows the optical transmittance in the wavelength range of 300-1000 nm of the as-deposited and post-growth annealed ZnO films deposited on glass substrates as a function of annealing temperature. The ZnO films show a slight increase of transmittance with annealing temperature, which probably indicates that the annealing treatment could slightly improve the crystallinity (see Figure 4-46). This also further confirms the Rusop *et al.* research [66] that higher transmittance in the visible region indicates that the films have fewer defects and better crystallinity. However, the difference of transmittance with different annealing temperature is not significant, so we need to do more experiments to confirm this result, even taking account of experimental errors.

4.3.3 Surface morphology

Figure 4-47 shows the AFM images of as-grown and annealed samples at various temperatures for 2h in oxygen, and Figure 4-48 illustrates the SEM images of as-grown and annealed samples for 2h at 500°C in oxygen. It is clearly observed that the morphology was improved by annealing at 500°C and the needle-like shape was observed in Figure 4-48b-annealed sample. Furthermore, this result also can be observed in Figure 4-49 which shows the roughness of ZnO films deposited at various annealing

temperatures. Therefore, we probably can deduce that the quality of ZnO thin films was improved by the re-crystallization of ZnO thin film by supplying sufficient thermal energy.

4.3.4 Structural properties

Figure 4-51 shows XRD patterns of ZnO films deposited by PLD on glass substrates at 200°C with ambient oxygen (as-deposited), and ZnO films post-growth annealed at various annealing temperatures. It is clearly observed that a (002) textured film is formed in an effective equilibrium state which gives enough surface mobility to impinge atoms. Even after the annealing treatment, the peak of diffraction (002) is still the only observed peak. Moreover, as shown in Figure 4-46, the peak intensity of ZnO thin films with annealing treatment is relatively higher than that of the as-deposited thin film. So, we probably can conclude that the post-annealing treatment of the films has a positive effect on the crystallization. Sun *et al.*[67] explained that high temperature could enhance the diffuse activation energy of the surface, as a result the Zn and O atoms occupy the correct site in the crystal lattice and grains with the lower surface energy will become larger at a high temperature.

4.4 Influence of the number of pulses on ZnO films

Table 4-5 shows that ZnO thin films were deposited on glass substrates with various thicknesses using the pulsed-laser deposition (PLD) technique in order to investigate the thickness dependence of the structural, electrical and optical properties of the films. The thickness of thin films is controlled by changing the number of pulses, and the structural, electrical and optical properties were characterized with XRD, resistance and transmittance measurement.

4.4.1 Structural properties

Figure 4-51 shows the XRD spectra of ZnO thin films deposited at the various number of laser pulses. Only (002) ZnO peaks were observed in the range 34°-35°, and it also further indicated that ZnO thin films deposited on glass substrates with various thicknesses are still strongly c-axis oriented. Additionally, as shown in Figure 4-52, the crystal quality of the ZnO films is enhanced with an increase in the number of laser pulses, from 5000 to 15000. However, when the number of laser pulses increases up to 20000, the crystal quality of ZnO films starts to degrade.

4.4.2 Optical properties

The transmittance spectra as a function of wavelength in the range 300-800 nm for three samples are shown in Figure 4-53. The average transmittance in the visible region for the number of pulses of 5000, 15000 and 20000 is 79 %, 65 % and 64 % respectively. With increase of thickness, the transmittance of ZnO thin films decreases due to the thickness effect. That the increase in thickness affects the optical properties can be explained by the Lambert-Beer Law [59], which can be expressed: $I/I_0 = \exp(-\alpha t)$, where I is the light intensity at a distance t into medium; α is the absorption coefficient of the material; I_0 is the incoming light intensity. Therefore, when the number of laser pulses or thickness of ZnO, increases, the transmittance accordingly decreases.

4.4.3 Electrical properties

Figure 4-54 shows the resistivity of ZnO thin films deposited at the various number of laser pulses. The observed resistivity decreased significantly with increasing thickness from 315 nm to 895 nm, but leveled off as the thickness increased over 895 nm. E.S Shim *et al.* [2] Indicated that the correlation between thickness and resistivity of ZnO thin films is negative due to the thicker films having fewer point defects like oxygen vacancies. Moreover, the conductivity of ZnO thin films can probably be attributed to oxygen vacancies and Zn interstitials which are donor type point defects. Therefore, the enhancement of the defects leads to the rise of carrier concentration. On the contrary, the decrease of defects with increase of the thickness of ZnO thin films causes the decline of carrier concentration, or the increase of resistivity.

4.5 Influence of laser fluence on ZnO films

To investigate the influence of laser energy density on the process parameters of ZnO films, a series of depositions were performed as follows: at a fixed oxygen pressure of 10 mTorr and a fixed substrate temperature of 200 °C; laser energy density was varied in the range from 1.16 J/cm² to 2.73 J/cm²; the target-substrate distance was kept at 55mm and the glass substrates were used for all samples. The detailed information is shown in Table 4 -4.

After deposition, the crystal structure of the film was investigated by X-ray diffraction (XRD) and the resistivity measured by four-point probe. The morphology of the film was studied using a JEOL scanning electron microscope (SEM).

4.5.1 Structural properties

The XRD spectra of ZnO films deposited at various laser fluences is shown in Figure 4-55. It can be observed that all films are c-axis oriented, exhibiting only (002) XRD diffraction. The peak intensity of the (002) diffraction of ZnO films deposited at various laser fluences, increases with increase of laser fluence, from 1.16 J/cm² to 2.27 J/cm². However, when the laser fluence increased up to 2.73 J/cm², the intensity of the (002) diffraction decreases dramatically (shown in Figure 4-56). The low laser fluence is related to the low kinetic energy of the species and it also leads to island growth.[55] Conversely, too high a laser fluence causes a degradation of the crystallinity of ZnO films through the bombardment of the growing film by energetic species.

4.5.2 Electrical properties

Figure 4-57 shows that the resistivity of ZnO thin films declines with increasing laser fluence up to 1.51 J/cm². However, at higher fluences up to 2.27 J/cm², the resistivity dramatically increases. The relatively low resistivity of the ZnO thin films of $3.1 \times 10^{-3} \Omega \text{ cm}$ is found at the laser fluence of 1.51 J/cm². From the particle energy point of view, with the increase of kinetic energy from raising the laser fluence, the ejected species cause some structural damage to the growing film reducing the mobility of free carriers. Thus, this is the reason why the increasing laser fluence increases the resistivity of ZnO thin film [55].

4.5.3 Optical properties

Figure 4-58 shows the optical transmittance spectrum of ZnO thin films which are deposited on glass substrates with the various laser fluences. It can be seen that the optical transmittance increases with increase of laser fluence, from 1.16 J/cm² to 2.27 J/cm² in the range of wavelength of 350 nm to 450 nm. However, as the laser fluence increases up to 2.73 J/cm², the optical transmittance significantly declines. If the thin film is deposited under too much laser fluence, it causes a degradation of optical properties of ZnO films due to the bombardment of the growing film by energetic species [55].

4.6 Influence of doping with silicon

According to previous research [68-70], it is well known that pure zinc oxide films usually exhibit high resistivity due to low carrier concentration. The electrical resistivity (ρ) of ZnO films depends on the carrier concentration (N) and carrier mobility (μ) as follows: $\rho = 1/(\mu N e)$, where e is the electron charge. Since e is a constant, to achieve lower resistivity of ZnO films, we should increase either the carrier concentration or the carrier mobility in ZnO films. For the purpose of increasing the carrier concentration, it can be achieved through oxygen or zinc non-stoichiometry and doping with an impurity.

Therefore, in this section, for studying the influence of doping with an impurity, we used a new target which is 2 wt % Si-doped ZnO to deposit new films to investigate the effect on electrical properties, optical properties and structural properties.

4.6.1 Electrical and optical properties

Figure 4-59 shows the difference of resistivity and carrier concentration between pure ZnO thin film and 2 wt% Si-doped ZnO thin film. The former is deposited under the relatively optimized parameters based on the result of sections 4.1 and 4.2 while 2 wt% Si-doped ZnO thin films are deposited under substrate temperature of 200°C, oxygen pressure of 5mTorr and laser fluence of 2.7 J/cm². Consequently, as shown in Figure 4-59, it is evidently observed that the carrier concentration increases with content of SiO₂, which also causes a decrease in the resistivity. This phenomenon could be explained by the amount of silicon which was introduced into the film; it is ionized to Si⁺⁴, normally replacing Zn⁺², with two electrons produced for each zinc atom replacement. Therefore, the resistivity of thin films should decrease significantly due to increase of the carrier concentration, from 9x10⁻³ Ω cm to 7x10⁻⁴ Ω cm.

Figure 4-60 shows optical absorption spectra of a pure ZnO thin film and a 2 wt% Si-doped ZnO film measured at room temperature. The pure ZnO thin film shows a sharp absorption edge at 3.25eV (Figure 4-60) while that of the 2wt% Si-doped ZnO thin film shifts to the higher energy of 3.5eV. Moreover, the absorption edge of the 2 wt% Si-doped ZnO thin film is less sharp than that of the pure ZnO thin film due to silicon states extending into the band gap (Figure 4-60). The shifted absorption edge and the development of states within the gap are indications that the Si ions have entered into the ZnO lattice. This characteristic has also been observed in Mn-doped ZnO thin films fabricated by pulsed laser deposition [71]. But, that of Si-doped ZnO fabricated by PLD presents another story [72]. As the Si was incorporated, the band gap shifted to lower energy. Therefore, from the above discussion, it can be seen that different doped

materials have different characteristics. However, Yoo *et al.* [72] also suggested that the reason for this phenomenon is still under dispute.

4.6.2 Structural properties

The crystalline structure of the pure ZnO thin film and the Si-ZnO (2 wt% silicon) thin film was investigated by X-Ray diffraction. Figure 4-61 shows the x-ray diffraction patterns for the undoped ZnO thin film, and it shows a discrete pattern with evidence of only the (002) peak, while the x-ray diffraction pattern for the Si-ZnO (2 wt% silicon) revealed a not very sharp diffraction peak at (002) orientation. This probably indicates that to dope ZnO thin films with silicon deteriorates the crystallinity of films due to the formation of stress by the difference in ionic size between zinc and the dopant [45]. However, in both thin films only diffraction peaks with (002) orientation can be observed and this result indicates that the Si-ZnO (2 wt% silicon) thin film and the pure ZnO thin film were strongly orientated with the c-axis perpendicular to the glass substrate plane.

5 Conclusions

5.1 Conclusions

The main PLD growth parameters, i.e. the oxygen pressure, the substrate temperatures, the laser fluence and the number of pulses were varied one by one. The effect of each parameter on the physical and structural properties were investigated and explained. Furthermore, the physical properties of the ZnO thin films were also optimized.

Initially, for obtaining the optimized oxygen pressures all parameters were kept at the same level except oxygen pressure. As a result, we found that the ambient oxygen pressure is sensitive relative to the electrical resistivity of ZnO films because of mobility of species and stoichiometry effects. As the oxygen pressure increases, the electron concentration tends to decrease while the resistivity of the film increases, being associated with a decrease in the density of oxygen vacancies as shallow donors; this also is a sign that the ZnO film approaches an improved stoichiometry with an increase in oxygen supply. Thus, for achieving low resistivity of ZnO films, the supply of the ambient oxygen pressure would be at around 10 mTorr, and the relative lower resistivity is $1.89 \times 10^{-2} \Omega \text{ cm}$. But a high transmittance of 91 % can be achieved at the ambient oxygen pressure of 50 mTorr. This result indicates that one important quality of the UV emission may be the stoichiometry of the ZnO which usually has many oxygen vacancies in its lattice. It is thus expected that the ZnO film grown at higher oxygen pressure of 50 mTorr probably has more improved stoichiometry with fewer oxygen vacancies.

From the above discussion, it can be concluded that for obtaining a more highly conductive ZnO film, a relatively optimized oxygen pressure would be 10 mTorr. So, as Table 4-2 shows, using the PLD technique, ZnO films of 10 mTorr oxygen pressure were grown for various substrate temperatures on to glass substrates and the effect of the substrate temperatures were investigated. The resistivity decreases from 8×10^{-2} to $9 \times 10^{-3} \Omega \text{ cm}$ with substrate temperature increase from 100°C to 200°C but on increasing the substrate temperature from 200°C to 500°C, the resistivity increases from 9×10^{-3} to $4 \times 10^{-1} \Omega \text{ cm}$, It is believed that as the substrate temperature increases, the number of oxygen atoms absorbed on the thin film will increase, causing a decrease of the defect density. So the optimized substrate temperature for obtaining lower resistivity of ZnO thin films would be at substrate temperature of 200°C, which is $9 \times 10^{-3} \Omega \text{ cm}$ and the average transmittance is 80 % in the visible region.

After discussing the effect of oxygen pressures and the substrate temperatures, we

obtained the relatively optimized deposition parameters as $P_{O_2}=10\text{mTorr}$, $T_s=200^\circ\text{C}$. However, for further improving the electrical properties, we examined the effect of post-growth annealing (for 2 hours) of ZnO thin films on the structural as well as electrical properties. For annealing temperature $< 300^\circ$, it is observed that the resistivity of the ZnO films decreases slightly. So, the resistivity improves to $7\times 10^{-3}\ \Omega\ \text{cm}$ and transmittance still remains at the same level. Furthermore, it can be observed that the post-annealing treatment of the films has a positive effect on the crystallization.

For achieving high conductivity ZnO thin films, we turned to study the next parameter, the value of laser fluence. The result shows that the resistivity of ZnO thin films decreases with increasing laser fluence up to $1.51\text{J}/\text{cm}^2$. However, at higher fluences up to $2.27\text{J}/\text{cm}^2$, the resistivity dramatically increases. The relatively low resistivity of the ZnO thin films of $3\times 10^{-3}\ \Omega\ \text{cm}$ is found at the laser fluence of $1.51\text{J}/\text{cm}^2$, and the average transmittance is 82 % in the visible region..

Finally, summarizing all the results, we can conclude that the optimized parameters are: oxygen pressure of 10 mTorr, substrate temperature of 200°C and laser fluence of $1.51\ \text{J}/\text{cm}^2$, and we can obtain the relative lower resistivity of $3\times 10^{-3}\ \Omega\ \text{cm}$ and the transmittance is 85 % at light wavelength of 625 nm. But, this result compared to ITO thin films (resistivity= $1\times 10^{-4}\ \Omega\ \text{cm}$) is still not enough to replace the ITO in flat-panel display and solar energy applications. Therefore, thin films were deposited from a 2 wt% Si - ZnO target, and then the physical properties were investigated. As a result, it is evidently observed that the carrier concentration increases with content of SiO_2 , which also causes the decrease of the resistivity. This phenomenon could be explained by the amount of silicon which was introduced into film, it is ionized to Si^{+4} , normally replacing Zn^{+2} , with two electrons produced for each zinc atom replaced. Therefore, the resistivity of thin films should decrease significantly from $3\times 10^{-3}\ \Omega\ \text{cm}$ to $6\times 10^{-4}\ \Omega\ \text{cm}$ due to the increase of the carrier concentration,. Furthermore, the introduced 2 wt% silicon causes the absorption edge of the 2 wt% Si-doped ZnO thin film to be less sharp than that of the pure ZnO thin film and the sharp absorption edge of pure ZnO thin films of 3.25eV was shifted to that of the 2 wt% Si-doped ZnO thin film of 3.5eV due to silicon states extending into the band gap. On the other hand, the average transmittance increases to 85% in the visible region due to doping with 2 wt% silicon.

6 Future work

In order to obtain the optimized parameters of ZnO thin films, the influence of oxygen pressure, substrate temperature, the numbers of pulses, annealing treatment and laser fluence have been studied. However, the influence of the number of pulses on resistivity is not very clear, and further work is needed to use 1000 pulses, 2000 pulses, and 3000 pulses and up to 5000 pulses. Also the laser energy as the pulses increase up to 5000 pulses should be measured because the laser energy may decrease with rise of laser pulses.

In section 4.6, although the Si-doped ZnO has been investigated, and the resistivity also improved, the resistivity of ITO is still lower than the optimized 2wt% Si-doped ZnO thin film (ITO: $1\sim 2\times 10^{-4}\Omega\text{cm}$ vs. 2wt%Si-ZnO: $7\times 10^{-4}\Omega\text{cm}$). In order to attain the high potential offered by ZnO, both high-quality n- and p-type ZnO are indispensable. However, ZnO is easily doped to n-type, while p-type is difficult [73]. Thus, the future work can be categorized into two projects:

A. n-type doping

Group-III elements, such as Al, Ga and In, and Group-IV elements (Ge, Ti and Zr) as substitutional elements for Zn and Group-VII elements Cl and I as substitutional elements for O can be used as n-type dopants [74]. Doping with Al, Ga and In has been attempted by many groups, resulting in high-quality conductive n-type ZnO films. For example, Ataev *et al.* reported resistivity as low as $1\times 10^{-4}\Omega\text{cm}$ for Ga-doped ZnO films grown by chemical-vapour deposition, which is quite close to the electrical properties of ITO. While group-IV and group VII elements have been widely investigated, and that is a future potential project.

B. p-type doping

For obtaining p-type ZnO, known acceptors in ZnO include group-I element such as lithium (Li)[75, 76], Na and K, copper (Cu) [77], silver (Ag)[78], Zn vacancies, and group-V elements such as N, P, and As. However, among those acceptors, only Group-V elements are believed as the most promising dopants for p-type ZnO [77]. On the other hand, p-type doping still needs exploring.

7 References

1. Bae, S.H., et al., *Effects of post-annealing treatment on the light emission properties of ZnO thin films on Si*. Optical Materials. ,2001, **17**(1-2): p. 327-330.
2. Shim, E.S., et al., *Effect of the variation of film thickness on the structural and optical properties of ZnO thin films deposited on sapphire substrate using PLD*. Applied Surface Science, 2002. **186**(1-4): p. 474-476.
3. Bagnall, D.M., et al., *Optically pumped lasing of ZnO at room temperature*. Applied Physics Letters, 1997. **70**(17): p. 2230-2232.
4. Service, R.F., *Materials Science: Will UV Lasers Beat the Blues?* Science, 1997. **276**(5314): p. 895-.
5. Ondo-Ndong, R., et al., *Properties of RF magnetron sputtered zinc oxide thin films*. Journal of Crystal Growth, 2003. **255**(1-2): p. 130-135.
6. Ono, S., et al., *SAW resonators using rf-sputtered ZnO films on glass substrates*. Applied Physics Letters, 1978. **33**(3): p. 217-218.
7. Tiku, S.K., C.K. Lau, and K.M. Lakin, *Chemical vapor deposition of ZnO epitaxial films on sapphire*. Applied Physics Letters, 1980. **36**(4): p. 318-320.
8. Li, B.S., et al., *High quality ZnO thin films grown by plasma enhanced chemical vapor deposition*. Journal of Applied Physics, 2002. **91**(1): p. 501-505.
9. OHRING, M., *Materials science of thin films*. 1991.
10. J.L. Vossen, in G. Hass, M.H. Francombe and R.W. Hoffmann (eds.), **Physics of Thin Films**, Academic Press, New York, **1977**, p. **1**.
11. Ma, Y., et al., *Control of conductivity type in undoped ZnO thin films grown by metalorganic vapor phase epitaxy*. Journal of Applied Physics, 2004. **95**(11): p. 6268-6272.
12. Kumar, M., et al., *Epitaxial growth of high quality ZnO:Al film on silicon with a thin gamma-Al₂O₃ buffer layer*. Journal of Applied Physics, 2003. **93**(7): p. 3837-3843.
13. Bian, J.M., et al., *Deposition and electrical properties of N--In codoped p-type ZnO films by ultrasonic spray pyrolysis*. Applied Physics Letters, 2004. **84**(4): p. 541-543.
14. Kang, S., et al., *Effect of substrate temperature on structural, optical and electrical properties of ZnO thin films deposited by pulsed laser deposition*. Journal of Materials Science: Materials in Electronics, 2008. **19**(11): p. 1073-1078.
15. Hu, W.S., et al., *OPTICAL PROPERTIES OF PULSED LASER DEPOSITED ZnO THIN FILMS*. Journal of Physics and Chemistry of Solids, 1997. **58**(6): p. 853-857.
16. Badeker, *Electrical Conductivity and Thermo-Electromotive Force of Some Metallic Compounds*, Ann. Phys.(Leipzig), 1907. **22**(1907): p. 749.
17. Kaminska, E., et al., *Transparent p-type ZnO films obtained by oxidation of*

- sputter-deposited Zn₃N₂*. Solid State Communications, 2005. **135**(1-2): p. 11-15.
18. Eason, R., PULSED LASER DEPOSITION OF THIN FILMS. 2007: WILEY-INTERSCIENCE, New York.
 19. Hu, J. and R.G. Gordon, *Textured aluminum-doped zinc oxide thin films from atmospheric pressure chemical-vapor deposition*. Journal of Applied Physics, 1992. **71**(2): p. 880-890.
 20. Johnson, V.A. and K. Lark-Horovitz, *Theory of Thermoelectric Power in Semiconductors with Applications to Germanium*. Physical Review, 1953. **92**(2): p. 226.
 21. William D. Callister, J., *Fundamentals of materials science and engineering. Fifth edition ed.* 2000: John Wiley & Sons, Inc, New York.
 22. Srikant, V. and D.R. Clarke, *On the optical band gap of zinc oxide*. Journal of Applied Physics, 1998. **83**(10): p. 5447-5451.
 23. Chopra, K.L., S. Major, and D.K. Pandya, *Transparent conductors--A status review*. Thin Solid Films, 1983. **102**(1): p. 1-46.
 24. Tauc, J., R. Grigorovici, and A. Vancu, *Optical Properties and Electronic Structure of Amorphous Germanium*. physica status solidi (b), 1966. **15**(2): p. 627-637.
 25. Lide, D.R., *Handbook of Chemistry and Physics* 71st edn ed ed. 1991: CRC, Boca Raton, FL
 26. Göpel, W. and U. Lampe, *Influence of defects on the electronic structure of zinc oxide surfaces*. Physical Review B, 1980. **22**(12): p. 6447.
 27. Minami, T., H. Nanto, and S. Takata, *Highly Conductive and Transparent Aluminum Doped Zinc Oxide Thin Films Prepared by RF Magnetron Sputtering*. Japanese Journal of Applied Physics. **23**(Part 2, No. 1): p. L280.
 28. Igasaki, Y. and H. Saito, *The effects of deposition rate on the structural and electrical properties of ZnO:Al films deposited on (112-bar 0) oriented sapphire substrates*. Journal of Applied Physics, 1991. **70**(7): p. 3613-3619.
 29. Minami, T., et al., *Group III Impurity Doped Zinc Oxide Thin Films Prepared by RF Magnetron Sputtering*. Japanese Journal of Applied Physics. **24**(Part 2, No. 10): p. L781.
 30. Kim, H., et al., *Effect of aluminum doping on zinc oxide thin films grown by pulsed laser deposition for organic light-emitting devices*. Thin Solid Films, 2000. **377-378**: p. 798-802.
 31. Kim, H., et al., *Indium tin oxide thin films for organic light-emitting devices*. Applied Physics Letters, 1999. **74**(23): p. 3444-3446.
 32. Kim, H., et al., *Electrical, optical, and structural properties of indium--tin--oxide thin films for organic light-emitting devices*. Journal of Applied Physics, 1999. **86**(11): p. 6451-6461.
 33. Kim, H., et al., *Electrical and optical properties of indium tin oxide thin films grown by pulsed laser deposition*. Applied Physics A: Materials Science & Processing, 1999. **69**(7):

- p. S447-S450.
34. Kim, H., et al., *Epitaxial growth of Al-doped ZnO thin films grown by pulsed laser deposition*. Thin Solid Films, 2002. **420-421**: p. 107-111.
 35. Lv, M., et al., *Structural, electrical and optical properties of zirconium-doped zinc oxide films prepared by radio frequency magnetron sputtering*. Thin Solid Films, 2008. **516**(8): p. 2017-2021.
 36. Li, S.Y., et al., *Effect of Sn dopant on the properties of ZnO nanowires*. Journal of Physics D: Applied Physics, 2004. **37**(16): p. 2274-2282.
 37. Markov, V.A., et al., *Molecular beam epitaxy with synchronization of nucleation*. Surface Science, 1991. **250**(1-3): p. 229-234.
 38. E. Bauer, Z.K., *Phänomenologische Theorie der Kristallabscheidung an Oberflächen*, 1958. **110**: p. 372.
 39. Chen, K.R., et al., *Mechanisms affecting kinetic energies of laser-ablated materials*. in *The 42nd national symposium of the American Vacuum Society*. 1996. Mineapolis, Minnesota (USA): AVS.
 40. Belouet, C., *Thin film growth by the pulsed laser assisted deposition technique*. Applied Surface Science, 1996. **96-98**: p. 630-642.
 41. Jackson, T.J. and S.B. Palmer, *Oxide superconductor and magnetic metal thin film deposition by pulsed laser ablation: a review*. Journal of Physics D: Applied Physics, 1994. **27**(8): p. 1581-1594.
 42. Cho, A.Y., *Film Deposition by Molecular-Beam Techniques*. Journal of Vacuum Science and Technology, 1971. **8**(5): p. S31-S38.
 43. Alivov, Y., M. Chukichev, and V. Nikitenko, *Green luminescence band of zinc oxide films copper-doped by thermal diffusion*. Semiconductors, 2004. **38**(1): p. 31-35.
 44. Yoo, Y.Z., et al., *High temperature growth of ZnS films on bare Si and transformation of ZnS to ZnO by thermal oxidation*. Applied Physics Letters, 2001. **78**(5): p. 616-618.
 45. Lee, J.-H. and B.-O. Park, *Transparent conducting ZnO:Al, In and Sn thin films deposited by the sol-gel method*. Thin Solid Films, 2003. **426**(1-2): p. 94-99.
 46. Huang, Y.-C., et al., *Characterizations of gallium-doped ZnO films on glass substrate prepared by atmospheric pressure metal-organic chemical vapor deposition*. Thin Solid Films. **In Press, Corrected Proof**.
 47. Masuda, S., et al., *Transparent thin film transistors using ZnO as an active channel layer and their electrical properties*. Journal of Applied Physics, 2003. **93**(3): p. 1624-1630.
 48. Xiao, R.F., et al., *Growth of c-axis oriented gallium nitride thin films on an amorphous substrate by the liquid-target pulsed laser deposition technique*. Journal of Applied Physics, 1996. **80**(7): p. 4226-4228.
 49. **PI-KEM_LTD**, Unit 20 Tame Valley Business Centre Tilley, Magnus, Tamworth, Staffordshire. B77 5BY. UK.

50. Corning_Incorporated, Corning Incorporated One Riverfront Plaza Corning, NY 14831 USA
51. **Scientific_Ltd., A.**, Unit 7, M11 Business Link Parsonage Lane Stansted Essex CM24 8GF England
52. Hartnagel, *Semiconducting Transparent Thin Films*,. 1995: Hartnagel .Limited, B.S.
53. Cullity, B.D., *Elements of x-ray diffraction*. Addison Wesley Publishing Company, 2001, USA.
54. Triboulet, R. and J. Perri re, *Epitaxial growth of ZnO films*. Progress in Crystal Growth and Characterization of Materials, 2003. **47**(2-3): p. 65-138.
55. Jin, B.J., et al., *Effects of native defects on optical and electrical properties of ZnO prepared by pulsed laser deposition*. Materials Science and Engineering B, 2000. **71**(1-3): p. 301-305.
56. Zhang, Z.G., et al., *Effects of oxygen pressures on pulsed laser deposition of ZnO films*. Physica E: Low-dimensional Systems and Nanostructures, 2007. **39**(2): p. 253-257.
57. Zheng, J.P. and H.S. Kwok, *Low resistivity indium tin oxide films by pulsed laser deposition*. Applied Physics Letters, 1993. **63**(1): p. 1-3.
58. Hubler, D.B.C.a.G.K., *Pulsed Laser Deposition of Thin Films*. May 2003, New York: Wiley.
59. Suche, M., et al., *Structural and morphological properties of thin ZnO films grown by pulsed laser deposition*. Applied Surface Science, 2008. **254**(17): p. 5475-5480.
60. Bae, S.H., et al., *Growth and characterization of ZnO thin films grown by pulsed laser deposition*. Applied Surface Science, 2001. **169-170**: p. 525-528.
61. Zhu, B.L., et al., *The effects of substrate temperature on the structure and properties of ZnO films prepared by pulsed laser deposition*. Vacuum, 2008. **82**(5): p. 495-500.
62. Fujimura, N., et al., *Control of preferred orientation for ZnOx films: control of self-texture*. Journal of Crystal Growth, 1993. **130**(1-2): p. 269-279.
63. Kang, H.S., et al., *Annealing effect on the property of ultraviolet and green emissions of ZnO thin films*. Journal of Applied Physics, 2004. **95**(3): p. 1246-1250.
64. Stamataki, M., et al., *Annealing effects on the structural, electrical and H2 sensing properties of transparent ZnO thin films, grown by Pulsed Laser Deposition*. Thin Solid Films. **In Press, Accepted Manuscript**.
65. Rusop, M., et al., *Post-growth annealing of zinc oxide thin films pulsed laser deposited under enhanced oxygen pressure on quartz and silicon substrates*. Materials Science and Engineering: B, 2006. **127**(2-3): p. 150-153.
66. Sun, J., et al., *Influence of annealing atmosphere on ZnO thin films grown by MOCVD*. Applied Surface Science, 2006. **253**(4): p. 2066-2070.
67. Zhao, J.-L., et al., *Structural, optical and electrical properties of ZnO films grown by pulsed laser deposition (PLD)*. Journal of Crystal Growth, 2005. **276**(3-4): p. 507-512.
68. Zeng, J.N., et al., *Effect of deposition conditions on optical and electrical properties of*

- ZnO films prepared by pulsed laser deposition*. Applied Surface Science, 2002. **197-198**: p. 362-367.
69. Grundmann, M., et al., *Electrical properties of ZnO thin films and optical properties of ZnO-based nanostructures*. Superlattices and Microstructures, 2005. **38**(4-6): p. 317-328.
 70. Cheng, X.M. and C.L. Chien, *Magnetic properties of epitaxial Mn-doped ZnO thin films*. Journal of Applied Physics, 2003. **93**(10): p. 7876-7878.
 71. Yoo, Y.Z., et al., *S doping in ZnO film by supplying ZnS species with pulsed-laser-deposition method*. Applied Physics Letters, 2002. **81**(20): p. 3798-3800.
 72. Neumark, G.F., *Achievement of well conducting wide band-gap semiconductors: Role of solubility and of nonequilibrium impurity incorporation*. Physical Review Letters, 1989. **62**(15): p. 1800.
 73. Kato, H., et al., *Growth and characterization of Ga-doped ZnO layers on a-plane sapphire substrates grown by molecular beam epitaxy*. Journal of Crystal Growth, 2002. **237-239**(Part 1): p. 538-543.
 74. Schirmer, O.F., *The structure of the paramagnetic lithium center in zinc oxide and beryllium oxide*. Journal of Physics and Chemistry of Solids, 1968. **29**(8): p. 1407-1429.
 75. Valentini, A., et al., *Preparation and characterization of Li-doped ZnO films*. Journal of Vacuum Science & Technology A: Vacuum, Surfaces, and Films, 1991. **9**(2): p. 286-289.
 76. Kanai, Y., *Admittance Spectroscopy of Cu-Doped ZnO Crystals*. Japanese Journal of Applied Physics. **30**(Part 1, No. 4): p. 703.
 77. Kanai, Y., *Admittance Spectroscopy of ZnO Crystals Containing Ag*. Japanese Journal of Applied Physics. **30**(Part 1, No. 9A): p. 2021.
 78. Ozerov, I., et al., *Production of gas phase zinc oxide nanoclusters by pulsed laser ablation*. Applied Surface Science, 2005. **247**(1-4): p. 1-7.
 79. Jin, B.J., S. Im, and S.Y. Lee, *Violet and UV luminescence emitted from ZnO thin films grown on sapphire by pulsed laser deposition*. Thin Solid Films, 2000. **366**(1-2): p. 107-110.

Appendix

Figures and tables from Chapter 2

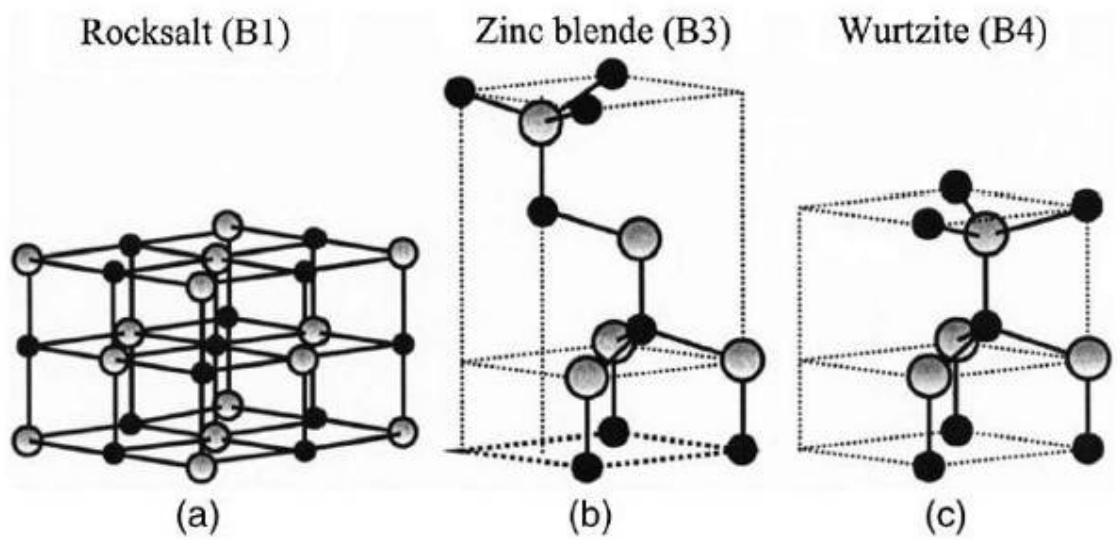


Figure 2-1 Stick and ball representation of ZnO crystal structures: (a) cubic rock-salt(B1), (b) cubic zinc blend (B3), and (c) hexagonal wurztie (B4). The shaded gray and black spheres denote Zn and O atoms, respectively.[79]

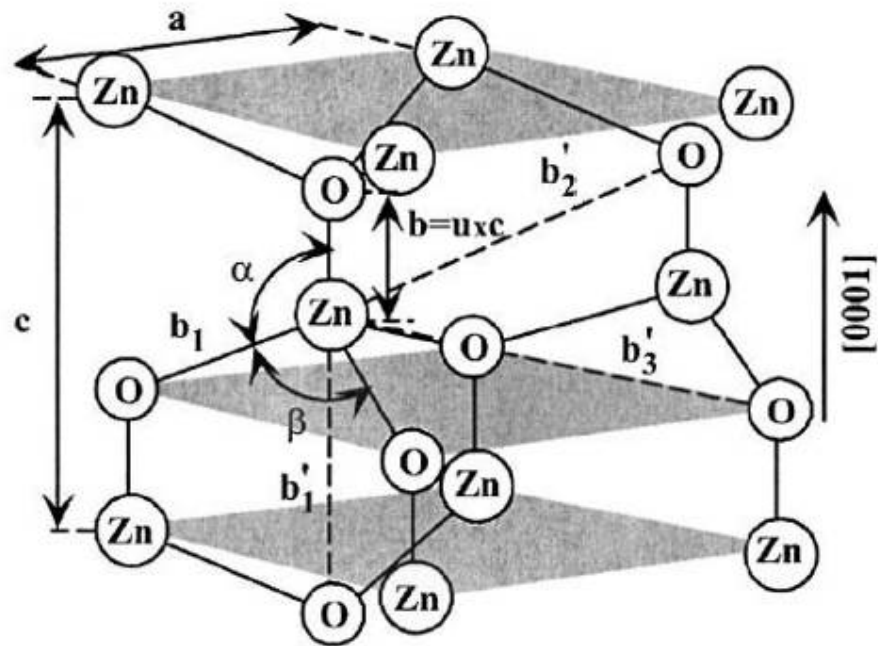


Figure 2-2 Schematic representation of a wurtzitic ZnO structure having lattice constant a in the basal plane and c in the basal direction; u parameter is expressed as the bond length or the nearest-neighbor distant b divided by c (0.375 in ideal crystal), and α and β (109.47° in ideal crystal) are the bond angles.[79]

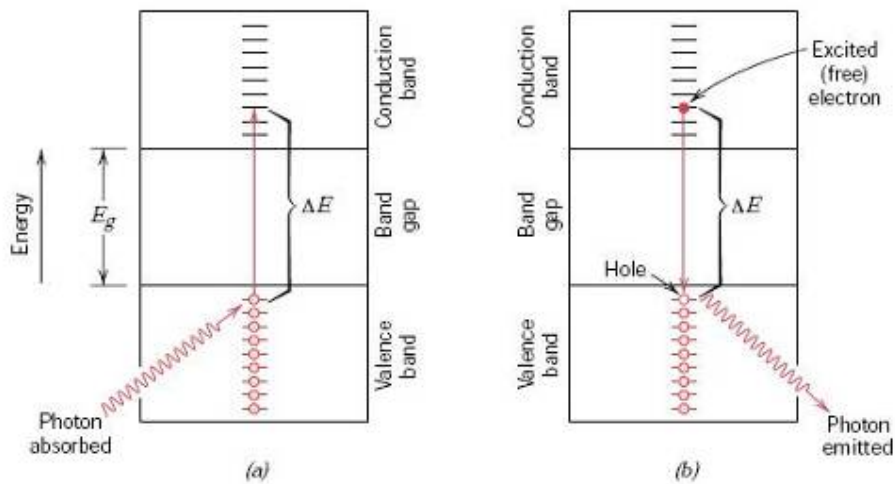


Figure 2-3 (a) Mechanism of photon absorption for non-metallic materials in which an electron is excited across the band gap, leaving behind a hole in the valence band. The energy of the photon absorbed is ΔE , which is necessarily greater than the band gap energy E_g . (b) Emission of a photon of light by a direct electron transition across the band gap. [21]

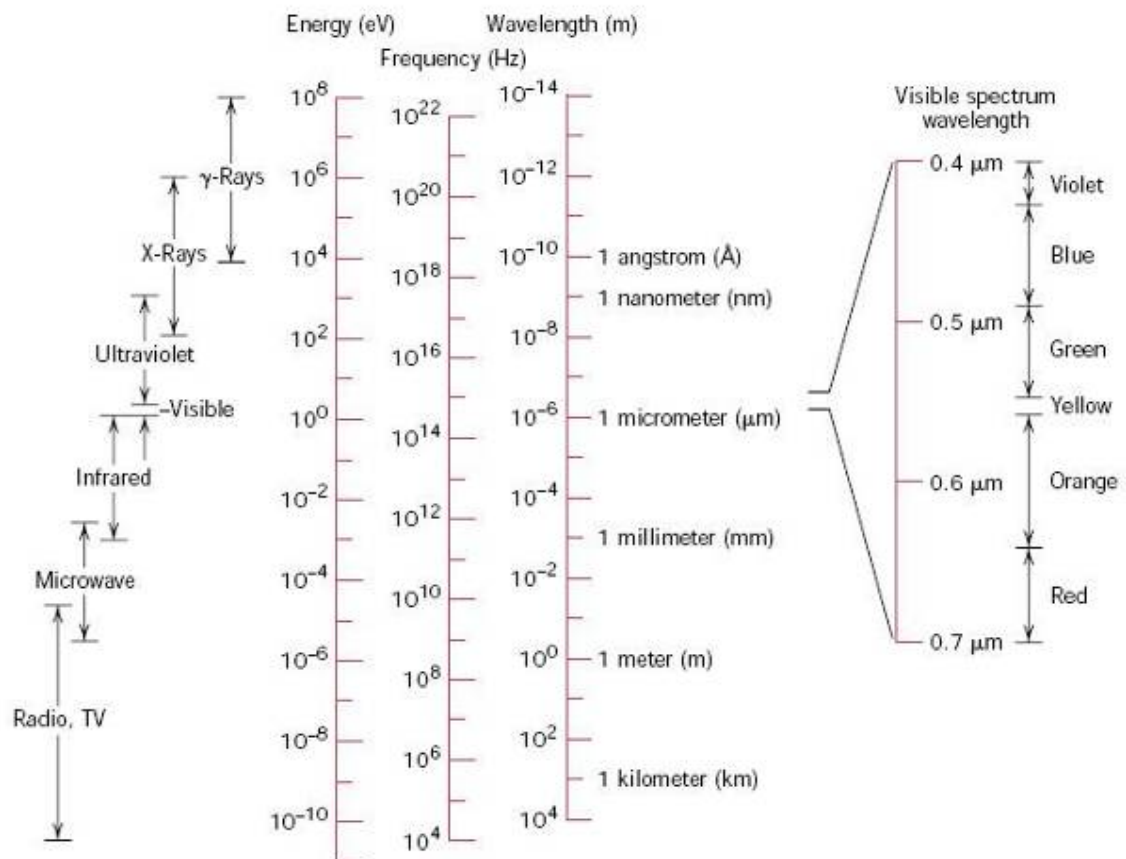


Figure 2-4 The spectrum of electromagnetic radiation, including wavelength ranges for the various colors in the visible

spectrum.[21]

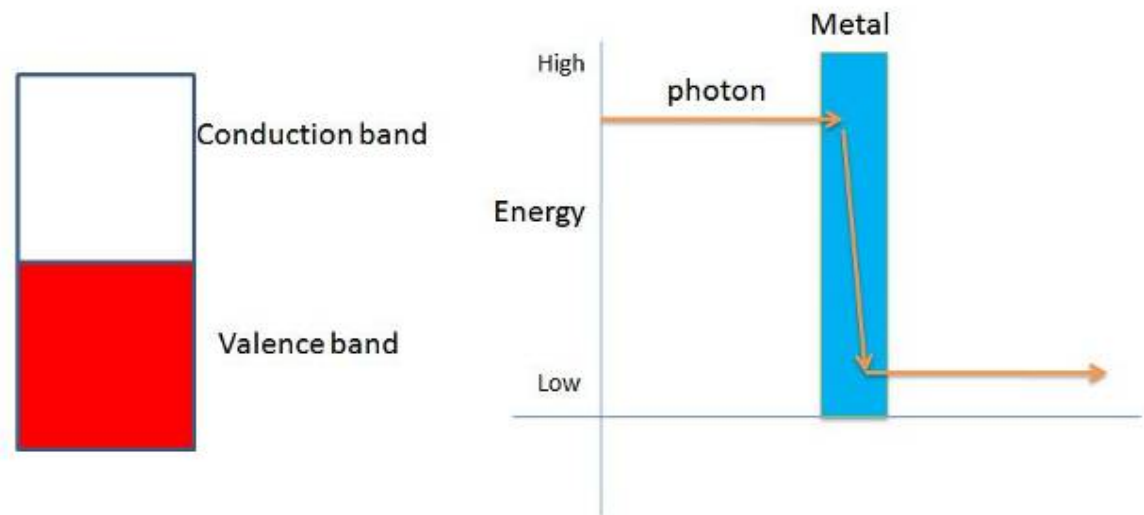


Figure 2-5 The relation between absorption and the energy band: Metal

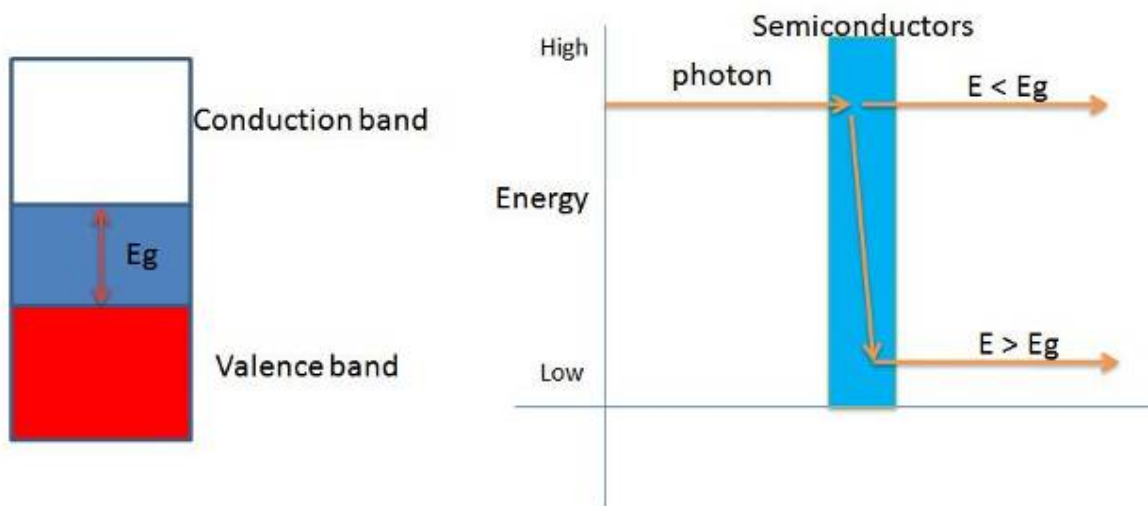


Figure 2-6 The relation between absorption and the energy band: Semiconductors

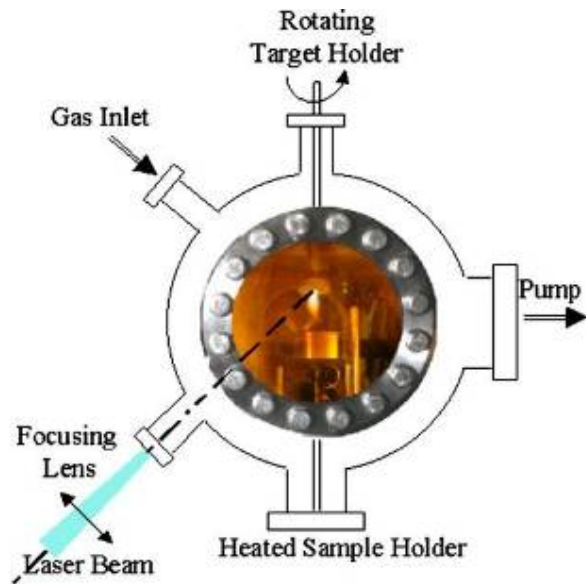


Figure 2-7 The Schematic description of a PLD experimental set-up[55]

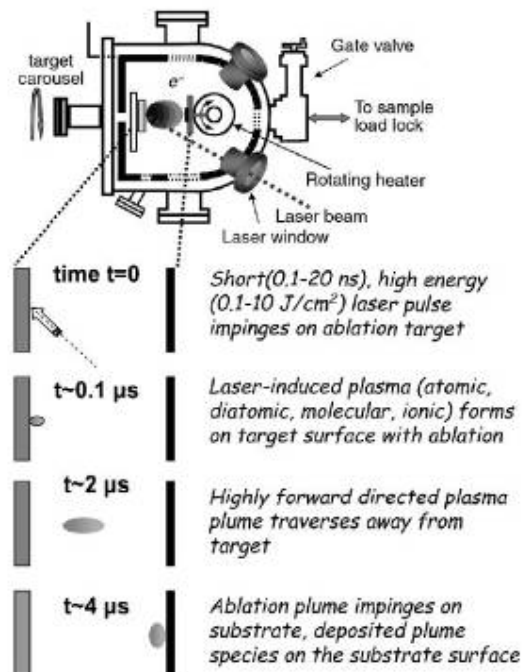


Figure 2-8 Schematic of the PLD process[18]

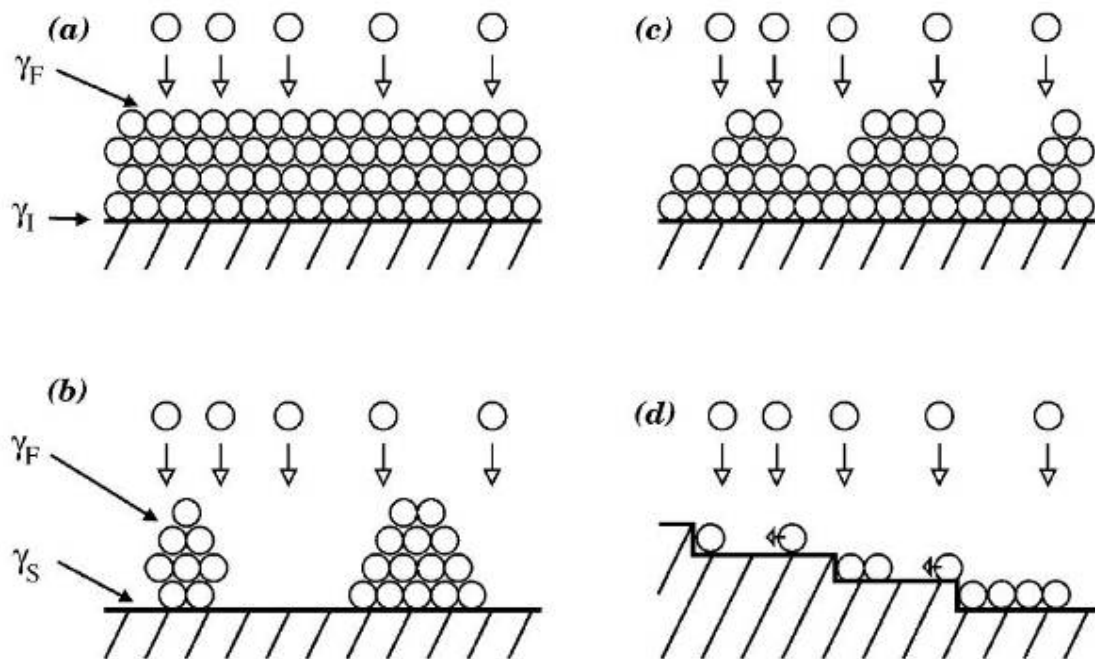


Figure 2-9 Film growth modes—layer-by-layer: (a) Frank-Van der Merwe, island; (b) Volmer-Weber (c), Stranski-Krastanov, (d) and step flow.[18]

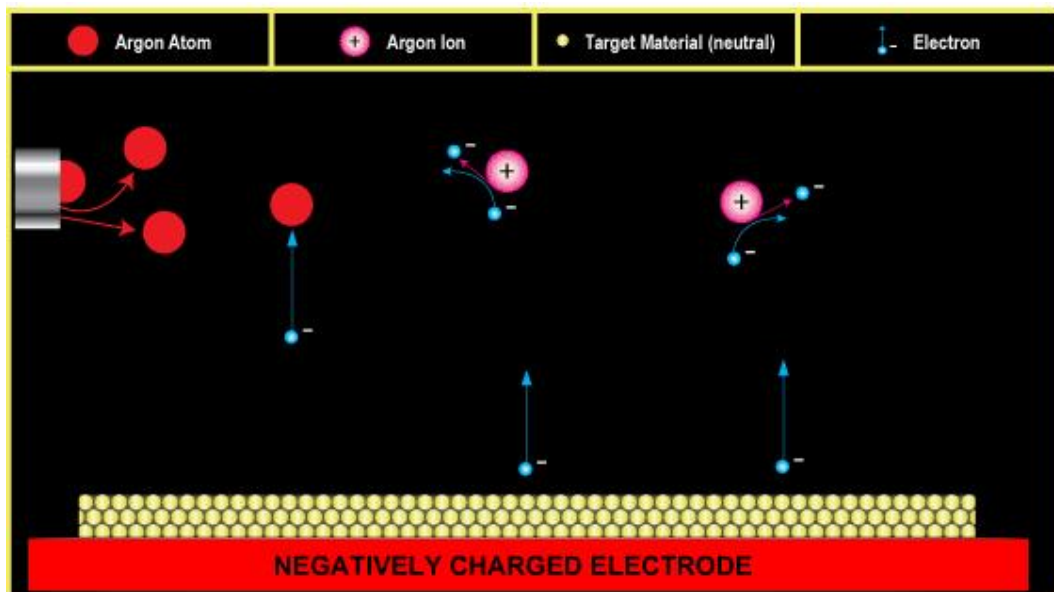


Figure 2-10 The process of sputter (1) (from <http://www.ajaint.com/whatis.htm>)

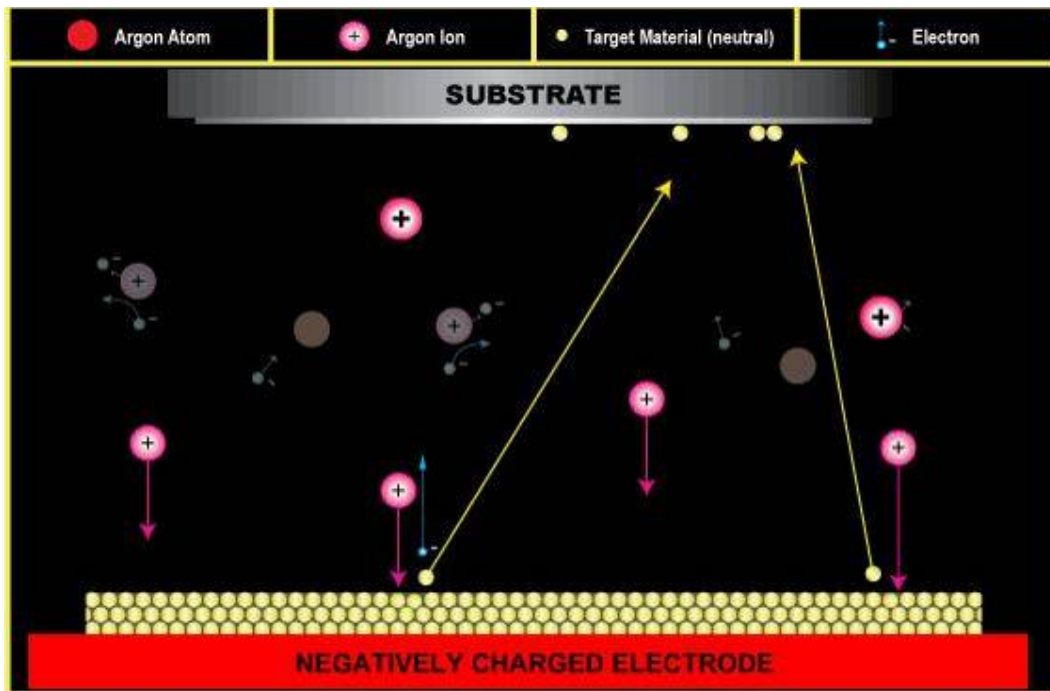


Figure 2-11 The process of sputter (2) (from <http://www.ajaint.com/whatis.htm>)

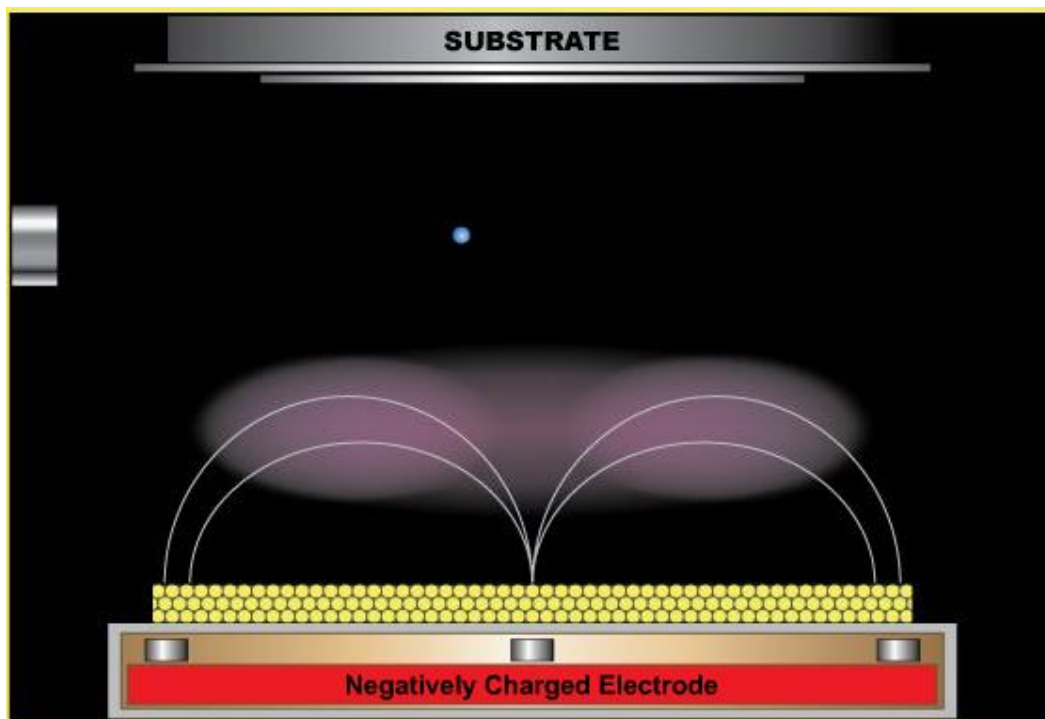


Figure 2-12 The magnet sputter (from <http://www.ajaint.com/whatis.htm>)

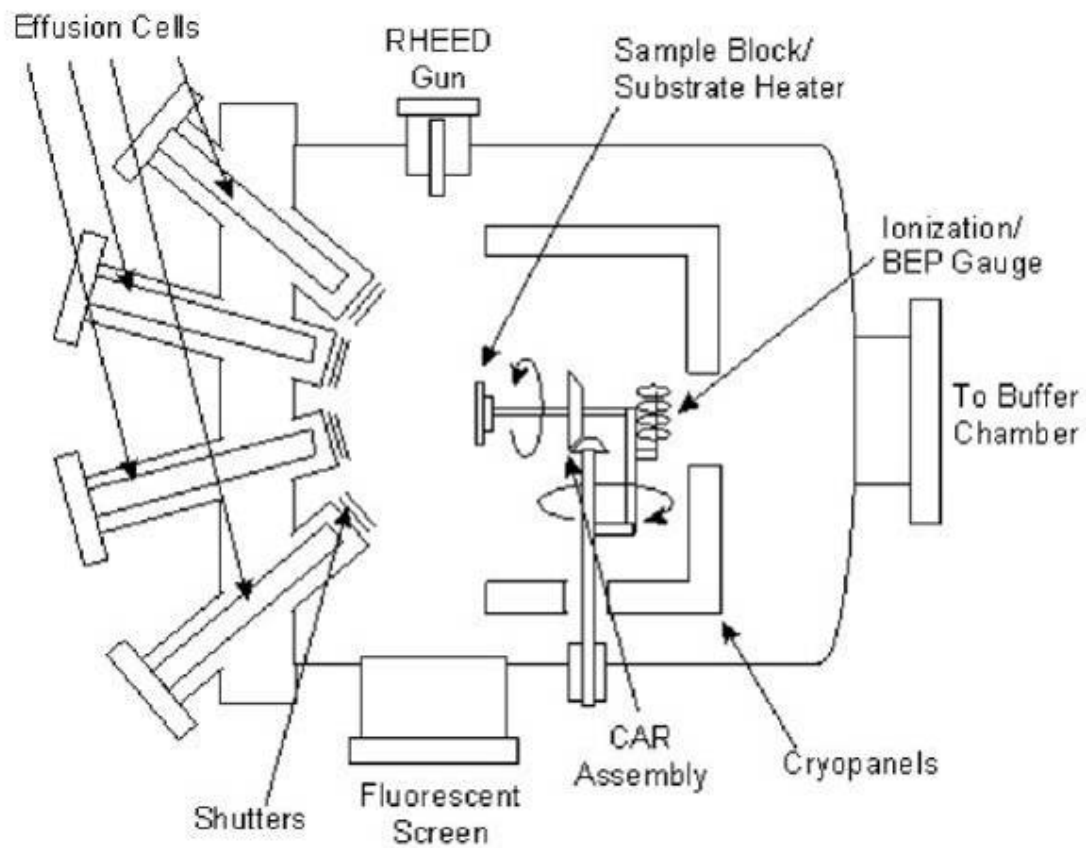


Figure 2-13 The Schematic description of MBE

(from http://projects.ece.utexas.edu/ece/mrc/groups/street_mbe/mbechapter.html)

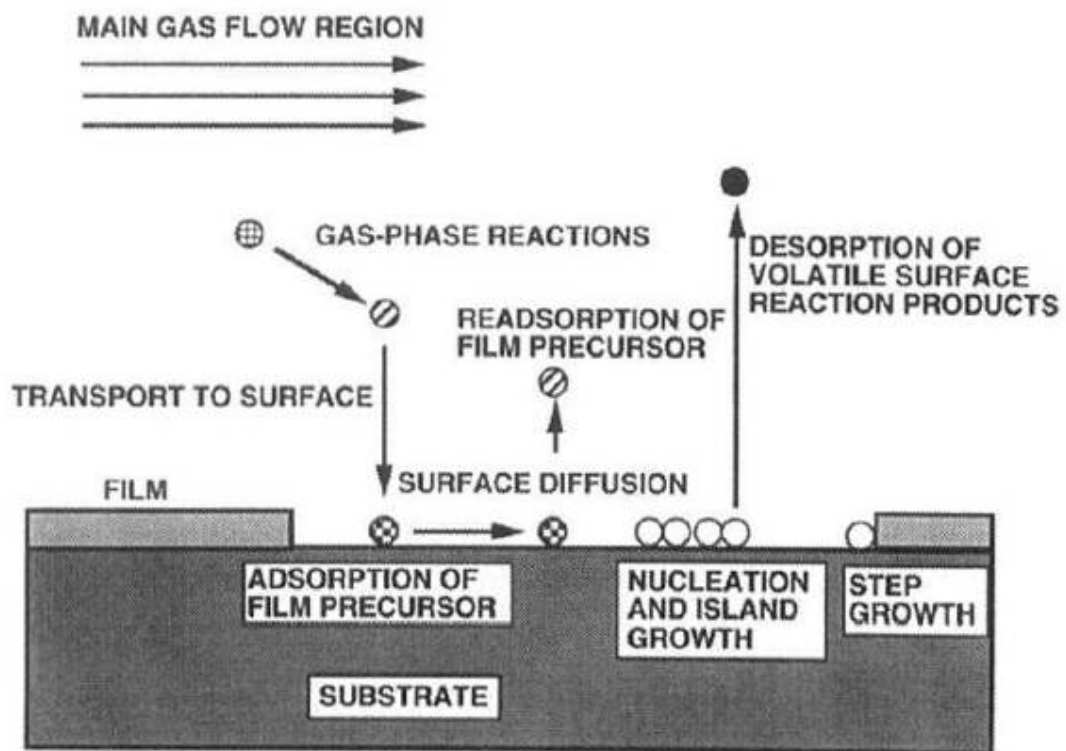


Figure 2-14 Sequence of gas transportation and reaction process contributing to CVD film growth[9]

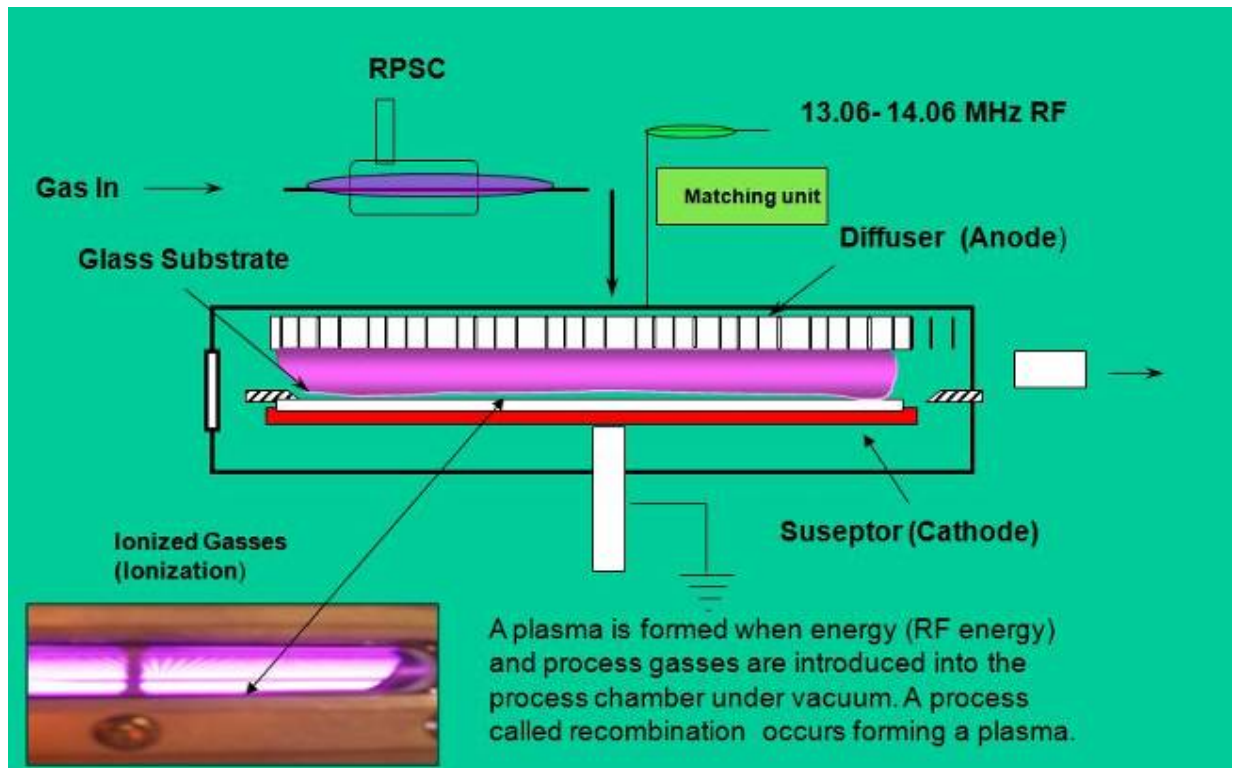


Figure 2-15 The Schematic of CVD (from Chi Mei Corporation established Chi Mei Optoelectronics LTD.)

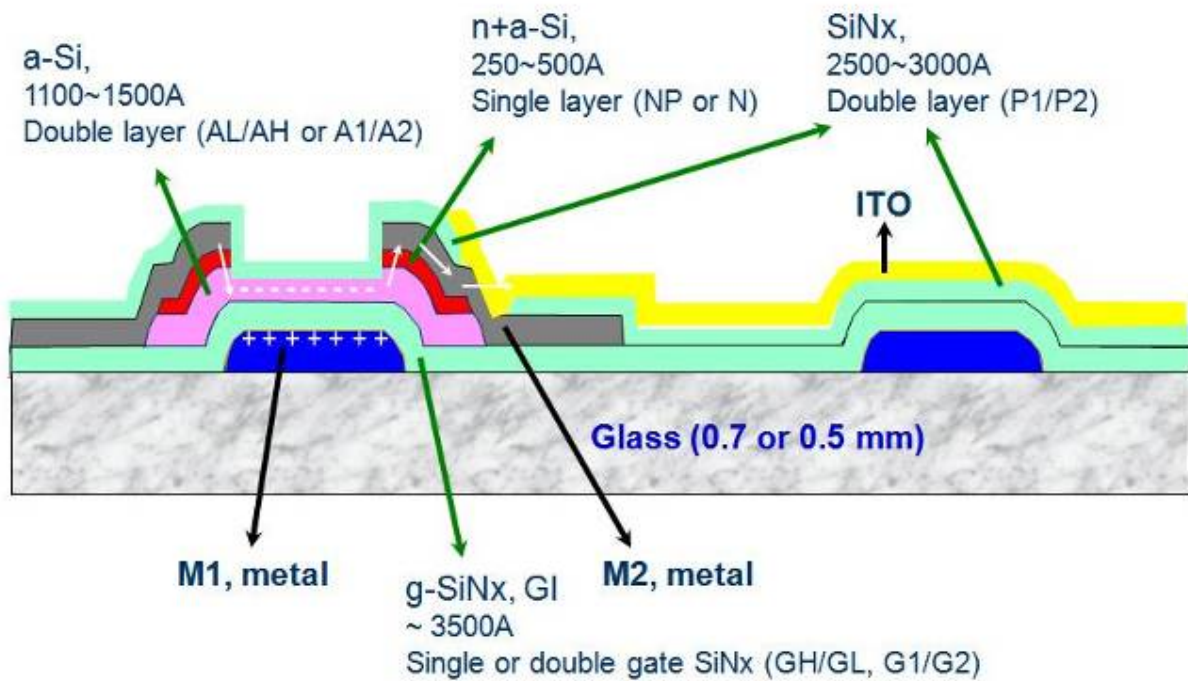


Figure 2-16 The structure of transparent thin-film transistor (from Chi Mei Corporation established Chi Mei Optoelectronics LTD.)



Figure 2-17 The picture of the PLD system used in University of Birmingham

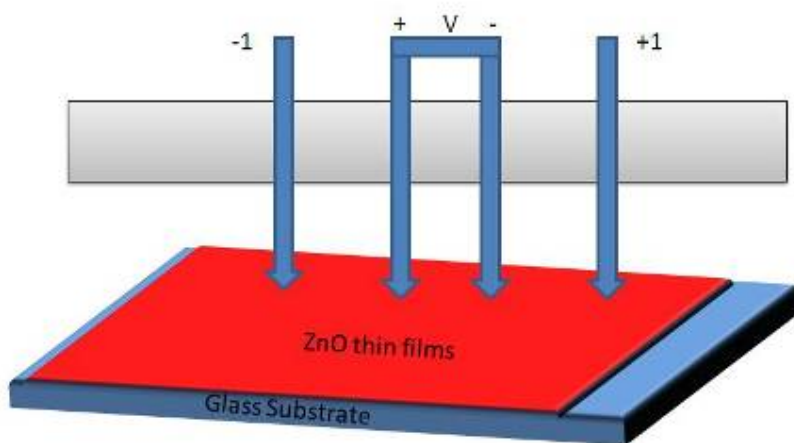


Figure 2-18 Schematic diagram of a Four point -Probe

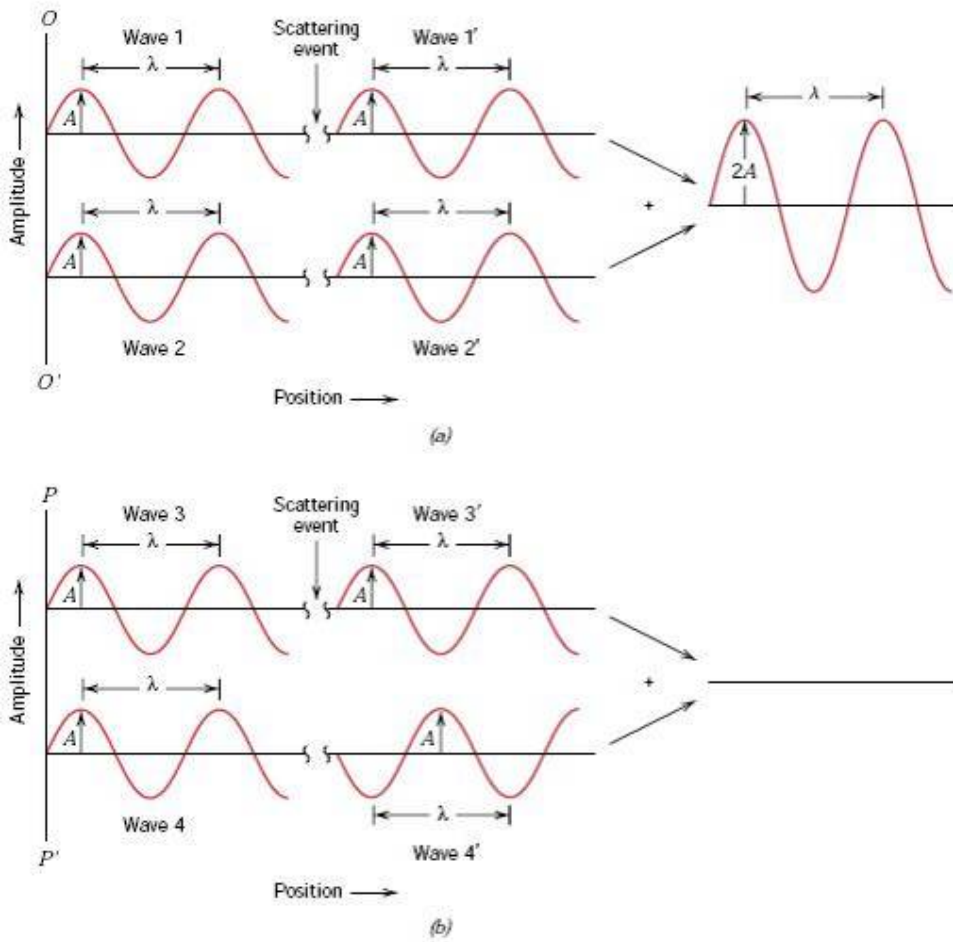


Figure 2-19 (a) Demonstration of how two waves that have the same wavelength λ and remain in phase after a scattering event (b) Demonstration of how two waves that have the same wavelength λ and become out of the phase after a scattering event after a scattering[21]

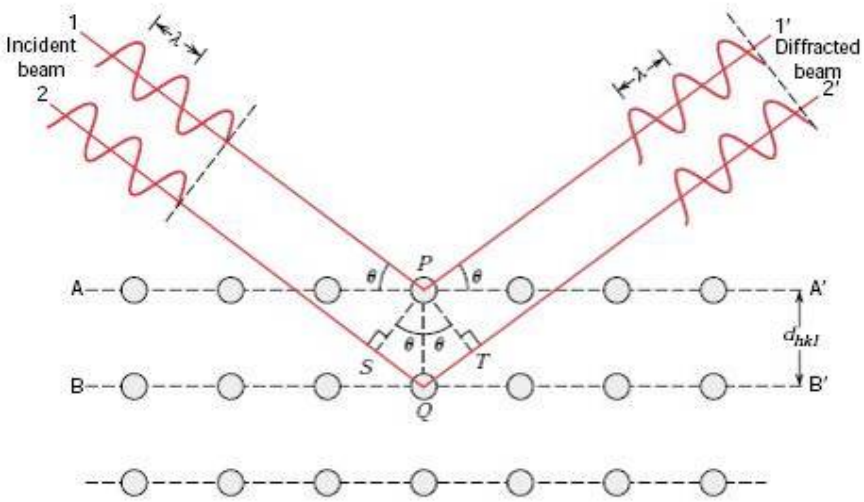


Figure 2-20 Diffraction of x-rays by plans of atoms.[21]

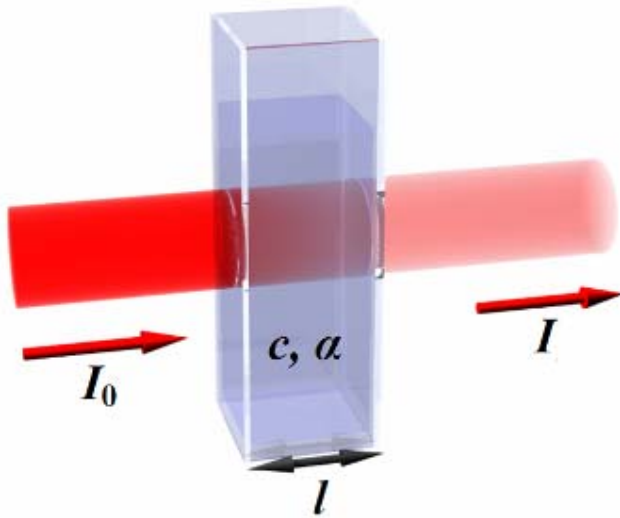


Figure 2-21 The Schematic diagram of transmittance (from <http://en.wikipedia.org/wiki/Wiki>)



Figure 2-22 The picture of Spectrophotometer

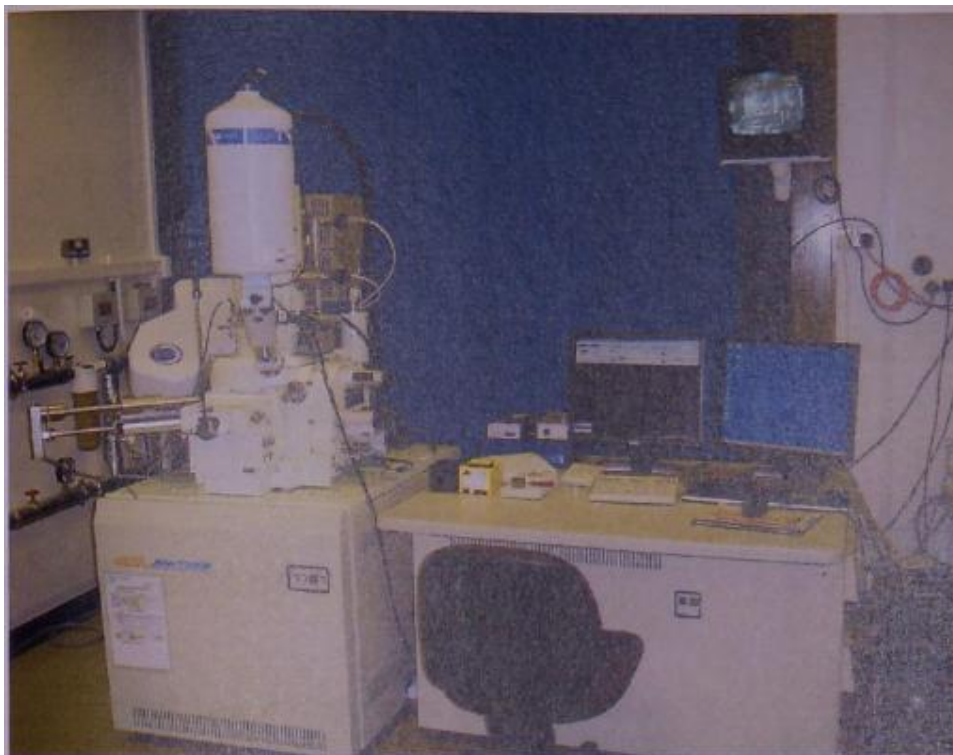


Figure 2-23 The picture of SEM JEOL 7000

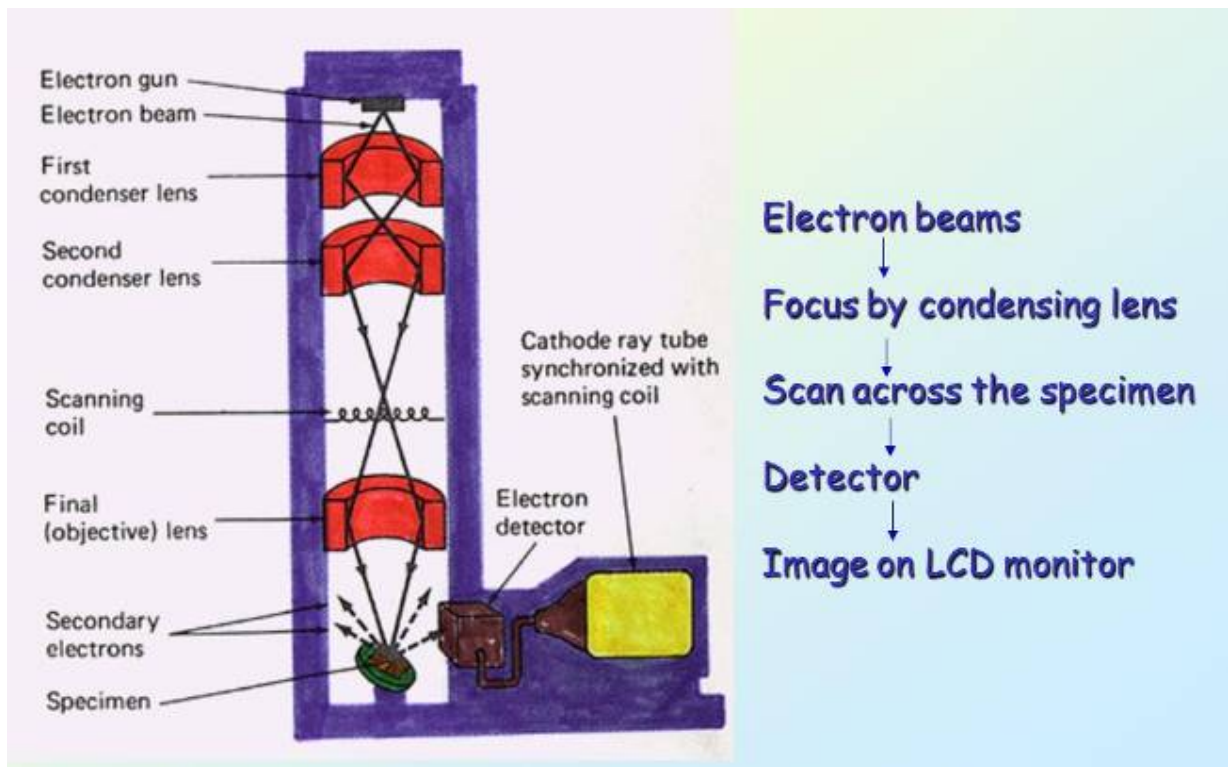


Figure 2-24 The Schematic diagram of a SEM (from Professor Ian Jones' lecture)

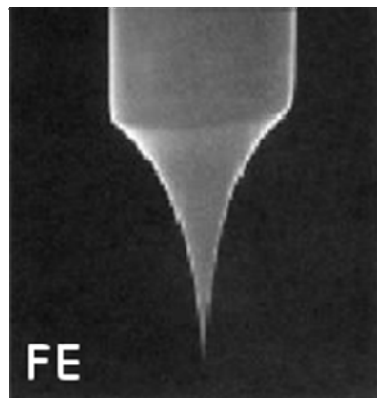


Figure 2-25 The picture of Field emission (from Professor Ian Jones' lecture)

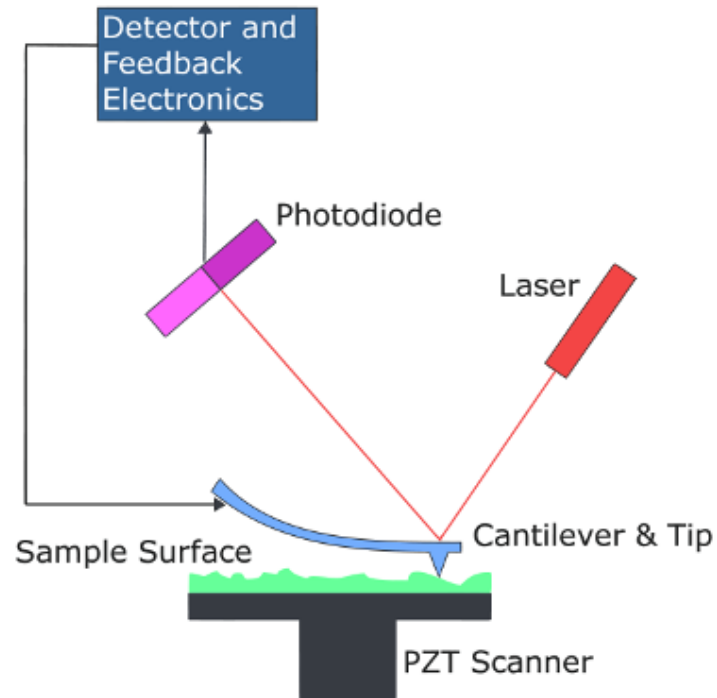


Figure 2-26 The Schematic diagram of AFM (from <http://en.wikipedia.org/wiki/Wiki>)

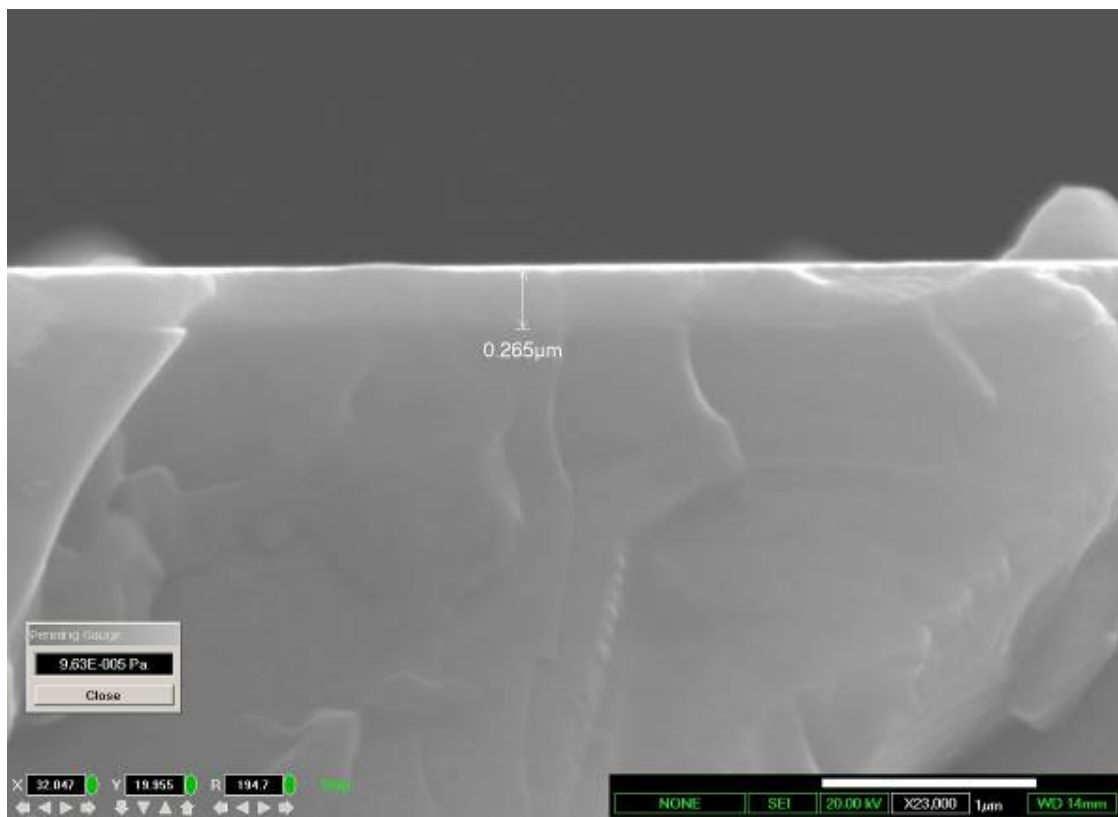


Figure 2-27 The picture of cross section of ZnO thin films by SEM

Figures and tables from Chapter 4

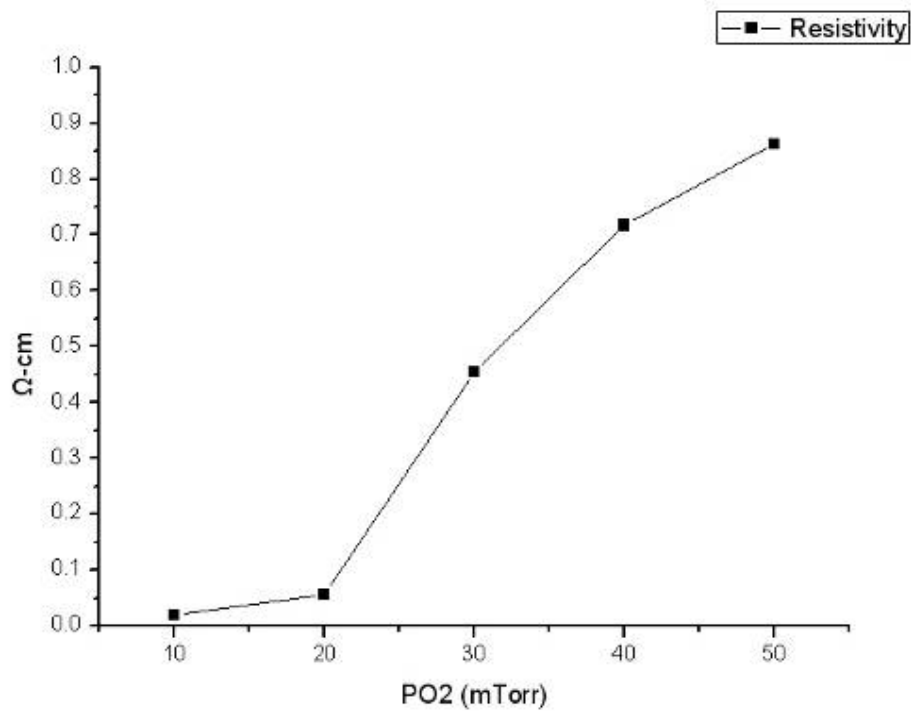


Figure 4-28 Resistivity of ZnO films deposited at various ambient oxygen pressures ($D=55\text{mm}$, $T_s=300^\circ\text{C}$, Laser fluence= $2.7\text{J}/\text{cm}^2$)

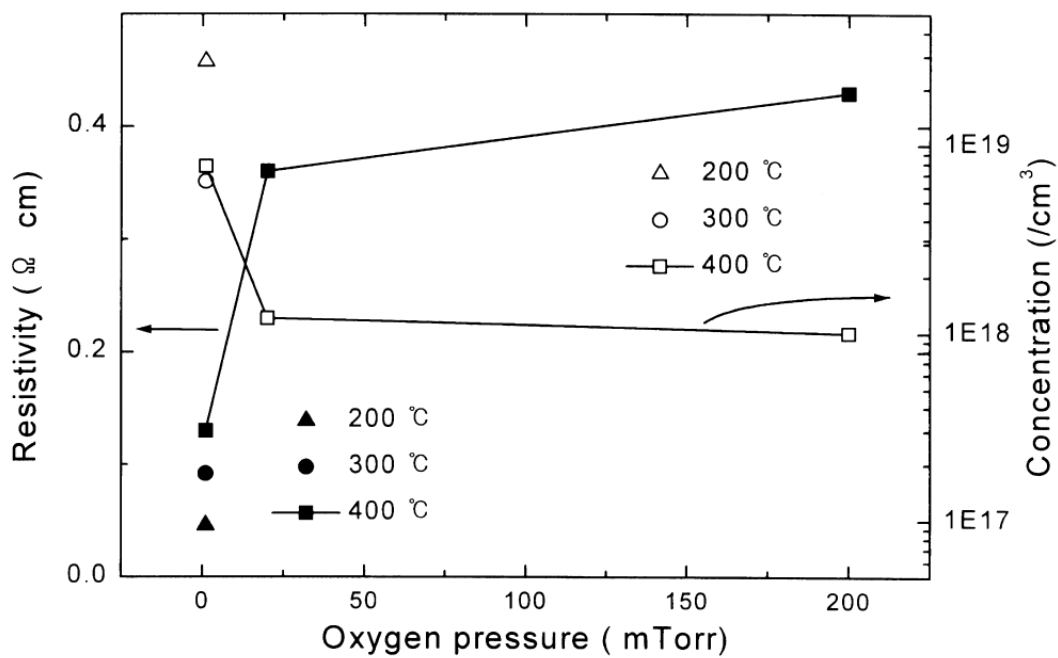


Figure 4-29 A plot of electron concentration and resistivity vs. oxygen pressure as result of Hall measurements. The results from samples grown with 1mTorr and 200°C and 300°C are also plotted.[80]

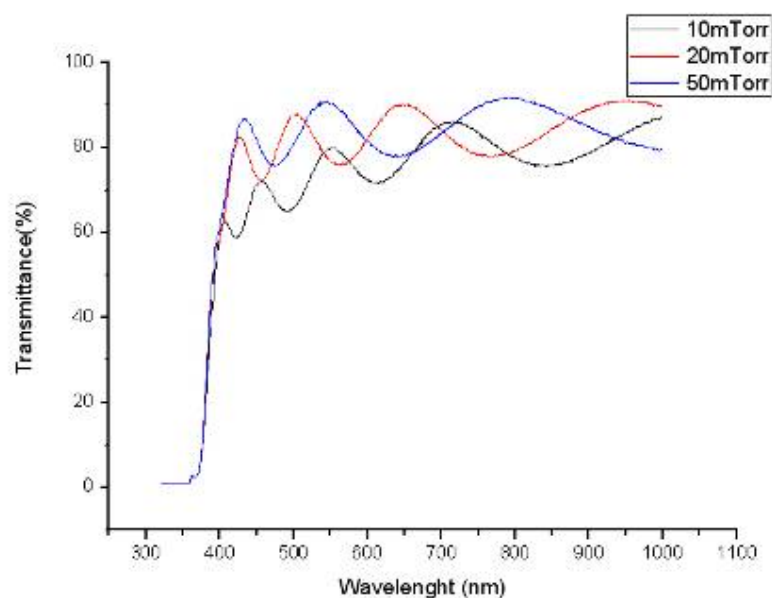


Figure 4-30 Transmittance spectra of ZnO films on glass substrate grown at different ambient oxygen pressures. (D=55mm, Ts=300°C, Laser fluence=2.7J/cm²)

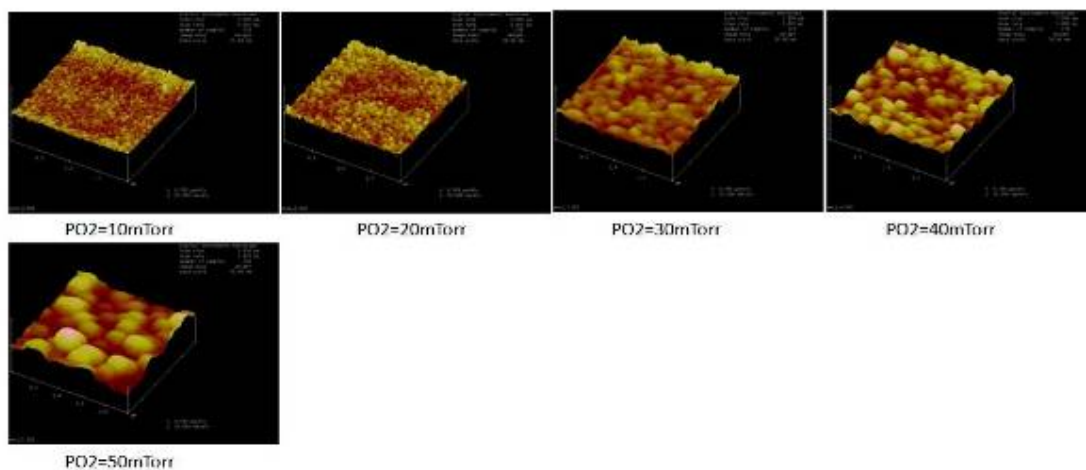


Figure 4-31 AFM 3D images (2×2μm) of ZnO with varying ambient oxygen pressure. (D=55mm, Ts=300°C, Laser fluence=2.7J/cm²)

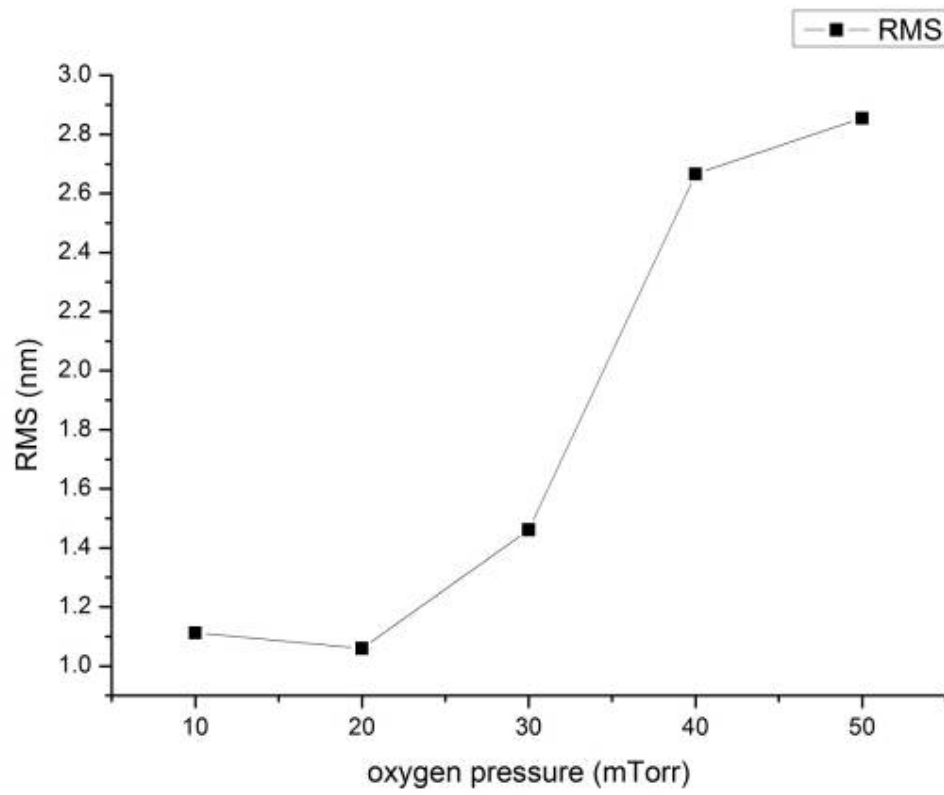


Figure 4-32 Roughness of ZnO films deposited by PLD (D=55mm, Ts=300°C, Laser fluence=2.7J/cm²)

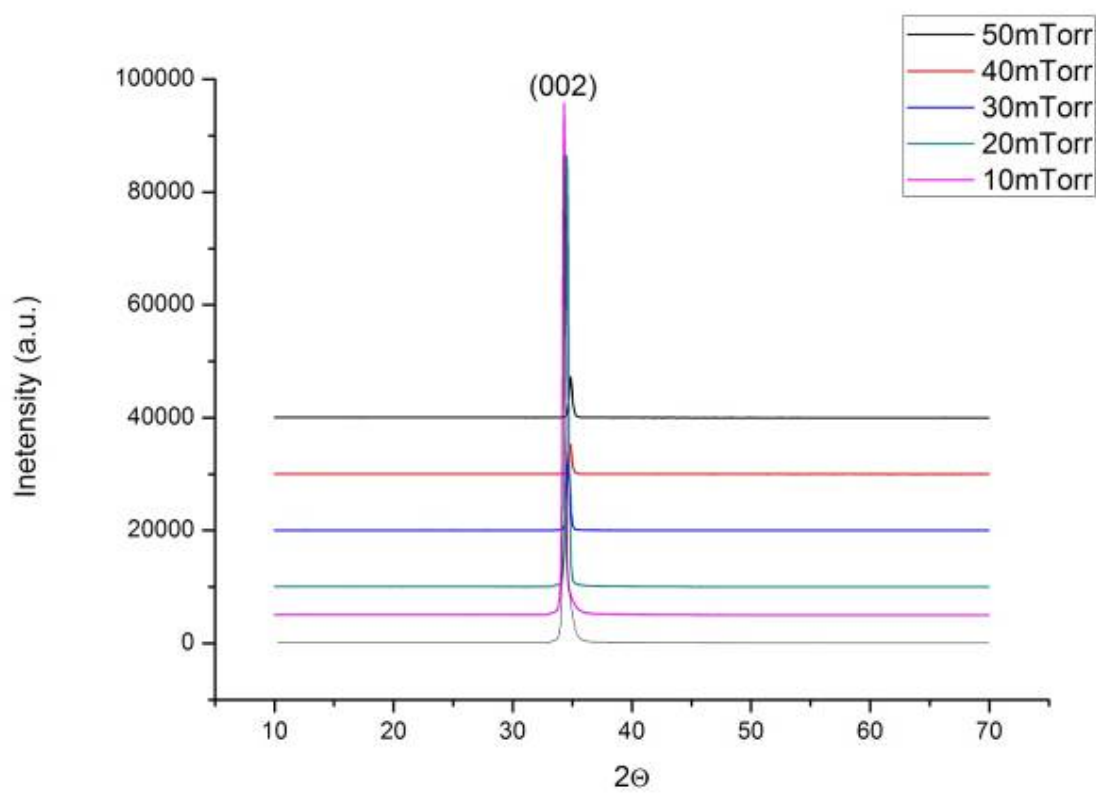


Figure 4-33 XRD pattern of ZnO films deposited by PLD with varying oxygen pressures. (D=55mm, $T_s=300^\circ\text{C}$, Laser fluence= $2.7\text{J}/\text{cm}^2$)

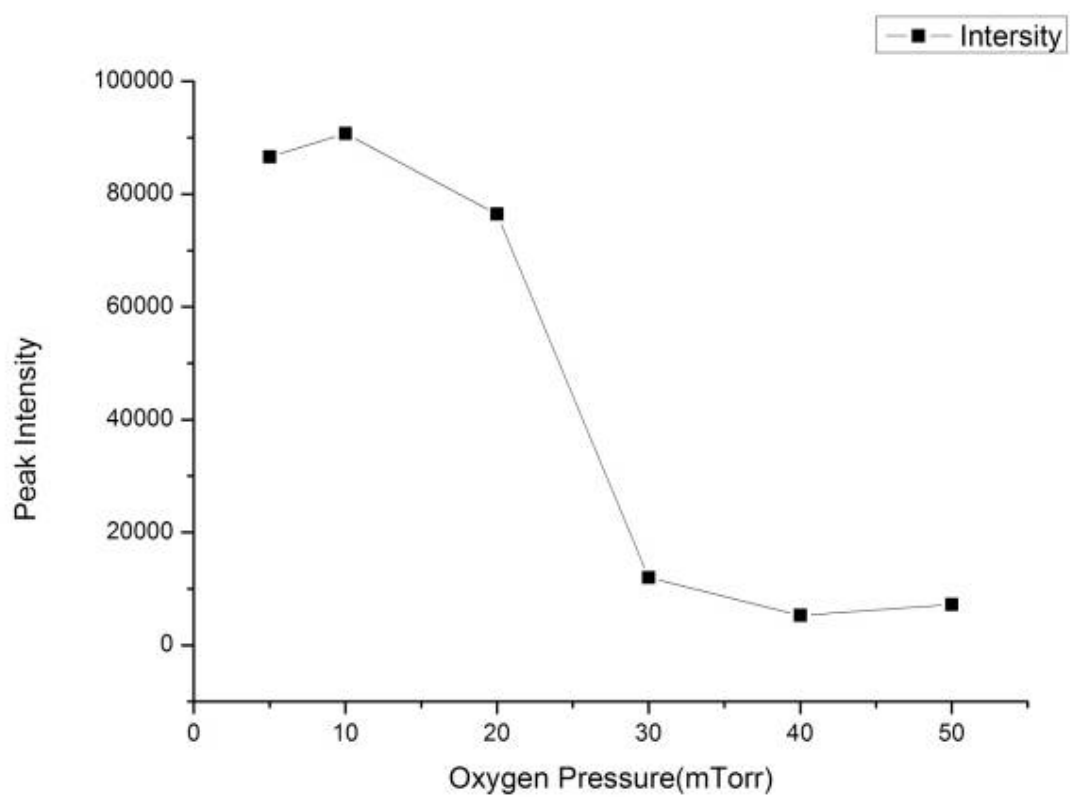


Figure 4-34 peak intensity of XRD pattern of ZnO films deposited by PLD with varying oxygen pressures. (D=55mm, Ts=300°C, Laser fluence=2.7J/cm²)

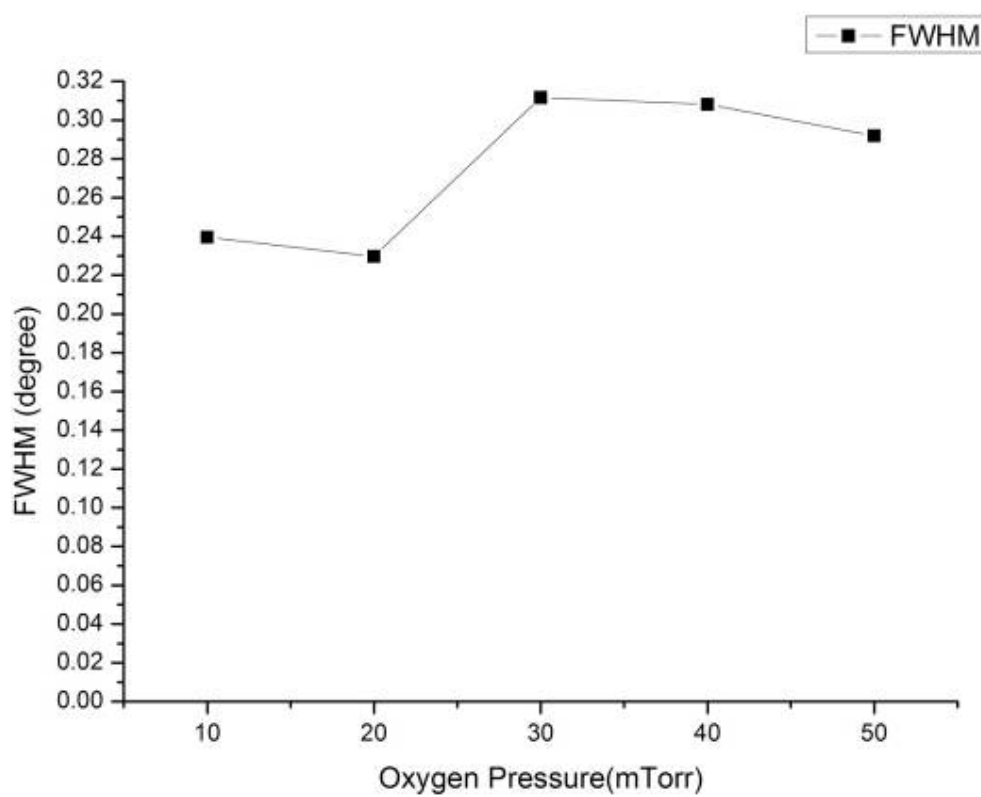


Figure 4-35 Variation in the FWHM of (002) reflections of The ZnO films as a function of oxygen pressures. (D=55mm, Ts=300°C, Laser fluence=2.7J/cm²)

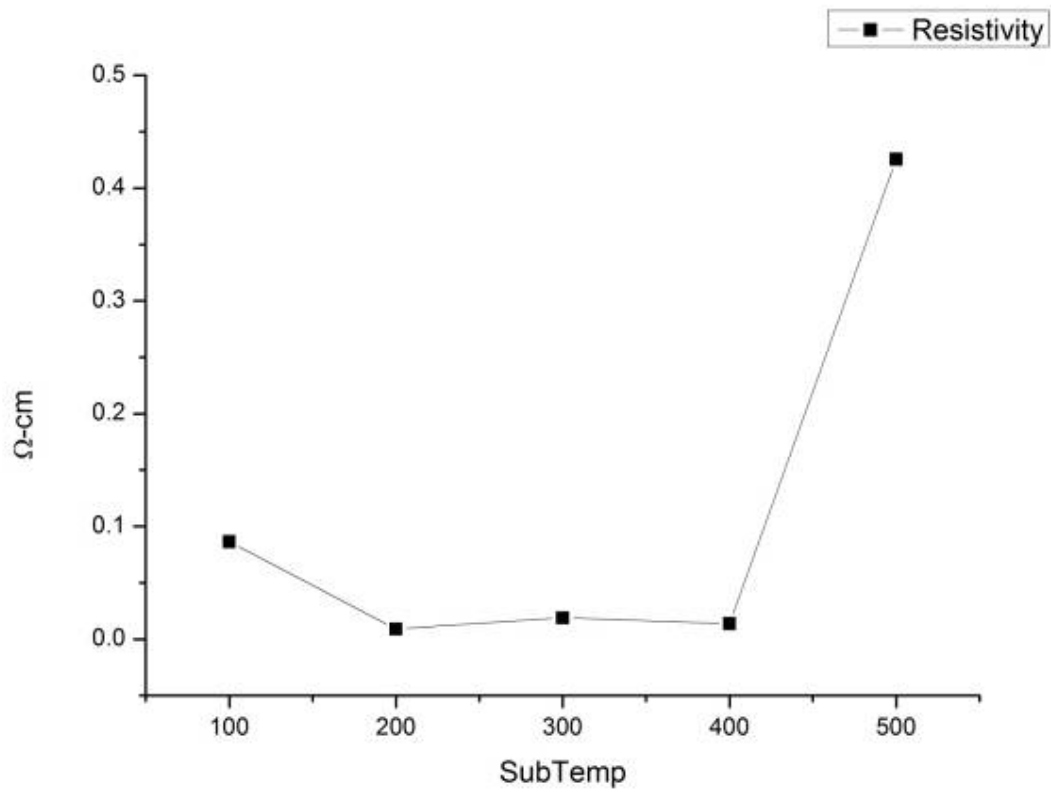


Figure 4-36 Resistivity of ZnO films deposited at various Substrate temperatures (D=55mm, Po₂=10mTorr, Laser fluence=2.7J/cm²)

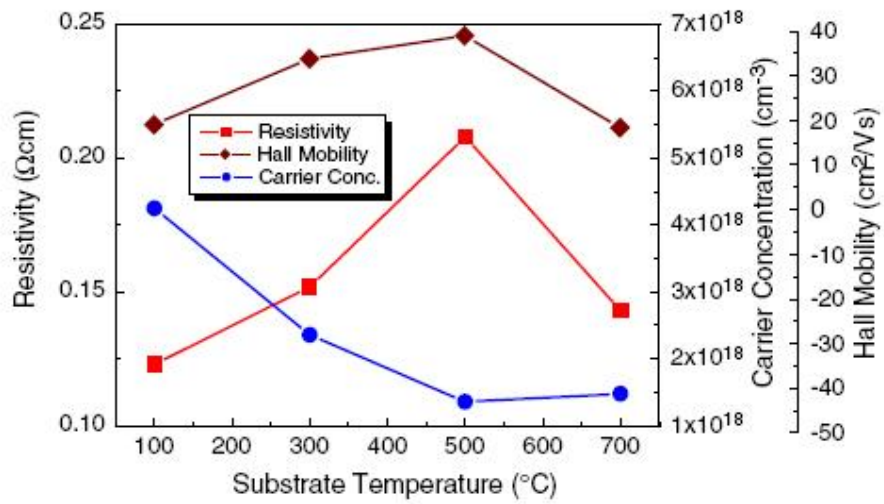


Figure 4-37 The electrical properties of ZnO thin films deposited at various temperatures[14]

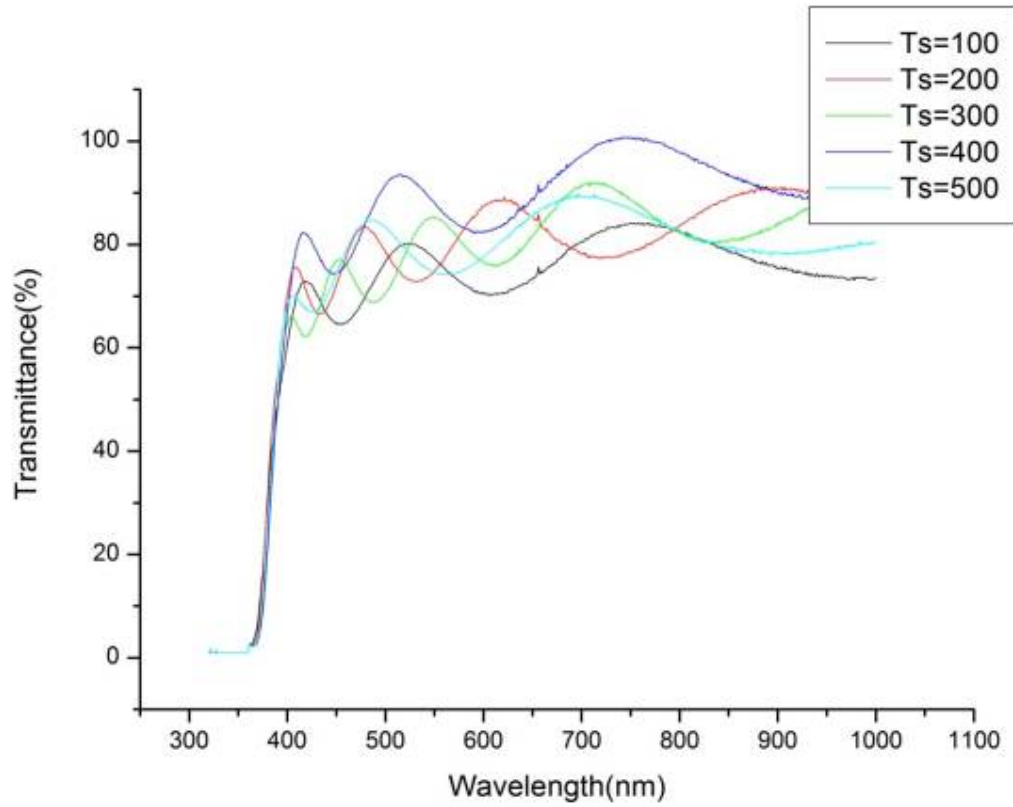


Figure 4-38 Optical transmittance spectra of the ZnO thin films grown at various substrate temperature. (D=55mm, Po2=10mTorr, Laser fluence=2.7J/cm²)

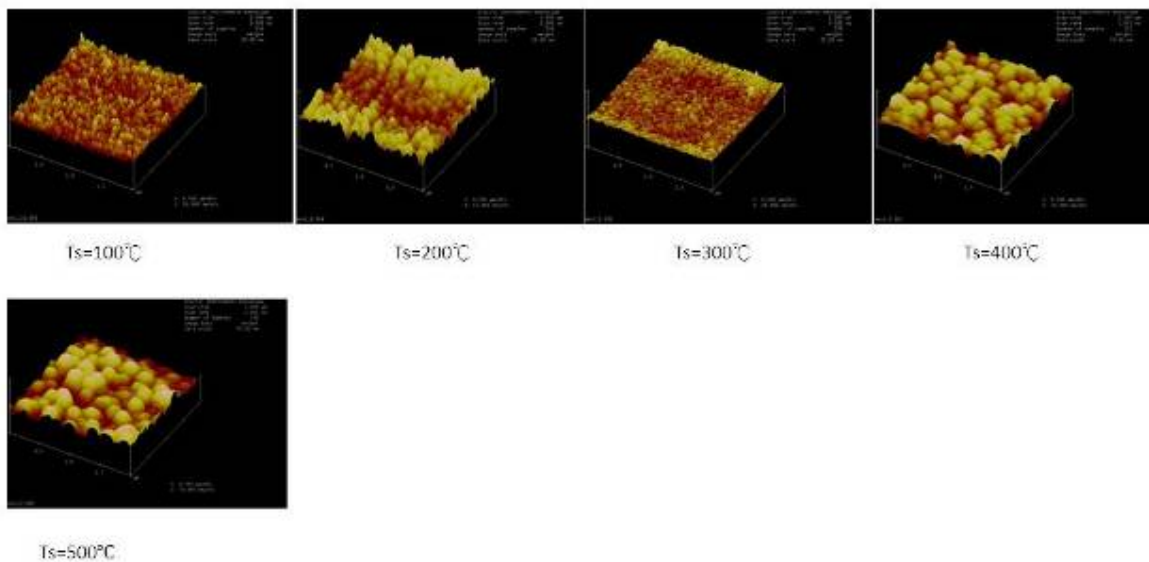


Figure 4-39 AFM image of ZnO thin films deposited at various substrate temperatures

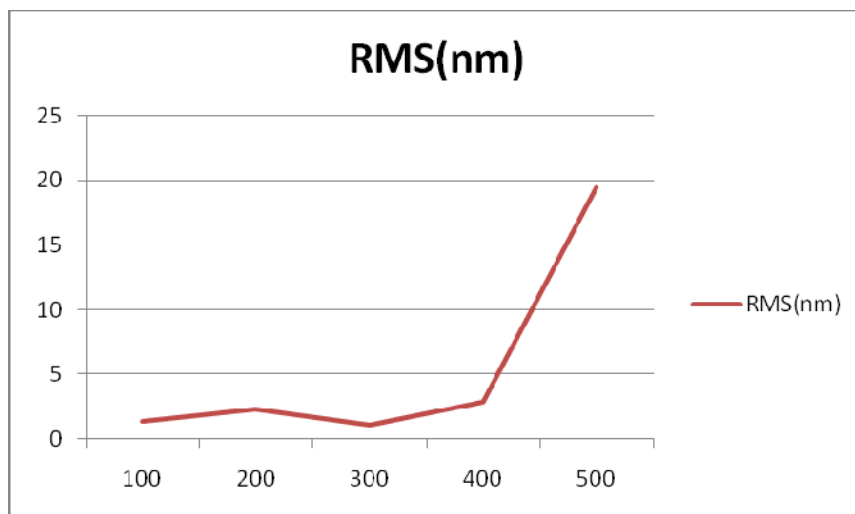


Figure 4-40 Roughness of ZnO thin films deposited at various temperatures

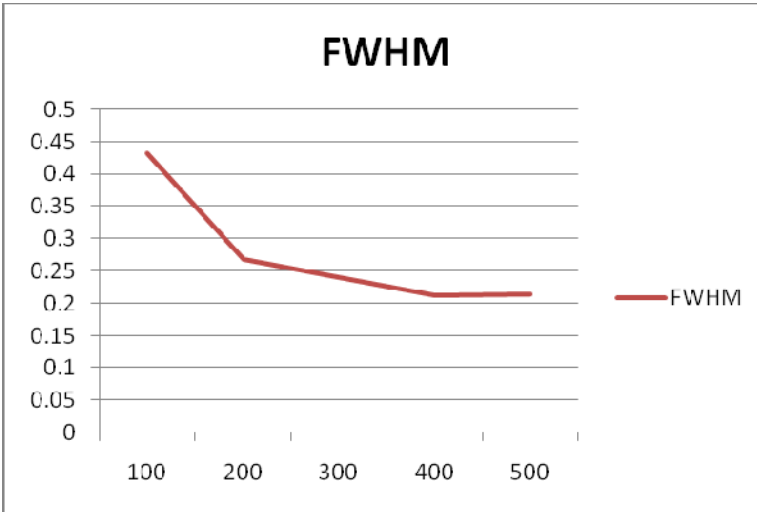


Figure 4-41 FWHM of (002) XRD peaks from ZnO thin films deposited at various temperatures

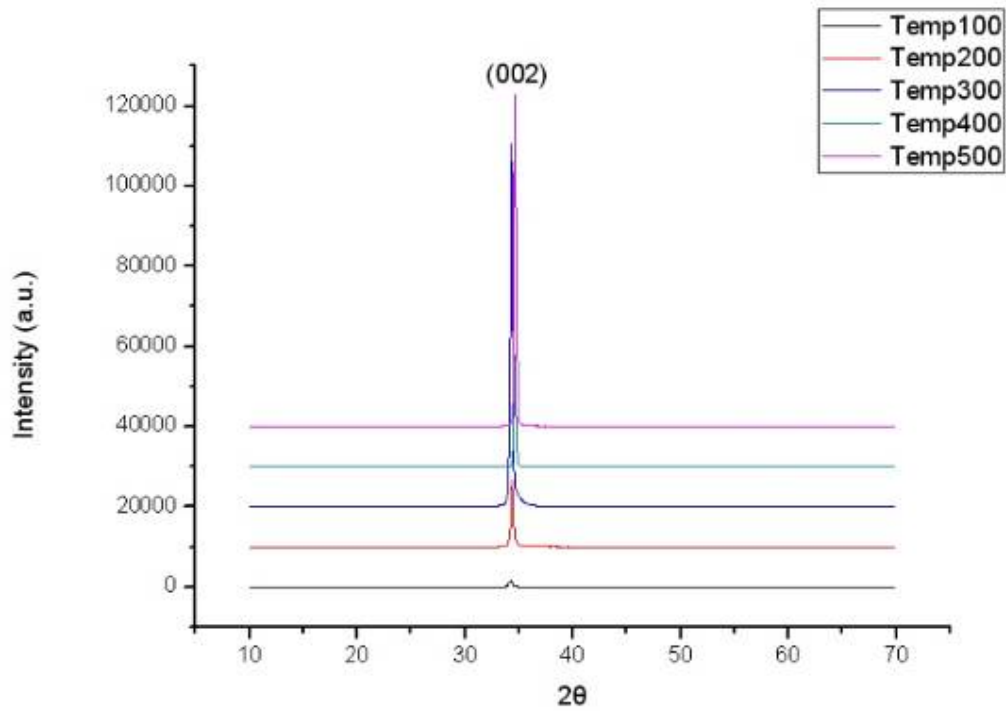


Figure 4-42 XRD patterns of ZnO thin films deposited at various substrate temperatures

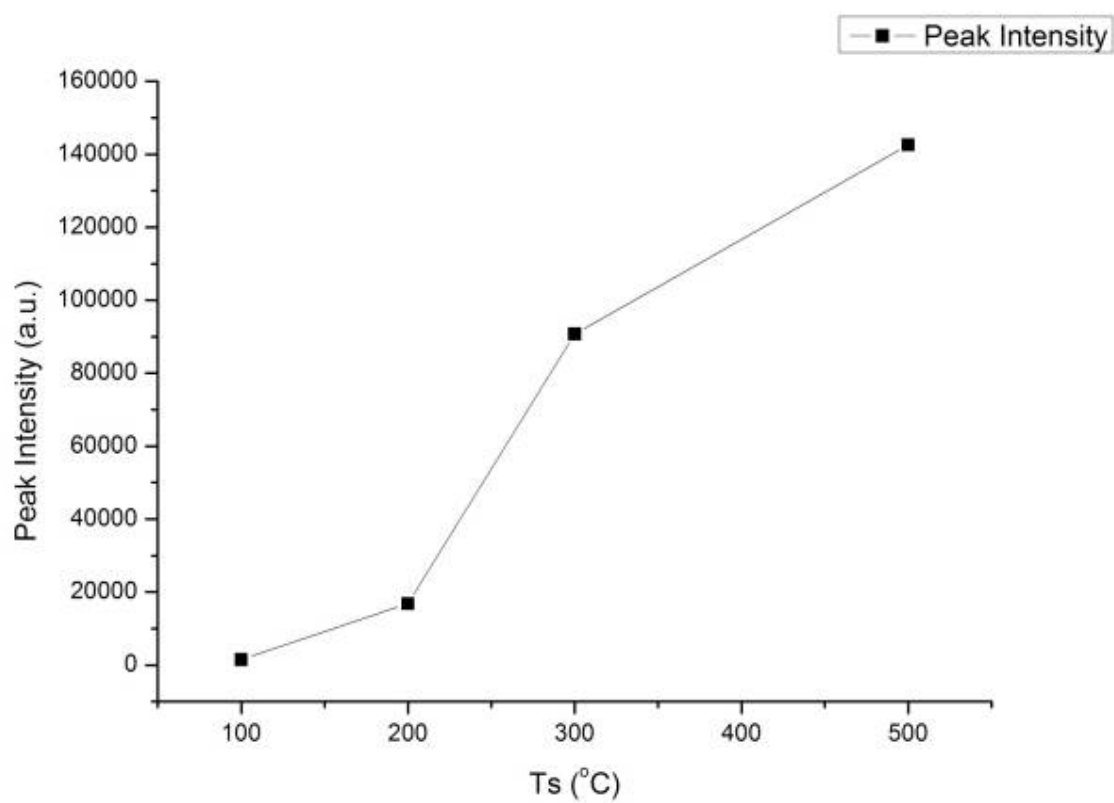


Figure 4-43 Peak intensity of (002) diffraction peak for the ZnO films deposited at various temperatures.

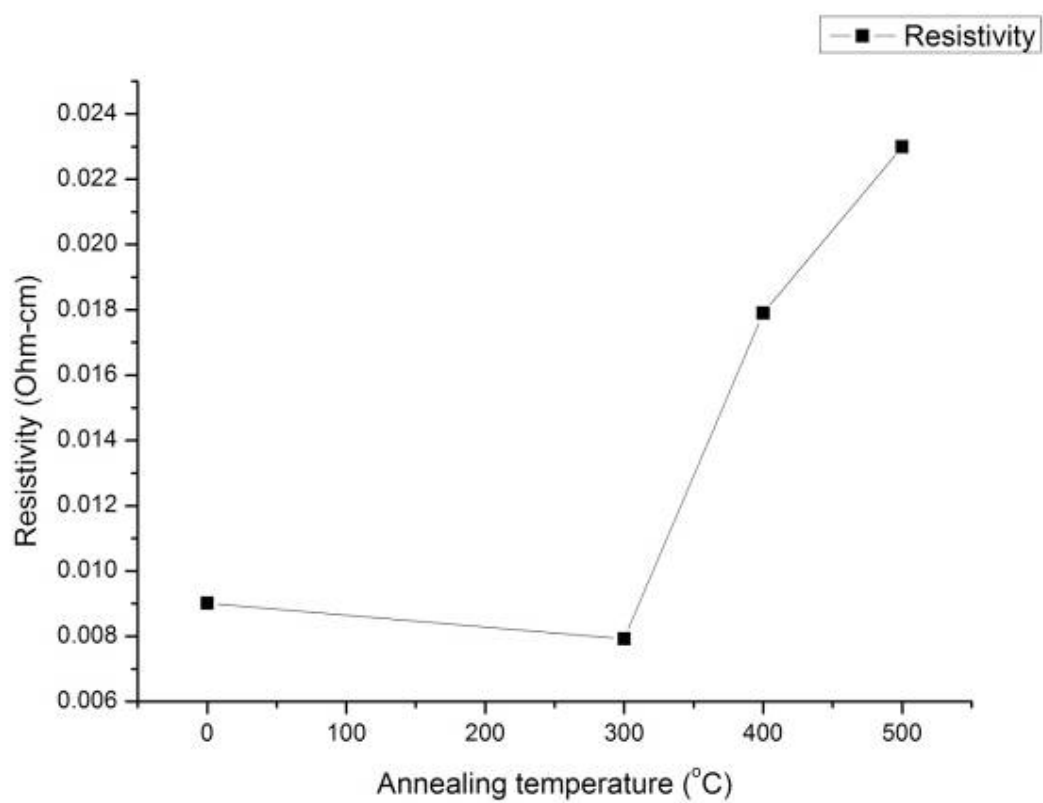


Figure 4-44 Resistivity of ZnO films deposited at various annealing temperatures (D=55mm, Po2=10mTorr, Ts=200°C, Laser fluence=2.7J/cm²)

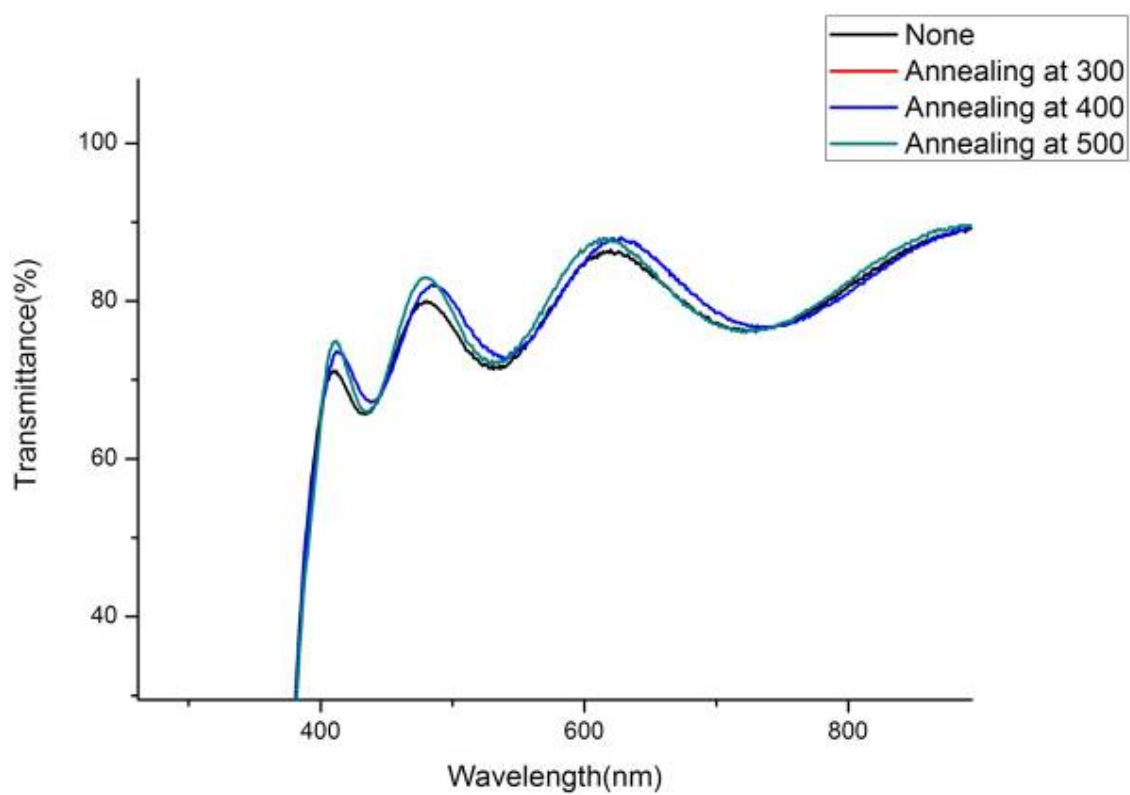


Figure 4-45 the optical transmittance spectrum of ZnO thin films deposited on glass substrate for as-deposited, and post-growth annealed at various annealing temperatures. (D=55mm, Po2=10mTorr, Ts=200°C, Laser fluence=2.7J/cm²)

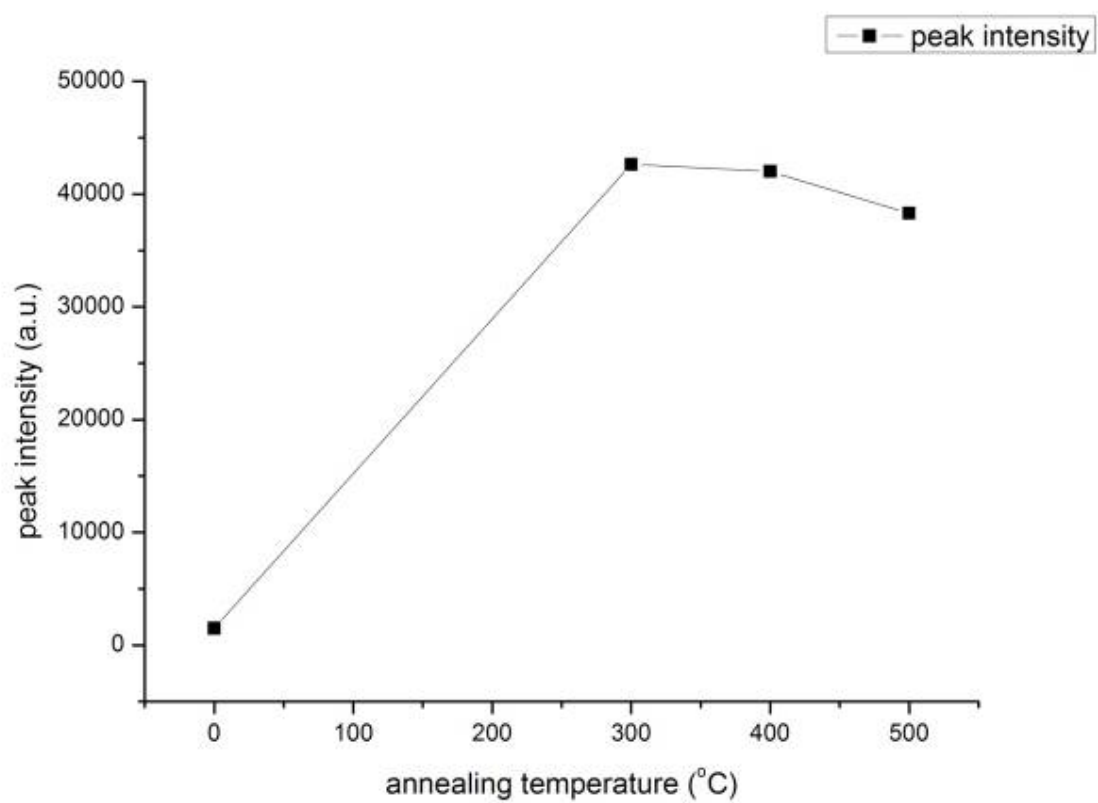
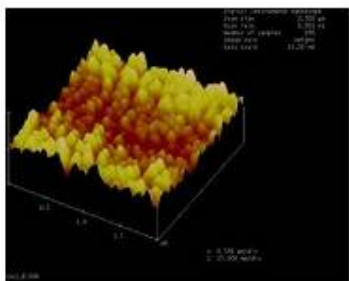
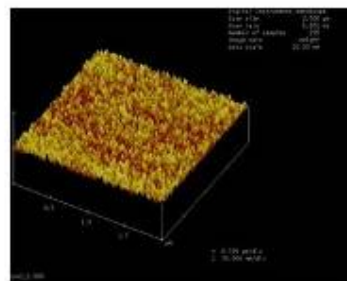


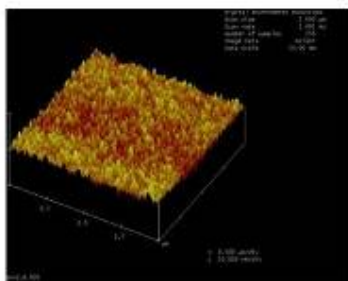
Figure 4-46 Peak intensity of (002) diffraction peak for the ZnO films deposited at various annealing temperatures (D=55mm, Po2=10mTorr, Ts=200°C, Laser fluence=2.7J/cm²)



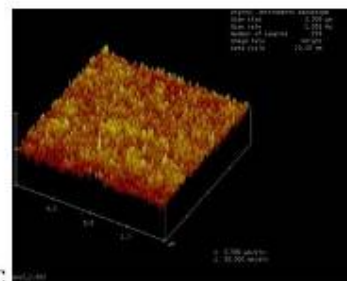
No annealing



Annealing for 2h at 300°C

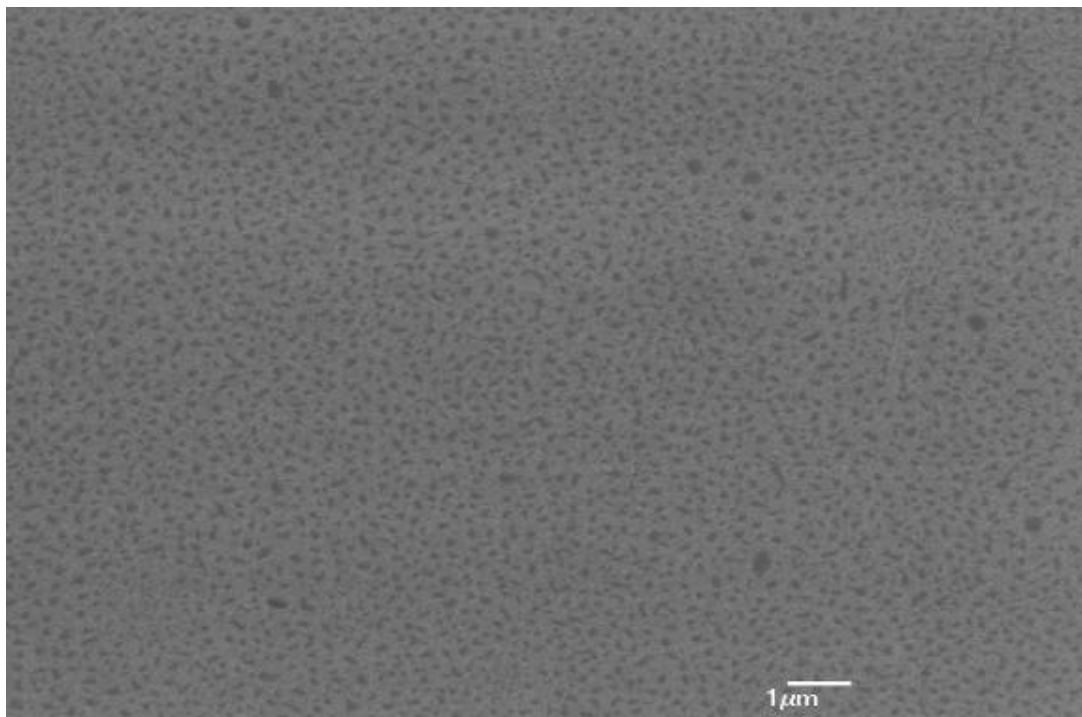


Annealing for 2h at 400°C

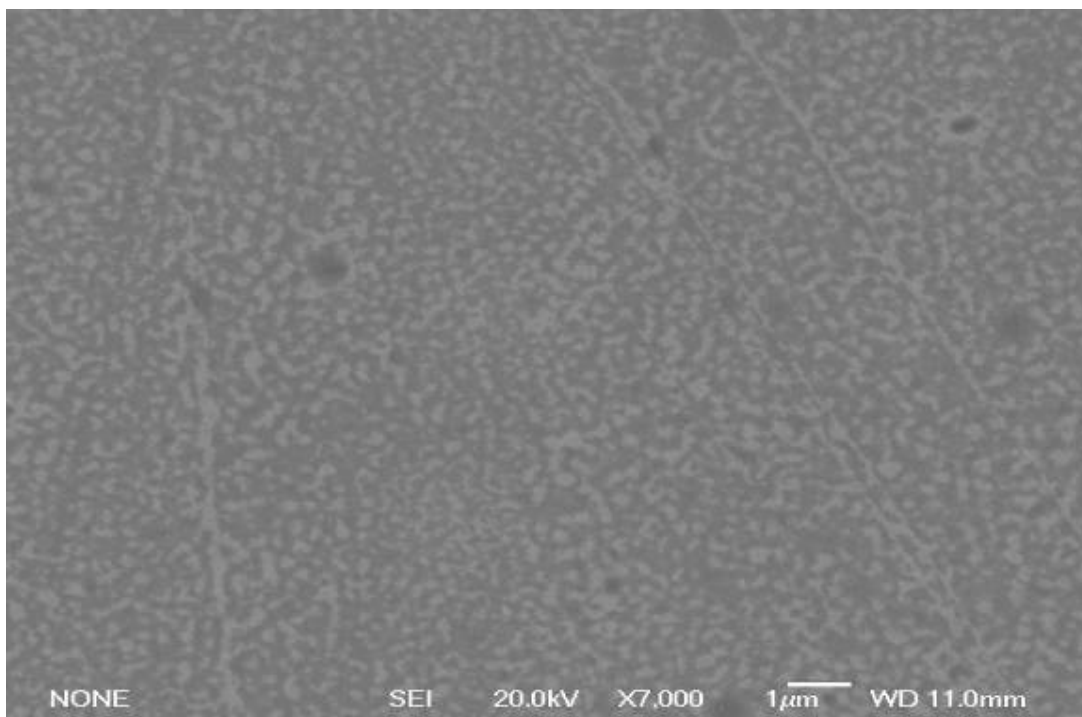


Annealing for 2h at 500°C

Figure 4-47 AFM image of ZnO thin films deposited at various annealing temperatures. (D=55mm, Po₂=10mTorr, Ts=200°C, Laser fluence=2.7J/cm²)



(a)



(b)

Figure 4-48 The SEM image of ZnO thin film: (a) as grow, and (b) annealing at 500°C for 2h in oxygen (D=55mm, Po2=10mTorr, Ts=200°C, Laser fluence=2.7J/cm²)

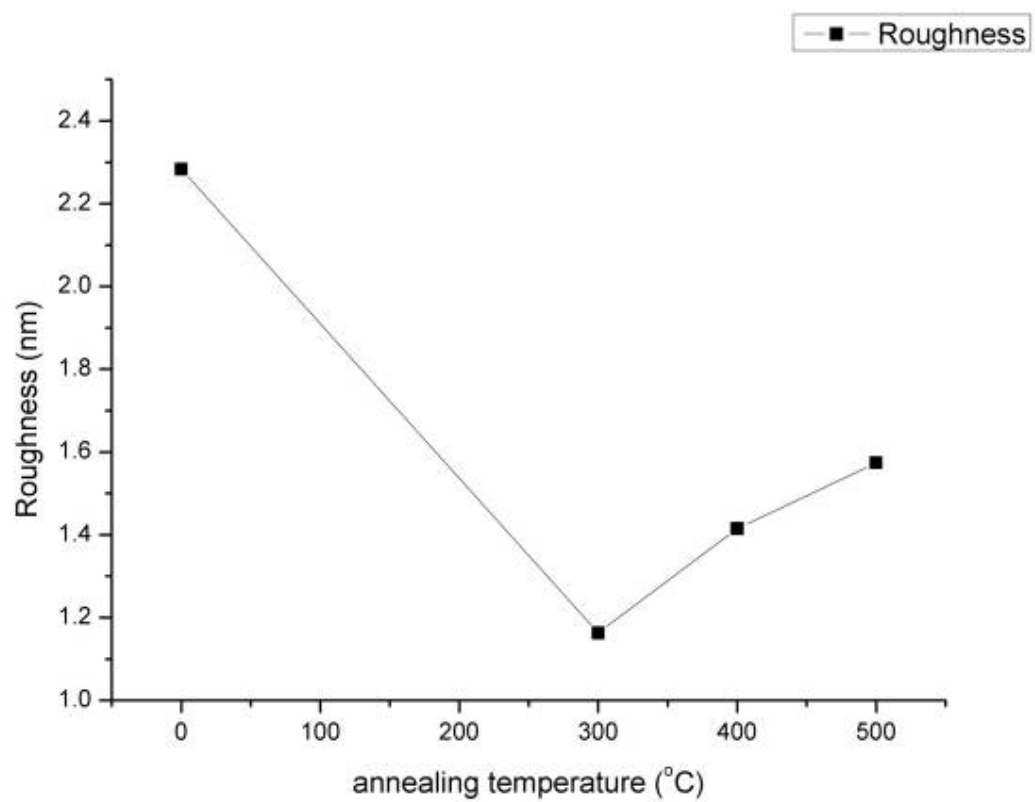


Figure 4-49 Roughness of ZnO thin film deposited at various annealing temperatures. (D=55mm, Po2=10mTorr, Ts=200°C, Laser fluence=2.7J/cm²)

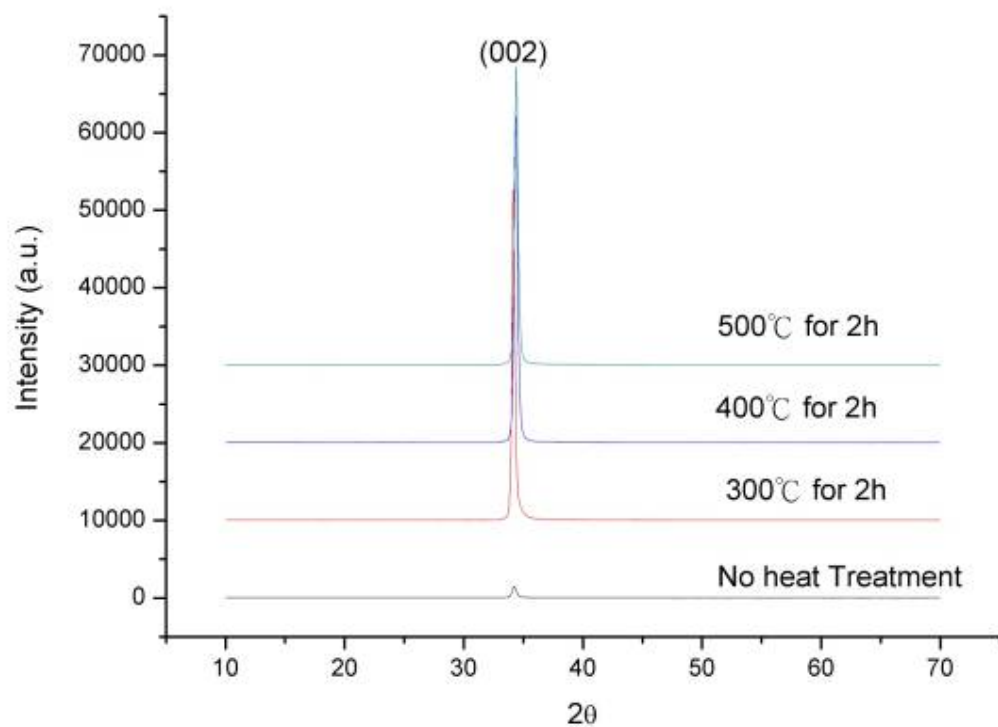


Figure 4-50 The XRD pattern of ZnO thin films deposited at various annealing temperatures. . (D=55mm, Po2=10mTorr , Ts=200°C, Laser fluence=2.7J/cm²)

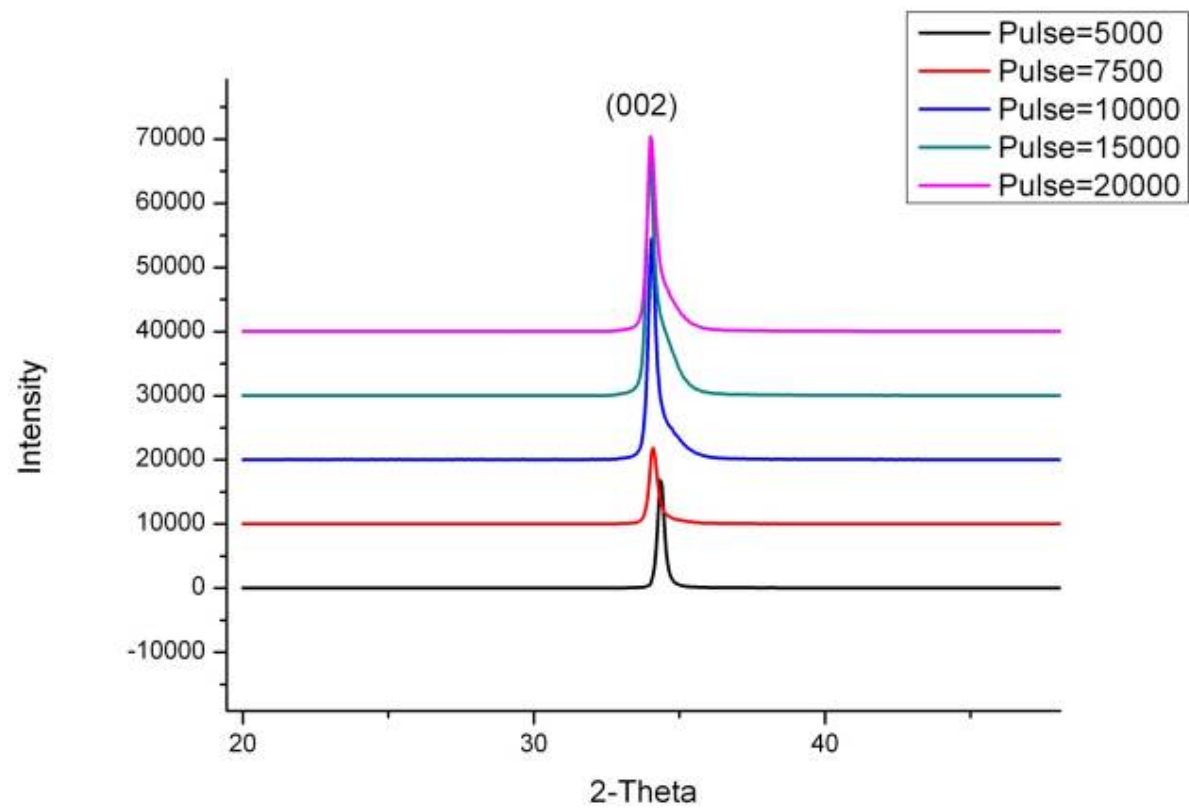


Figure 4-51 X-ray diffraction spectra of ZnO thin film deposited at the various number of laser pulses. (D=55mm, Po₂=10mTorr, T_s=200°C, Laser fluence=2.7J/cm²)

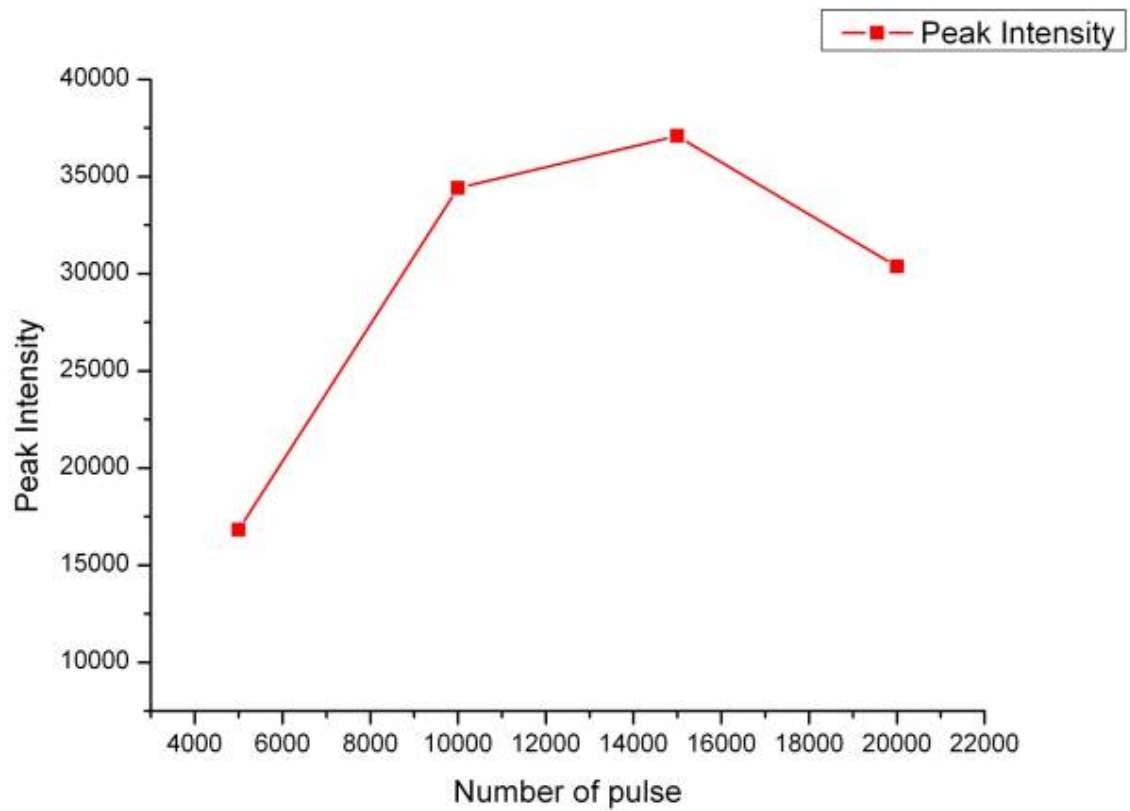


Figure 4-52 Peak intensity of (002) diffraction peak for the ZnO films deposited at the various number of laser pulses. (D=55mm, Po2=10mTorr, Ts=200°C, Laser fluence=2.7J/cm²)

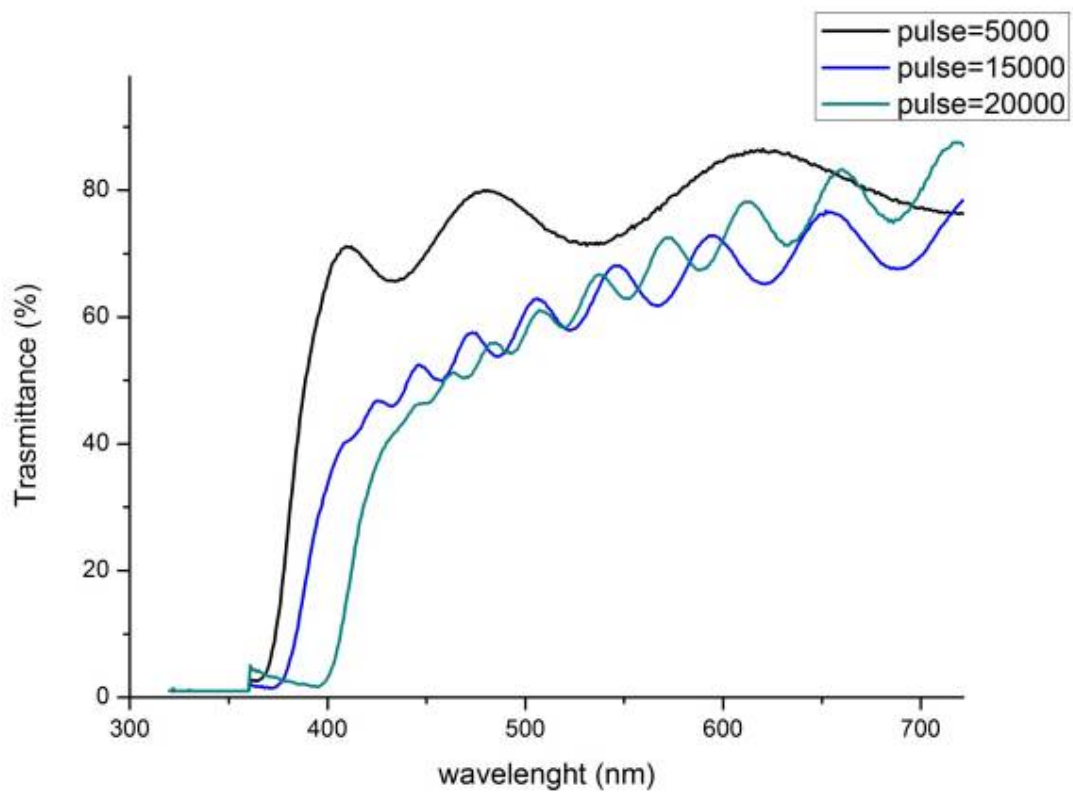


Figure 4-53 the optical transmittance spectrum of ZnO thin films deposited on glass substrate with the various number of laser pulses. (D=55mm, Po2=10mTorr, Ts=200°C, Laser fluence=2.7J/cm²)

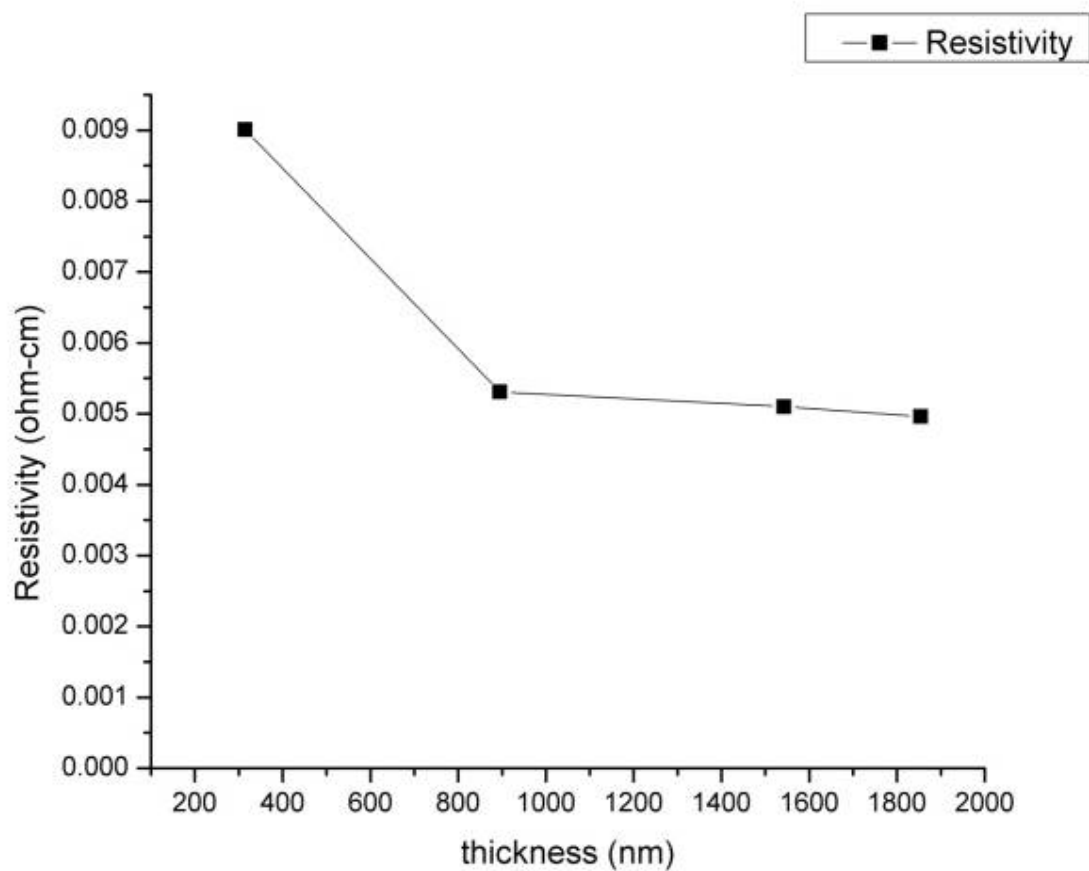


Figure 4-54 The resistivity of ZnO thin films deposited at the various number of laser pulses

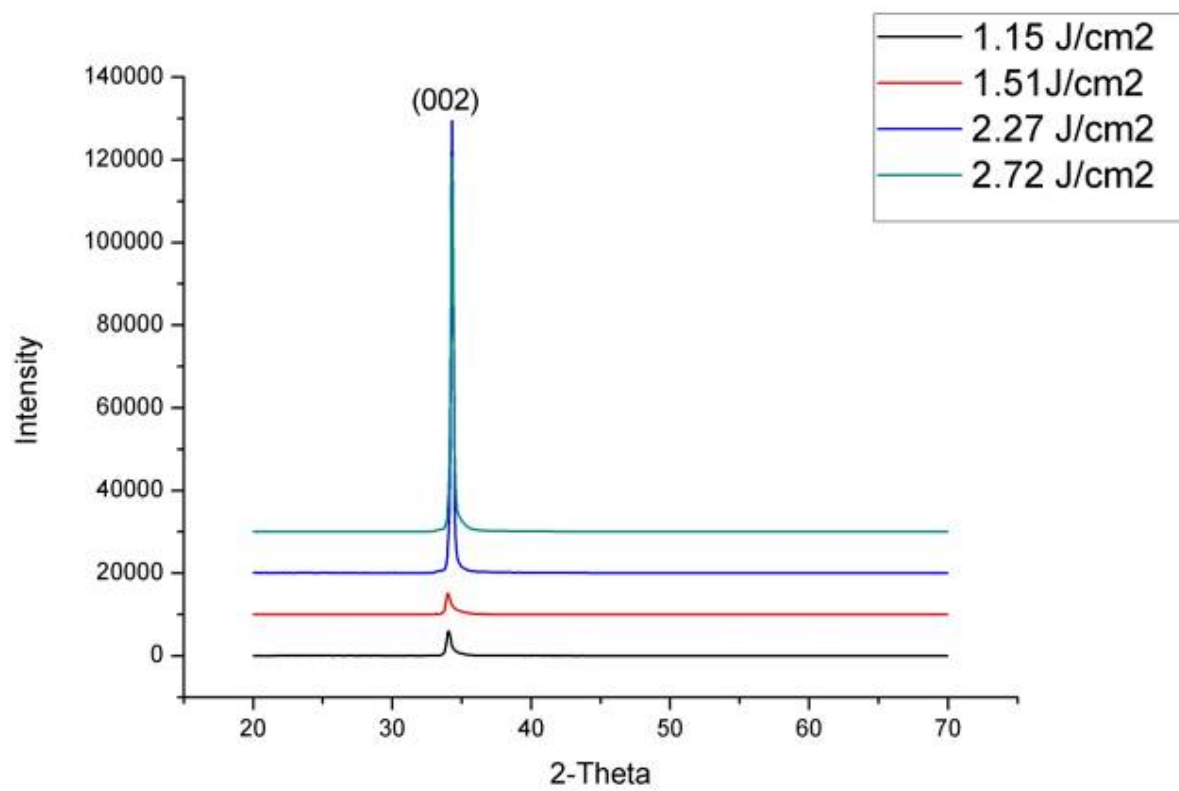


Figure 4-55 X-ray diffraction spectra of ZnO thin film deposited at various laser fluence. (D=55mm, Po₂= 10mTorr, Ts=200°C)

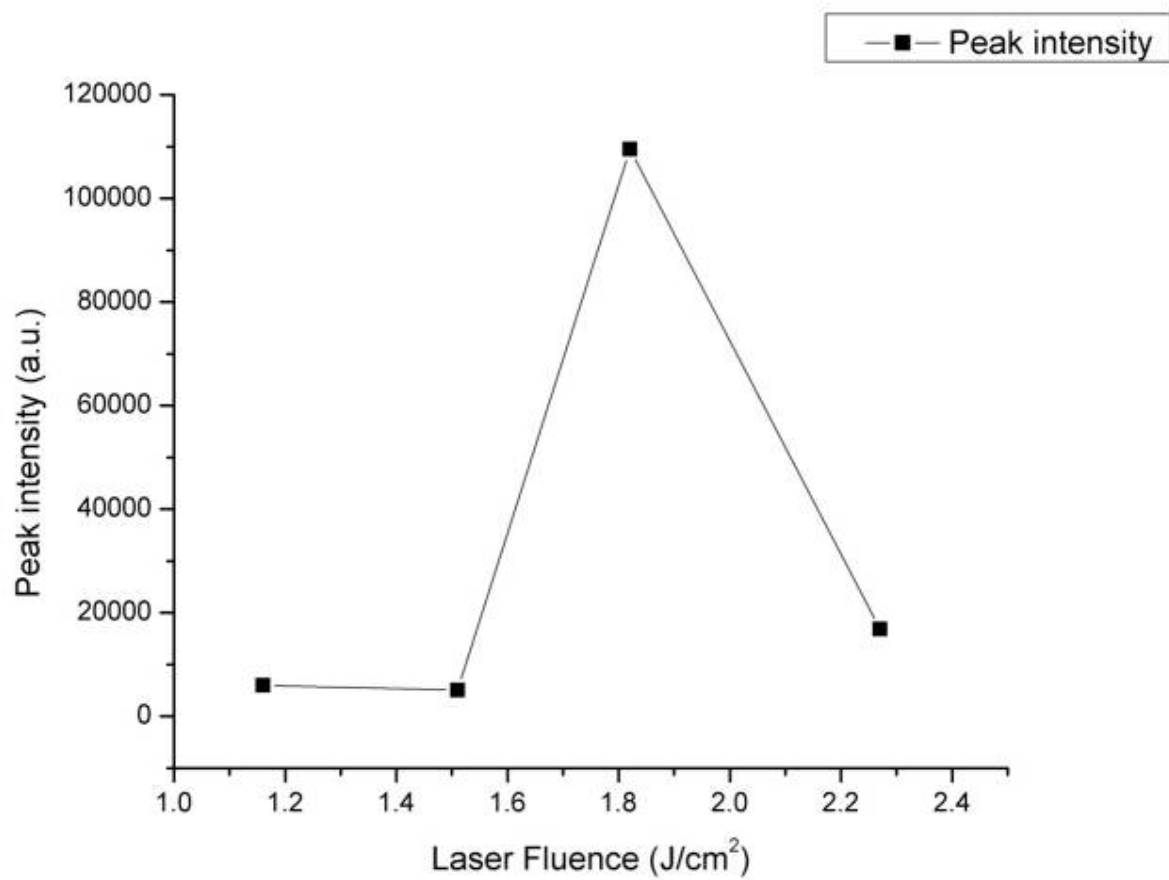


Figure 4-56 Peak intensity of (002) diffraction peak for the ZnO films deposited at various laser fluence (D=55mm, Po2=10mTorr, Ts=200°C)

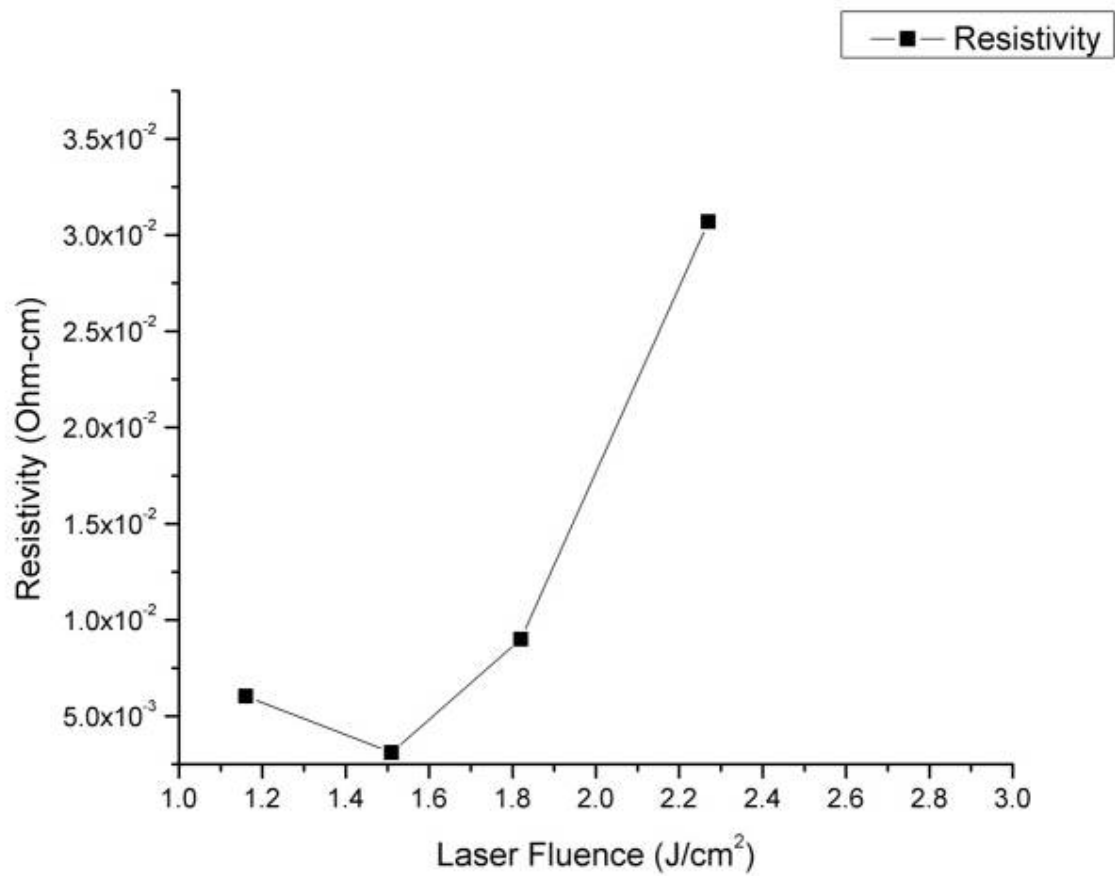


Figure 4-57 Resistivity of ZnO thin films deposited at various laser fluence

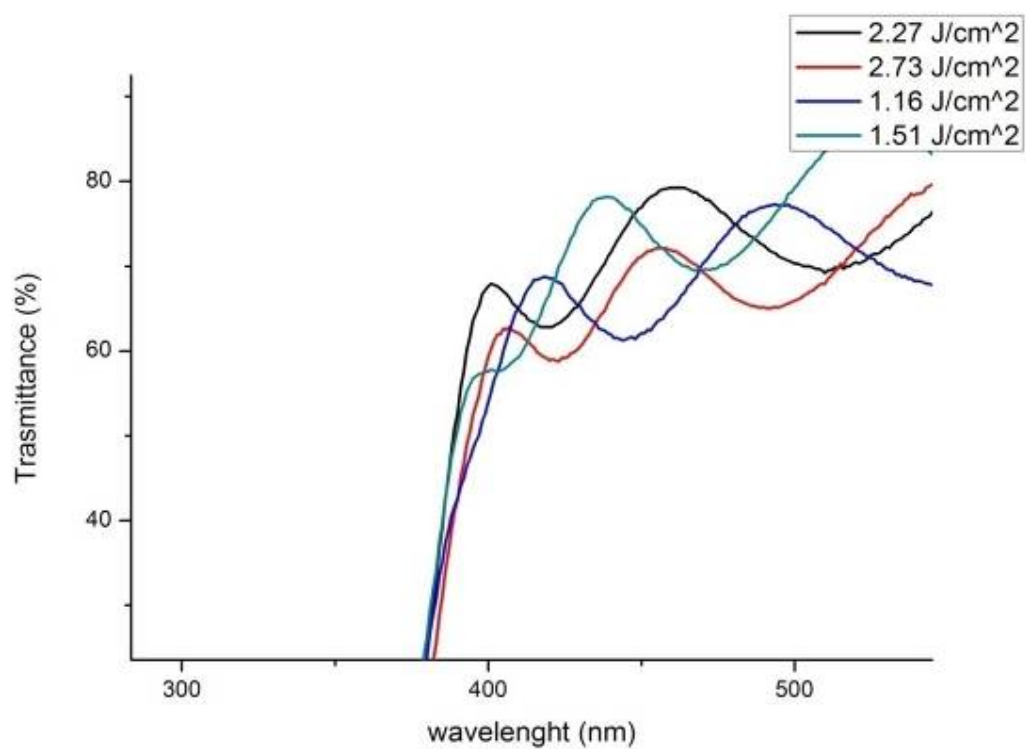


Figure 4-58 the optical transmittance spectrum of ZnO thin films deposited on glass substrates with the various laser fluence ($D=55\text{mm}$, $P_{O2}=10\text{mTorr}$, $T_s=200^\circ\text{C}$, the number of laser pulse=5000)

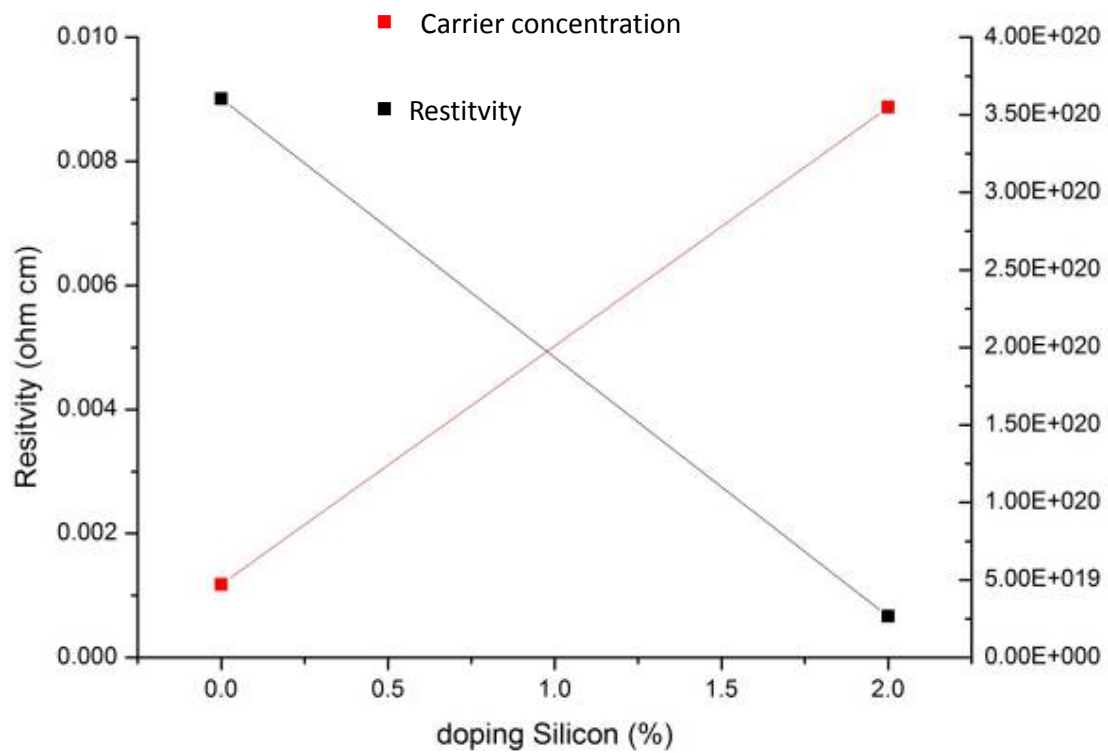


Figure 4-59 Resistivity, and carrier concentration as a function of Si-ZnO thin films (D=55mm, Po2=5mTorr, Ts=200°C, the number of laser pulse=5000)

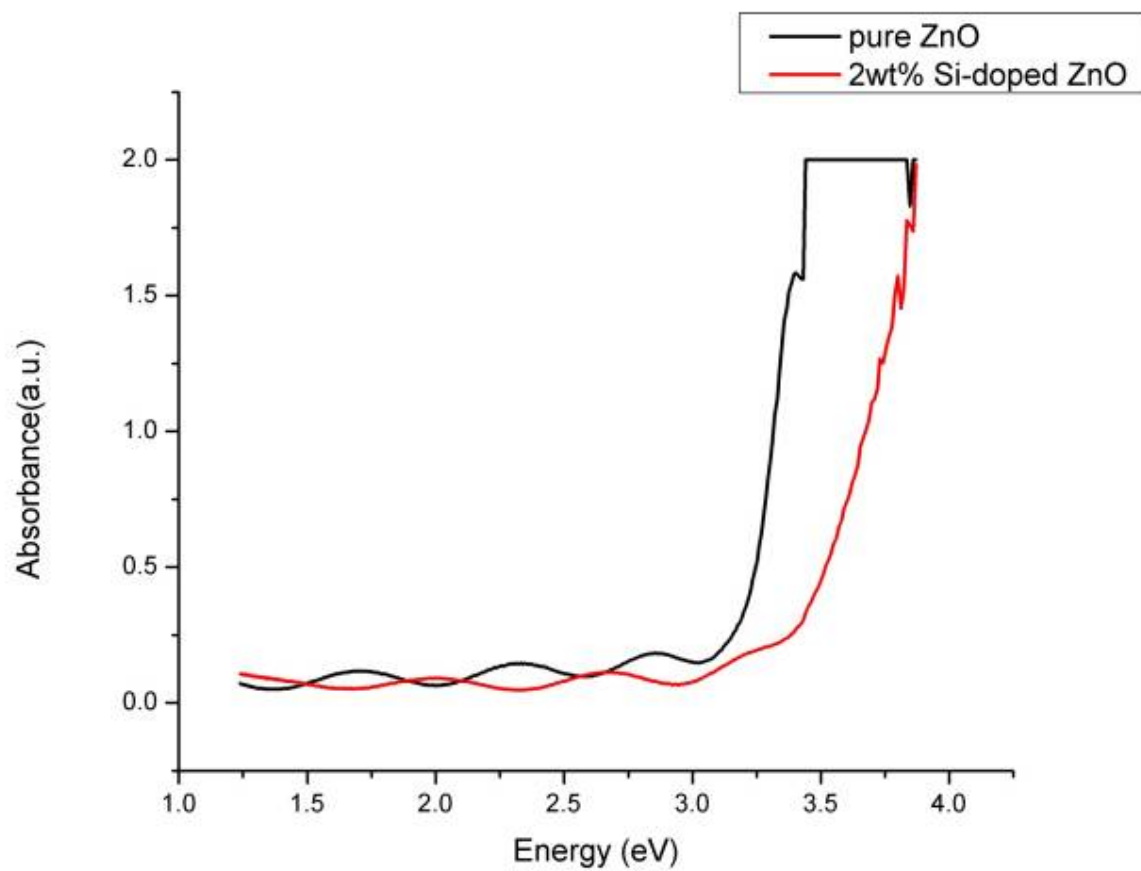


Figure 4-60 Absorption spectra of pure ZnO thin film and 2wt% Si-doped ZnO

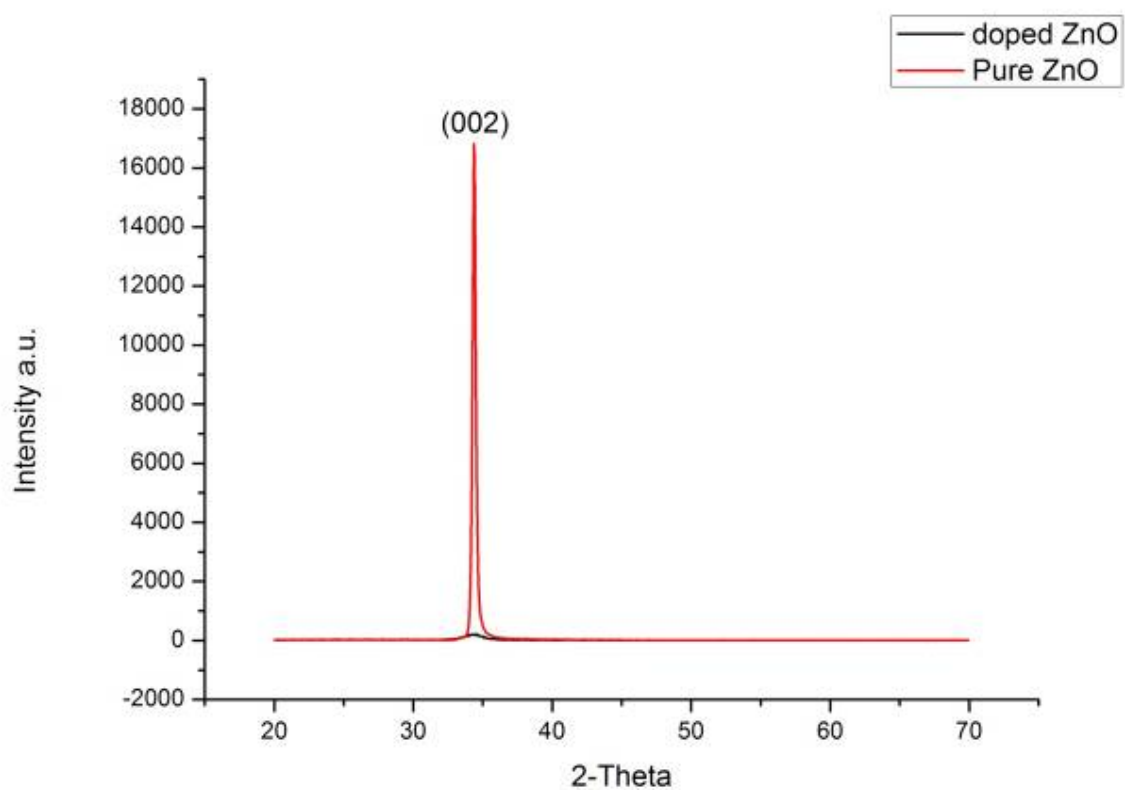


Figure 4-61 X-ray diffraction spectra of ZnO thin film and Si-ZnO thin film (D=55mm, Po2= 5mTorr & 10mTorr, Ts=200°C, Laser fluence=2.7J/cm²)

Substrate	Target	Distance (mm)	PO ₂ (mTorr)	T _s (°C)	Laser energy (mJ)	Resistivity (Ω-cm)	Transmittance
Glass	ZnO	55	10	300	350	1.89E-02	71.6
Glass	ZnO	55	20	300	350	5.70E-02	90.5
Glass	ZnO	55	30	300	350	4.49E+00	84.3
Glass	ZnO	55	40	300	350	7.43E-01	77.5
Glass	ZnO	55	50	300	350	8.73E-01	77.5

Table 4-1 Summarizing the electrical and optical properties of ZnO films on glass substrates at a temperature of 300°C with varying oxygen pressure

Substrate	Target	Distance (mm)	PO ₂ (mTorr)	T _s (°C)	Laser energy (mJ)	Resistivity (Ω-cm)	Transmittance
Glass	ZnO	55	10	100	350	8.63E-02	79.6
Glass	ZnO	55	10	200	350	9.01E-03	86.9
Glass	ZnO	55	10	300	350	1.89E-02	71.6
Glass	ZnO	55	10	400	350	1.37E-02	78.1
Glass	ZnO	55	10	500	350	4.26E-01	80.3

Table 4-2 Summarizing the electrical and optical properties of ZnO films on glass substrates at the oxygen pressure of 10mTorr with varying substrate temperature.

Substrate	Target	Annealing for 2h	D (mm)	PO ₂ (mTorr)	T _s (□)	Laser energy (mJ)	Resistivity (Ω-cm)
Glass	ZnO	none	55	10	200	350	0.009014043
Glass	ZnO	300	55	10	200	350	0.007925144
Glass	ZnO	400	55	10	200	350	0.01790256
Glass	ZnO	500	55	10	200	350	0.022995634

Table 4-3 Summarizing the electrical and optical properties of ZnO films on glass substrates under optimized conditions with varying annealing temperature

Substrate	Target	Distance(mm)	PO2(mTorr)	Ts(°C)	Laser energy(mJ)	laser fluence
Glass	ZnO	55	10	200	127.2	1.16
Glass	ZnO	55	10	200	166.3	1.51
Glass	ZnO	55	10	200	250	2.27
Glass	ZnO	55	10	200	300	2.73

Table 4 -4 Summarizing the growth parameters of ZnO films on glass substrates with varying laser fluence

Pulse	Target	Distance(mm)	PO2(mTorr)	Ts(°C)	Laser energy(mJ)	thickness(nm)
5000	ZnO	55	10	200	350	315
10000	ZnO	55	10	200	350	895.5
15000	ZnO	55	10	200	350	1542.6
20000	ZnO	55	10	200	350	1854

Table 4-5 Summarizing the growth parameters of ZnO films on glass substrates with various thickness